

1N-32
3005
54 P

Defocussing Characteristics of the ACTS, T1-VSAT Earth Terminal Antennas

Kevin M. Lambert
Analex Corporation
Brook Park, Ohio

and

Walter M. Strickler
Lewis Research Center
Cleveland, Ohio

January 1994

(NASA-TM-106420) DEFOCUSSING
CHARACTERISTICS OF THE ACTS,
T1-VSAT EARTH TERMINAL ANTENNAS
(NASA. Lewis Research Center) 54 p

N94-28826

Unclas



G3/32 0003005

DEFOCUSING CHARACTERISTICS OF THE ACTS, T1-VSAT EARTH TERMINAL ANTENNAS

*Kevin M. Lambert
Analex Corporation
3001 Aerospace Parkway
Brook Park, Ohio 44142*

*Walter M. Strickler
National Aeronautics and Space Administration
Lewis Research Center
Cleveland, Ohio 44135*

ABSTRACT

This report describes a study, the purpose of which was to determine the characteristics of two reflector antennas, as the reflector feed is moved away from the focus. The antennas are a 1.2 meter and a 2.44 meter reflector that will be used in the T1-VSAT earth terminals for the Advanced Communications Technology Satellite (ACTS). These terminals have been constructed in such a way that is inconvenient to use attenuators to control the gain of the signal that is directed toward the satellite. Feed defocussing was proposed as a simple, convenient way to achieve the required gain control. The study was performed in two parts. In order to determine the feasibility of the technique, a theoretical analysis was performed to obtain the gain, beamwidth and far-field pattern of the antennas, as a function of feed displacement. An experimental investigation followed in which patterns of the 1.2 meter antenna were obtained through measurement in the NASA Lewis Research Center, Near-Field Antenna Test Facility. Results of the theoretical and experimental investigation are presented for both uplink (30 GHz) and downlink (20 GHz) frequencies.

INTRODUCTION

The general effects which result from defocussing the feed of a reflector antenna have been studied in the past [1,2]. From those studies it is known that an axial displacement of the feed in a symmetric system introduces phase errors in the aperture field of the reflector. This phase error produces a wider main beam in the far-field pattern and in most cases, lower gain for the antenna. Although typically not desirable, there are some situations in which defocussing can be used to benefit the overall performance of the system in which the antenna is but a single component. The T1-VSAT terminals being discussed in this report are one example.

The Advanced Communication Technology Satellite (ACTS) Project Office (APO) had identified a need to control the effective isotropic radiated power (EIRP) of their T1-VSAT earth terminals [3]. Control is needed on the uplink in order to keep the signal within the dynamic range of the spacecraft demodulators [4]. Downlink signal control is required because the T1-VSAT's use the downlink signal to sense the need for forward error correction encoding of both their uplink and downlink. To meet these needs, APO determined that the EIRP of the terminals needed to be variable over a 9 dB range, with a resolution of 1 dB. Control of the uplink EIRP by means of microwave attenuators was considered impractical because of the inaccessibility of the attenuators, once they were in place, and because of the thermal load they would place on the T1-VSAT. Because of these restrictions, the APO sought alternative means to obtain signal control of the terminals.

Since feed defocussing was known to generally reduce the gain of a reflector antenna, it was suggested as an alternative approach to signal control for the T1-VSAT terminals. However, it was necessary to establish the relationship between feed displacement and antenna performance for the actual T1-VSAT antennas. This was the goal of this study. It was necessary to determine if 9 dB of signal control could be achieved by defocussing. Furthermore, it was necessary to determine the feed positions which would result in providing the required 1 dB of resolution. The previous referenced studies were of insufficient detail to apply to this particular problem. Also those studies assumed a symmetric system whereas the T1-VSAT antennas are offset reflectors.

This study will present the calculated far-field patterns of both the 1.2 meter antenna and the 2.44 meter antenna. The calculations are performed at 29.126 GHz, representing the uplink, and at 19.44 GHz, representing the downlink. The patterns are shown for a series of feed displacements until the maximum desired gain loss is achieved. Data is also presented to show the behavior of the gain of the antennas as the feed is defocussed. Furthermore, the far-field patterns are used to show the broadening of the main beam as the antennas are defocussed.

A prototype 1.2 meter antenna was configured and measured in the Near-Field Antenna Test Facility at the NASA Lewis Research Center. These measurements were taken to verify the predicted signal control established by the calculated patterns. Also the measurement could serve to provide calibration curves of signal control, once the T1-VSAT terminals are used in the field. Measurements were taken at both a representative uplink and downlink frequency, for 10 feed positions. Each feed position was chosen to produce a series of 1 dB gain decrements of the antenna gain at the uplink frequency. A description and the results of this experimental study are provided in this report.

DESCRIPTION OF THE T1-VSAT ANTENNAS

The T1-VSAT antennas are offset parabolic reflector antennas with aperture diameters of 1.2 meters and 2.44 meters respectively. The complete geometry for each antenna is shown in Figure 1. The reflectors are fed by a dual frequency corrugated horn that has an 2.299 inch

aperture diameter with a 96° flare angle. At the input to the feed is an orthomode transducer (OMT) that provides 20 GHz operation through the side port and 30 GHz operation at the thru port. The entire feed assembly is supported in the focal region of the reflectors by the supporting arm shown in Figure 2. The boresight of the feed assembly is directed toward the center of the reflector and thus the feed axis has a tilt angle of 44.60° . Defocussing of the antenna was done by moving the feed along the feed axis, away from the reflector. To enable this action, the feed support was modified to allow the feed assembly to slide continuously. Ten stops were included in this modification to allow for repeatable measurements.

CALCULATED PERFORMANCE

The far-field patterns of the T1-VSAT antennas were calculated by using the Ohio State University Reflector Antenna Code [3]. This code has the capability to calculate the far-field patterns and gain of various types of microwave feed and reflector antennas. The accuracy of this code has been demonstrated by comparison with measurements taken in a compact range [4]. The code is capable of calculating the performance of both the T1-VSAT feed and reflector antennas as will be shown below.

The spherical coordinate system used to define the pattern cuts for both the feed antenna and the reflector antennas, is shown in Figure 3. Patterns are calculated for constant values of ϕ with $\phi=0^\circ$ and $\phi=90^\circ$. The electric field of the feed is oriented along the y axis of the reflector and thus the $\phi=0^\circ$ pattern is the H-plane of the antenna and the $\phi=90^\circ$ pattern is the E-plane. For each value of ϕ , the pattern is calculated as a function of θ . The antenna boresight axis corresponds to the pattern angle $\theta=0^\circ$. Because of the offset geometry, the far-field patterns of the reflector are symmetric in the H-plane but are asymmetric in the E-plane.

The OSU Reflector Code utilizes a Method of Moments, Body of Revolution technique [5] to calculate the far-field patterns of a circularly symmetric horn antenna such as the T1-VSAT feed. Measured amplitude and phase patterns of the feed, at 19.3 GHz were available from the manufacturer. Figure 4 shows a comparison between those measurements and the calculated pattern. Note that the beamwidth of the calculated pattern is wider than that of the measured pattern. The reason that this occurs is unknown to the authors, but it may be the result of some higher order modes that are launched by the interaction between the feed and the OMT. The model does not account for the presence of the OMT. The beamwidth of wide angle corrugated horns is controlled by the flare angle. Therefore in order to match the measured data, a calculation was performed assuming that the feed had a 90° flare angle rather than the actual 96° angle of the horn. Figure 5 shows the comparison between this calculation and the measurement. As can be seen, the agreement here is very good. Therefore, the calculations for the reflector patterns will be made using the patterns of the 90° flare angle feed. Measured data was also available for the feed at 29.3 GHz. Figure 6 compares that data with calculations for both a 90° flare angle and a 96° flare angle feed. Again the agreement is good so it can be concluded that the feed is being accurately modeled.

The defocussing study used an uplink frequency of 29.126 GHz and a downlink frequency of 19.44 GHz. These frequencies were somewhat arbitrarily chosen, however they are within the operating band of the T1-VSAT terminal. The calculated feed patterns at these frequencies are shown in Figure 7 and Figure 8. Since the feed is a circularly symmetric structure, the patterns are symmetric about the boresight axis and they are independent of ϕ .

At the uplink frequency, patterns were generated from 0λ to 3.5λ in 0.5λ increments where λ is the free space wavelength. At 29.126 GHz a wavelength is 0.405 inch. Thus the antenna is modeled with the feed being moved from the focussed position to 1.42 inches in 0.203 inch increments. Figure 9 through Figure 16 is the series of far-field plots which show the changes in the patterns as the 1.2 meter antenna is defocussed. The calculated maximum gain for this antenna when it is focussed is 50.11 dBi.

A similar series of plots is shown in Figure 17 through Figure 28. In these figures, the frequency is 19.44 GHz. Here, the feed had to be displaced to a total of 2.23 inches in order to obtain 9 dB of gain loss. Again the increment between feed spacing is 0.203 inch. The maximum calculated gain is 46.56 dBi with the antenna focussed.

The pattern plots show that the defocussing has the anticipated effect. The movement of the feed away from the focus introduces phase errors in the reflector aperture and cause a broadening of the main beam. The broader main beam results in the antenna having lower gain. A summary of the defocussing effects on the boresight gain is given in Figure 29. This plot shows the gain loss at both frequencies as a function of feed displacement. Both curves are plotted on a relative scale, normalized to a value of 0 dB when the feed is focussed. As can be seen, signal control of the terminal can be achieved by feed displacement. 9 dB of loss is obtained at a feed displacement of about 2 inches at the downlink frequency and at about 1.3 inches at the uplink frequency. Also the slope of the curve is such that selecting 1 dB increments is mechanically reasonable.

Finally, the changes in the beamwidth are summarized in Figure 30 for the uplink and in Figure 31 for the downlink. Here the -3 dB and -10 dB beamwidths are shown as a function of the feed displacement. This beamwidth data is for the H-Plane patterns only. As can be seen in the far-field patterns, the main beam in the E-Plane becomes too distorted to accurately describe.

A set of patterns, calculated for the same feed positions described above, were calculated for the 2.44 meter antenna. Figure 32 through Figure 39 show the patterns of the antenna at 29.126 GHz for the eight feed positions leading up to the 9 dB gain loss level. Figure 40 through Figure 51 show the patterns for the defocus position for the downlink frequency of 19.44 GHz. The maximum gain of the antenna at 19.44 GHz is 52.72 dBi and it is 56.28 dBi at 29.126 GHz. The patterns are essentially the same as those calculated for the 1.2 meter antenna, except that the pattern is narrower by a factor of 2. This occurs because the 2.44 meter antenna geometry is almost double the scale of the 1.2 meter antenna. Thus, the results of the relative gain change, as a function of feed displacement, is the same as with the smaller antenna. These results are

shown in Figure 52. A summary of the beamwidth as a function of feed displacement is shown in Figure 53 for the uplink frequency and in Figure 54 for the downlink frequency.

MEASURED PERFORMANCE

A prototype 1.2 meter T1-VSAT antenna was configured and experiments were performed to obtain the far-field patterns of the antenna. The experiments were conducted in order to validate the modeling analysis presented above and to obtain a typical defocussing calibration of the T1-VSAT antennas. The tests were done at both the uplink and downlink frequencies in the Near-Field Antenna Test Facility at the NASA Lewis Research Center. A schematic diagram of the experiment configuration is shown in Figure 55.

The measurement was conducted by locating the antenna approximately 1250 mm away from the scan plane at an angle of approximately 5 degrees less than parallel. The antenna was positioned at this angle to neutralize the limitation of the pointing apparatus of the antenna which could only achieve an angle of 5 degrees greater than parallel with the scan plane. The RF source provided signals of -10.0 dBm and -7.5 dBm which were sent through a 30 dB travelling-wave-tube amplifier (TWTA) and fed to the antenna at two frequencies, 19.4 GHz and 29.2 GHz respectively. The transmitted energy was collected by an open-ended waveguide probe at each 1 wavelength, λ , spacing along the scan plane. The scan plane covers an area ± 2000 mm from boresight. The probe locations were arrived at by beginning at the bottom left corner of the scan plane, then moving vertically taking measurements at each 1 λ spacing. Once at the top of the scan plane, the probe was incremented 1 λ to the right and then descended vertically to the bottom of the scan plane. Again measurements were taken at each 1 λ spacing. The probe was incremented by 1 λ the right again and the cycle continued until the entire scan area was covered. The raw data was stored on a Concurrent 3250 Computer. Ten such experiments were conducted at the same feed displacements (see Table 1) for the two frequencies, a total of twenty experiments.

Table 1 - Feed Displacement of T1-VSAT Antenna Defocussing Experiment										
Position	1	2	3	4	5	6	7	8	9	10
Displacement (Inches)	0.00	0.40	0.61	0.75	0.88	0.99	1.09	1.18	1.28	1.37

These ten locations were selected from the curve of predicted gain versus feed displacement at 29.126 GHz to yield a 1 dB attenuation per location such that at the tenth location the gain would be attenuated by 9 dB.

Because the T1-VSAT will be used to communicate with the Advanced Communications Technology Satellite (ACTS), the observation point, from which to see the effects of defocussing, will be in the far-field of the antenna. Therefore, the

near-field data must be transformed into far-field data. One technique for transforming the data is the Fast Fourier Transform (FFT) [6]. It is optimal to perform a two dimensional FFT because we have two dimensional near-field data. However, the Concurrent Computer is only capable of performing a one dimensional FFT because of a memory limitation. Therefore, the near-field data must be reduced to one dimension. One technique for doing this is to approximate the aperture distribution with an equivalent line source. The proof of this follows.

Consider an arbitrary aperture field, E_a , as shown in Figure 56.

$$\vec{E}_a(x,y) = E_{ax}(x,y)\hat{x} + E_{ay}(x,y)\hat{y} \quad (1)$$

From Equation (8-26) of [7], the far-field electric field radiated by the aperture field is given by

$$E_\theta = j\beta \frac{e^{-j\beta r}}{2\pi r} (P_x \cos\phi + P_y \sin\phi) \quad (2)$$

and

$$E_\phi = j\beta \frac{e^{-j\beta r}}{t\pi r} \cos\theta (P_y \cos\phi - P_x \sin\phi) \quad (3)$$

where P_x and P_y are given by

$$P_x = \iint_{S_a} E_{ax}(x',y') e^{j\beta(x'\sin\theta\cos\phi + y'\sin\theta\sin\phi)} dx' dy' \quad (4)$$

and

$$P_y = \iint_{S_a} E_{ay}(x',y') e^{j\beta(x'\sin\theta\cos\phi + y'\sin\theta\sin\phi)} dx' dy' \quad (5)$$

Using (1) in (4) and applying the geometry of Figure 56,

$$P_x = \int_{-\frac{L_x}{2}}^{\frac{L_x}{2}} \int_{-\frac{L_y}{2}}^{\frac{L_y}{2}} E_{ax}(x',y') e^{j\beta(x'\sin\theta\cos\phi + y'\sin\theta\sin\phi)} dx' dy' \quad (6)$$

or

$$P_x = \int_{-\frac{L_x}{2}}^{\frac{L_x}{2}} e^{j\beta x' \sin\theta \cos\phi} \left[\int_{-\frac{L_y}{2}}^{\frac{L_y}{2}} E_{ax}(x',y') e^{j\beta y' \sin\theta \sin\phi} dy' \right] dx' \quad (7)$$

Let

$$I_x(x') = \int_{-\frac{L_y}{2}}^{\frac{L_y}{2}} E_{ax}(x', y') e^{j\beta y' \sin\theta \sin\phi} dy' \quad (8)$$

Using (8) in (7),

$$P_x = \int_{-\frac{L_x}{2}}^{\frac{L_x}{2}} I_x(x') e^{j\beta x' \sin\theta \cos\phi} dx' \quad (9)$$

This expression has the form of an unnormalized pattern factor of a line source with a current distribution given by $I_x(x')$.

Similarly, equation (5) can be written as

$$P_y = \int_{-\frac{L_x}{2}}^{\frac{L_x}{2}} I_y(x') e^{j\beta x' \sin\theta \cos\phi} dx' \quad (10)$$

where

$$I_y(x') = \int_{-\frac{L_y}{2}}^{\frac{L_y}{2}} E_{ay}(x', y') e^{j\beta y' \sin\theta \sin\phi} dy' \quad (11)$$

Therefore, P_x and P_y can be written in the form of equivalent line sources I_x and I_y . Consider the cases of the principal planes, $\phi = 0^\circ$ and $\phi = 90^\circ$. When $\phi = 0^\circ$ and $-180^\circ \leq \theta \leq 180^\circ$ (azimuth plane),

$$I_x(x') = \int_{-\frac{L_y}{2}}^{\frac{L_y}{2}} E_{ax}(x', y') dy' \quad (12)$$

and

$$I_y(x') = \int_{-\frac{L_y}{2}}^{\frac{L_y}{2}} E_{ay}(x', y') dy' \quad (13)$$

Using (12) in (9),

$$P_x = \int_{-\frac{L_x}{2}}^{\frac{L_x}{2}} I_x(x') e^{j\beta x' \sin\theta} dx' \quad (14)$$

or

$$P_x = \int_{-\frac{L_x}{2}}^{\frac{L_x}{2}} e^{j\beta x' \sin\theta} \left[\int_{-\frac{L_y}{2}}^{\frac{L_y}{2}} E_{ax}(x', y') dy' \right] dx' . \quad (15)$$

Similarly, using (13) in (10),

$$P_y = \int_{-\frac{L_x}{2}}^{\frac{L_x}{2}} I_y(x') e^{j\beta x' \sin\theta} dx' \quad (16)$$

or

$$P_y = \int_{-\frac{L_x}{2}}^{\frac{L_x}{2}} e^{j\beta x' \sin\theta} \left[\int_{-\frac{L_y}{2}}^{\frac{L_y}{2}} E_{ay}(x', y') dy' \right] dx' . \quad (17)$$

The integral

$$\int_{-\frac{L_y}{2}}^{\frac{L_y}{2}} E_{ax}(x', y') dy' \quad (18)$$

and

$$\int_{-\frac{L_y}{2}}^{\frac{L_y}{2}} E_{ay}(x', y') dy' \quad (19)$$

can be approximated by the Riemann sums

$$\sum_{i=1}^n E_{ax}(x', y_i) \delta y_i \quad (20)$$

and

$$\sum_{i=1}^n E_{ay}(x', y_i) \delta y_i \quad (21)$$

where $E_{ax}(x', y_i)$ and $E_{ay}(x', y_i)$ are measured quantities and δy_i are intervals between measurements, $1/\lambda$.

Noting that for $\phi = 0^\circ$ and $-180^\circ \leq \theta \leq 180^\circ$

$$E_\theta = j\beta \frac{e^{-j\beta r}}{2\pi r} P_x \quad (22)$$

and

$$E_\phi = j\beta \frac{e^{-j\beta r}}{4\pi r} \cos\theta P_y \quad (23)$$

where P_x and P_y are given by (16) and (17), it is shown that the near-field data can be reduced to a function in one dimension, x . This function is the equivalent line source current.

The same can be shown for the elevation plane, $\phi=90^\circ$ and $-180^\circ \leq \theta \leq 180^\circ$. Rearranging the order of integration, P_x and P_y can be written as

$$P_x = \int_{-\frac{L_y}{2}}^{\frac{L_y}{2}} e^{j\beta y' \sin\theta} \left[\int_{-\frac{L_x}{2}}^{\frac{L_x}{2}} E_{ax}(x', y') dx' \right] dy' \quad (24)$$

and

$$P_y = \int_{-\frac{L_y}{2}}^{\frac{L_y}{2}} e^{j\beta y' \sin\theta} \left[\int_{-\frac{L_x}{2}}^{\frac{L_x}{2}} E_{ay}(x', y') dx' \right] dy' \quad (25)$$

The integral

$$\int_{-\frac{L_x}{2}}^{\frac{L_x}{2}} E_{ax}(x', y') dx' \quad (26)$$

and

$$\int_{-\frac{L_x}{2}}^{\frac{L_x}{2}} E_{ay}(x', y') dx' \quad (27)$$

can be approximated by the Riemann sums

$$\sum_{i=1}^n E_{ax}(x'_i, y') \delta x_i \quad (28)$$

and

$$\sum_{i=1}^n E_{ay}(x_i', y') \delta x_i \quad (29)$$

where $E_{ax}(x_i', y')$ and $E_{ay}(x_i', y')$ are measured quantities and δx_i are intervals between measurements, 1λ .

Noting that for $\phi = 90^\circ$ and $-180^\circ \leq \theta \leq 180^\circ$

$$E_\theta = j\beta \frac{e^{-j\beta r}}{2\pi r} P_y \quad (30)$$

and

$$E_\phi = j\beta \frac{e^{-j\beta r}}{4\pi r} \cos\theta P_x \quad (31)$$

where P_x and P_y are given by (22) and (23), it is shown that the near-field data can be reduced to an equivalent line source current in one dimension, y .

In both cases, the two-dimensional near-field data was reduced to one dimension. We refer to this process as collapsing data.

The far-field patterns obtained from using the Concurrent computer to perform an FFT on the collapsed near-field data are shown in Figures 57 through 76.

From the far-field patterns, antenna characteristics, such as beamwidth and relative gain, can be ascertained. These parameters will serve as evaluation criteria for determining the effects of defocussing on the T1-VSAT and as criteria for verifying the theoretical analysis.

The 3 dB and 10 dB beamwidths of the antenna at both frequencies and at each feed displacement are shown in Figures 77 and 78. The beamwidths were determined by linear interpolation of the two far-field data points closest to 3 and 10 dB on both sides of the main beam.

The goal of these measurements was to obtain some indication of the gain of the antenna as the feed was defocussed. However, because of the nature of the near-field measurement, the antenna gain cannot be measured directly. Instead the gain must be calculated from the far-field patterns which were obtained as a result of the near-field measurement. The method in which this was done is described in the next section.

GAIN DETERMINATION FROM MEASURED PATTERNS

The directive gain of an antenna is defined as,

$$D(\theta, \phi) = \frac{U(\theta, \phi)}{U_{ave}} \quad (32)$$

where the $U(\theta, \phi)$ is the radiation intensity given by,

$$U(\theta, \phi) = \frac{1}{2} \text{Re}[\bar{E}(\theta, \phi) \times \bar{H}(\theta, \phi)^*] r^2 \hat{r} \quad (33)$$

and U_{ave} is the average radiation intensity,

$$U_{ave} = \frac{1}{4\pi} \iint U(\theta, \phi) d\Omega. \quad (34)$$

Here the integration is over all of space with the element of solid angle given by,

$$d\Omega = \sin\theta d\theta d\phi. \quad (35)$$

Using the plane wave relationship,

$$\bar{H}(\theta, \phi) = \frac{1}{\eta} \hat{r} \times \bar{E}(\theta, \phi) \quad (36)$$

where η is the free space impedance, Equation (33) becomes,

$$U(\theta, \phi) = \frac{1}{2} \frac{|\bar{E}(\theta, \phi)|^2}{\eta} r^2. \quad (37)$$

Using Equation (37) together with Equation (34), the expression for the directive gain becomes,

$$D(\theta, \phi) = 4\pi \frac{|\bar{E}(\theta, \phi)|^2}{\iint |\bar{E}(\theta, \phi)|^2 d\Omega}. \quad (38)$$

This is the form of the equation for directive gain that is needed to obtain the gain from the T1-VSAT measurements.

Two approximations occur when applying Equation (38) to the T1-VSAT patterns. The first occurs because the patterns are only known for $-30^\circ < \theta < 30^\circ$. The second occurs because only the $\phi=0^\circ$ pattern and the $\phi=90^\circ$ pattern were generated. The first approximation produces a negligible result on the calculation of gain because the antennas radiate very little power outside of that region. In fact, when doing the calculation, the integration over θ was restricted to the range $-10^\circ < \theta < 10^\circ$. The integration over ϕ was done through linear interpolation of the data between the two known pattern cuts. This approximation produces errors in the calculation of the absolute gain, however, the changes in relative gain, as a function of feed displacement is not affected. This can be shown through use of the OSU Reflector Antenna Code.

A computer program was written to implement Equation (38) with the limitations described above. The far-field patterns generated by OSU Reflector Antenna Code were then used in that code to calculate the gain of the antennas. Figure 79 shows the results of gain calculation along with the gain as predicted by the OSU code. The accuracy of this code in predicting gain was demonstrated in [4]. As can be seen, using the two pattern approximation produces a result which is a few dB higher than that calculated by the OSU code. However, when the gain curves are normalized, as shown in Figure 80, it can be seen that the relative changes in gain are the same. Thus two pattern approximation is an adequate method to use for this purpose since it is the relative gain change that is of interest.

The results of applying this technique to the gain calculation for the T1-VSAT antenna is shown in Figure 81. Also plotted with the measured results are those predicted by the OSU Reflector Code. The figure shows very good agreement between the curves at the downlink frequency. At the uplink frequency, the agreement is not as good but the measured curve appears to have the same slope as the predicted data. The discrepancy between the two curves may be due to increased error in the measured data at the focus point. If the gain of the antenna was actually higher than what had been measured, then that would have the effect of shifting the measured curve downward and hence results in better agreement between the curves. Another possible reason is that the near-field measurement is less accurate at the higher frequency. With the associated smaller wavelength, phase stability is much more difficult to maintain. A typical near-field measurement of these antennas took approximately one and a half hours to take. Over this time period, several factors such as temperature changes, ground vibrations and power fluctuations could degrade the accuracy of the measurement.

SUMMARY

This report has provided the results of an analytical and experimental study which was conducted to determine if defocussing is a viable way to control the gain of the

T1-VSAT antennas. The results show that the method works and the increments of feed displacement which are needed are mechanically convenient. A feed mount can be designed to make the gain control repeatable and easy to implement when the antennas are in the field. Other possible ways to describe the gain of the antenna were not considered. One alternative that has been suggested is to rotate the feed and thus lose gain through depolarization. The trade-off associated with this technique is that it increases the amount of power in the cross-polarized direction. The defocussing technique avoids this situation because the feed is displaced axially rather than rotated. As shown in the report, the trade-off in axial displacement is that the antenna has a broader, and in some cases, distorted main beam.

REFERENCES

- [1] P. G. Ingerson and W. V. T. Rusch, "Radiation from a Paraboloid with an Axially Defocused Feed," *IEEE Transactions on Antennas and Propagation*, vol. AP-21, pp. 339-345, May 1973.
- [2] Y. T. Lo and S. W. Lee, (ed.), Antenna Handbook, Van Nostrand Reinhold CO., New York, 1988, pg.15-49 - 15-51.
- [3] Advanced Communication Technology Satellite Project, Engineering Review Board #143, August 12, 1988.
- [4] Advanced Communication Technology Satellite Project, Engineering Review Board #221, January 15, 1993.
- [5] T. H. Lee, R. C. Rudduck, K. M. Lambert, "Pattern Measurements of Reflector Antennas in the Compact Range and Validation with Computer Code Simulation," *IEEE Transactions on Antennas and Propagation*, vol. 38, No. 6, pp.889-895, June 1990.
- [6] K. M. Lambert, R. C. Rudduck, T. H. Lee, "A new method for Obtaining Antenna Gain from Backscatter Measurements," *IEEE Transactions on Antenna and Propagation*, Vol. 38, No.6, pp. 896-902, June 1990.
- [7] T. H. Lee, K. M. Lambert, and R. C. Rudduck, "Pattern Measurements of Microwave Horn Antennas in the Compact Range and Comparisons with Moment Method Calculations," *AMTA Symposium Proceedings*, Seattle, WA, Sept., 1987.
- [8] E. O. Brigham, The Fast Fourier Transform and its Applications, Prentice-Hall, New Jersey, 1988, Section 14.6.

- [9] W. L. Stutzman, G. A. Thiele, Antenna Theory and Design, Wiley and Sons, New York, 1981, pg.381-383.

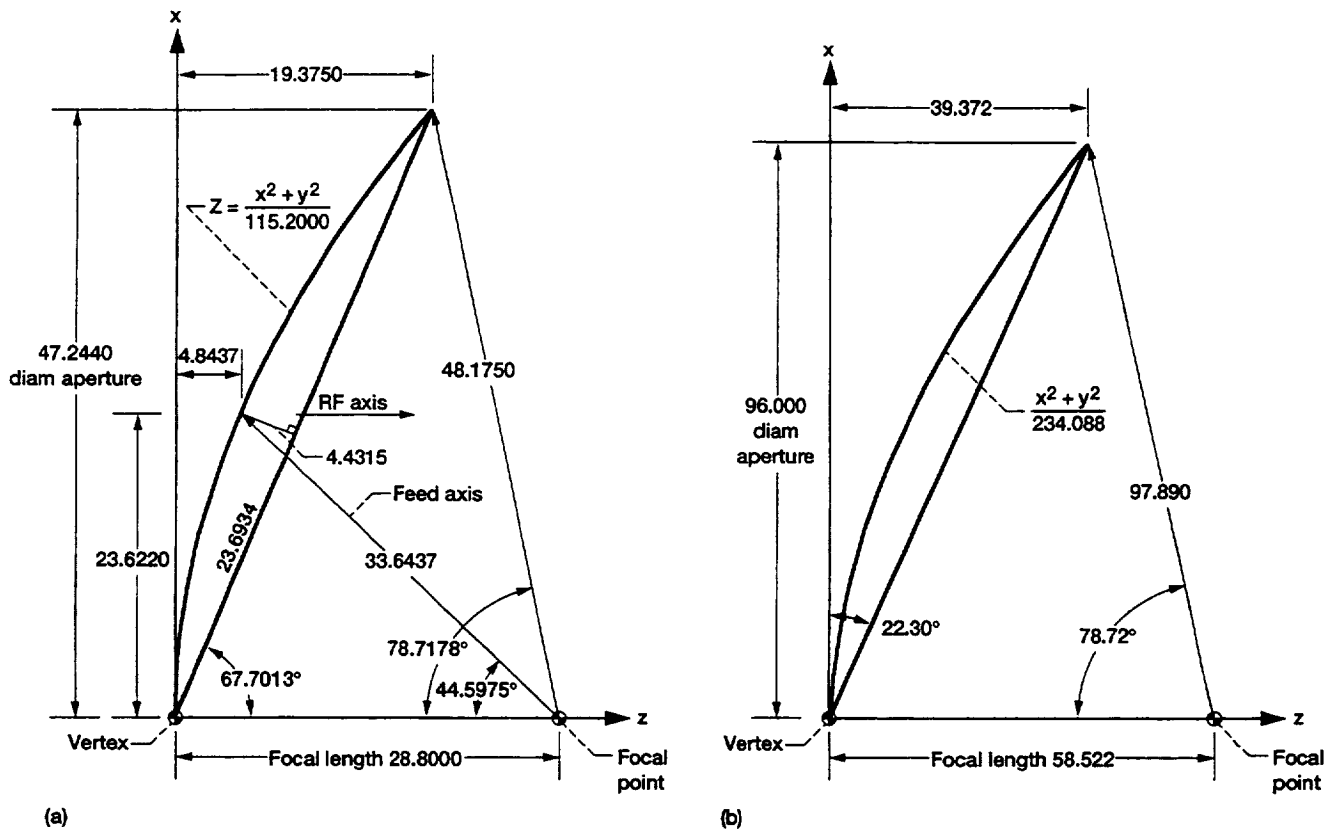


Figure 1.—Configuration of the T1-VSAT Earth Terminal Antennas. Linear dimensions are in inches. (a) 1.2 m reflector geometry. (b) 2.44 m reflector geometry.

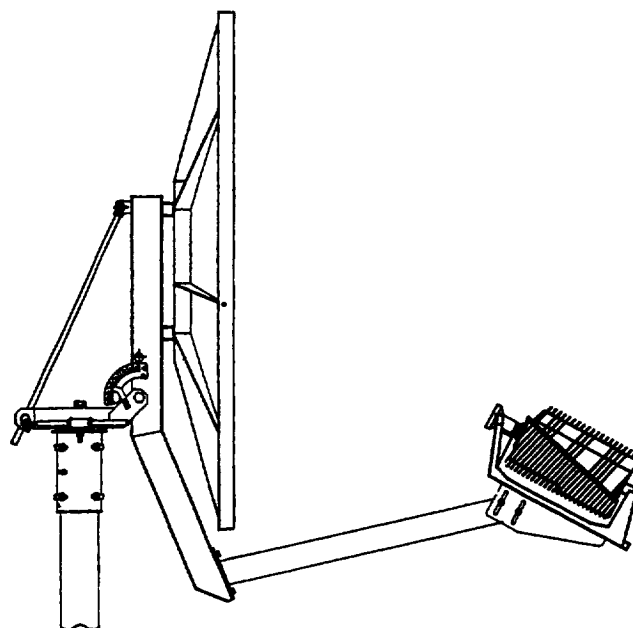


Figure 2.—Feed support for the T1-VSAT antennas.

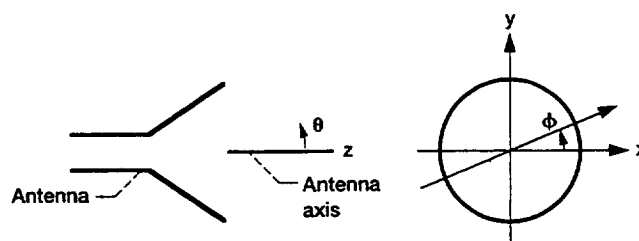


Figure 3.—The coordinate system used to define the far-field patterns of the antennas.

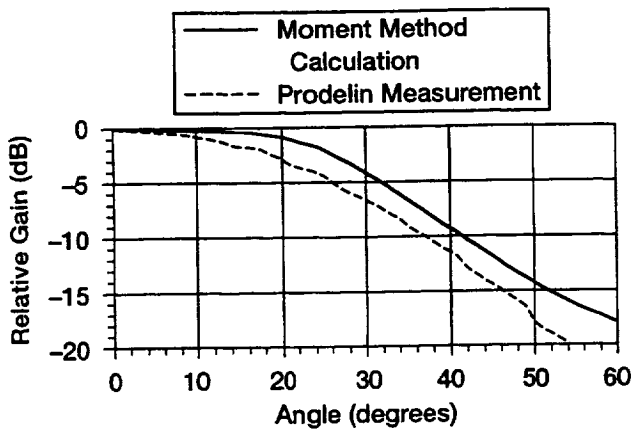


Figure 4.—Calculated and measured feed patterns at 19.3 GHz. Feed modeled with a 96° flare angle.

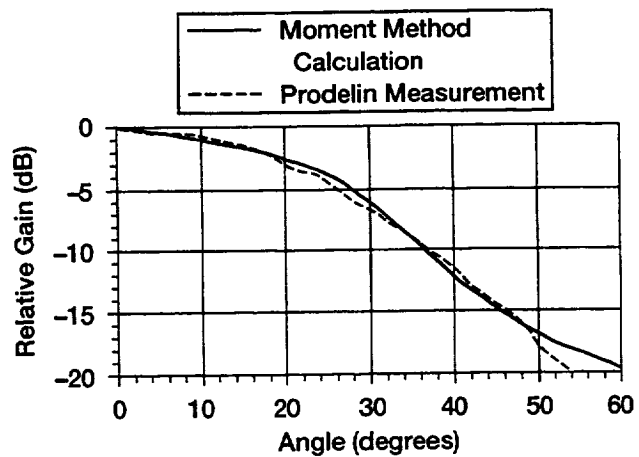
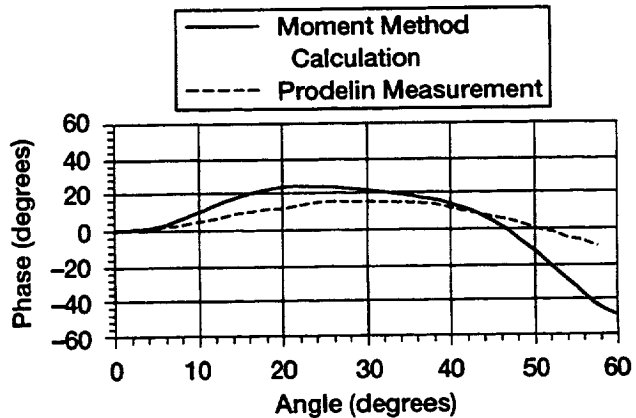
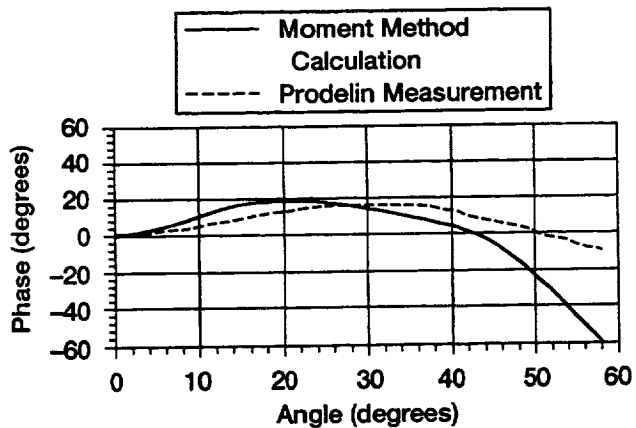


Figure 5.—Calculated and measured feed patterns at 19.3 GHz. Feed modeled with a 90° flare angle.



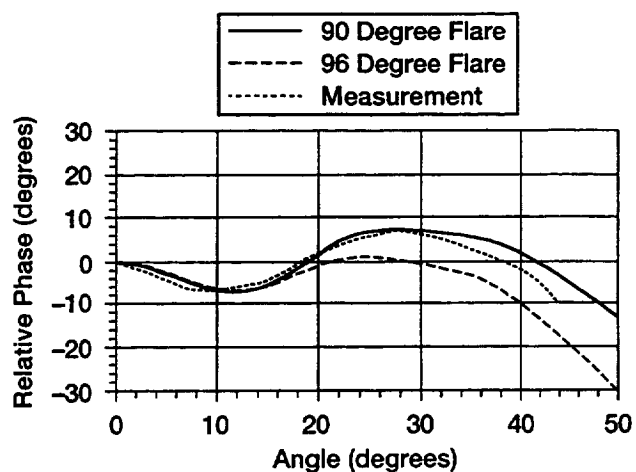
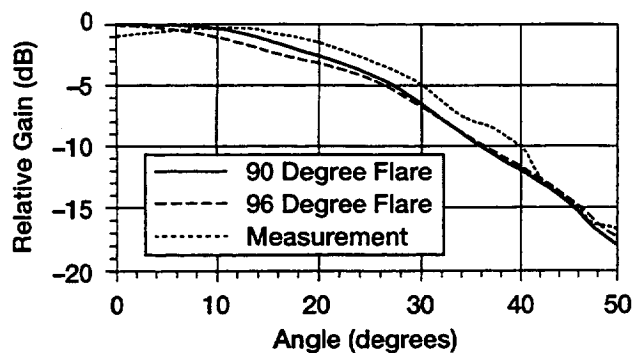


Figure 6.—Calculated and measured feed patterns at 29.3 GHz.

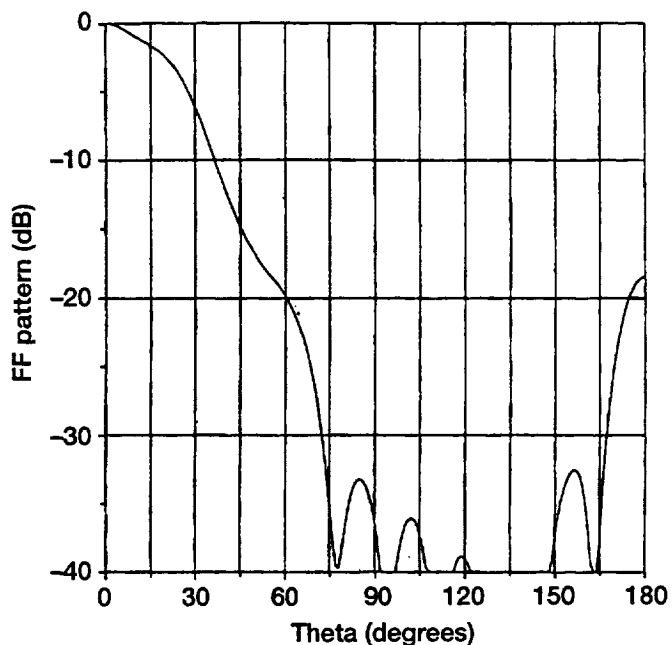


Figure 7.—Calculated feed pattern at 19.44 GHz.

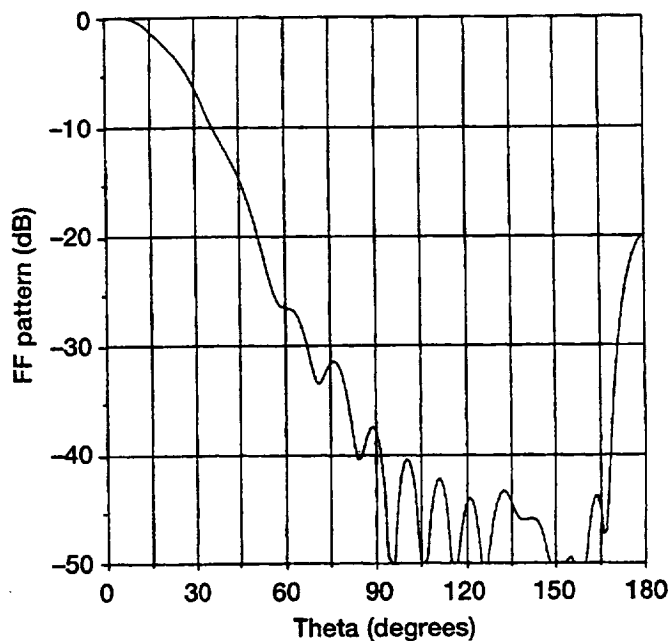


Figure 8.—Calculated feed pattern at 29.126 GHz.

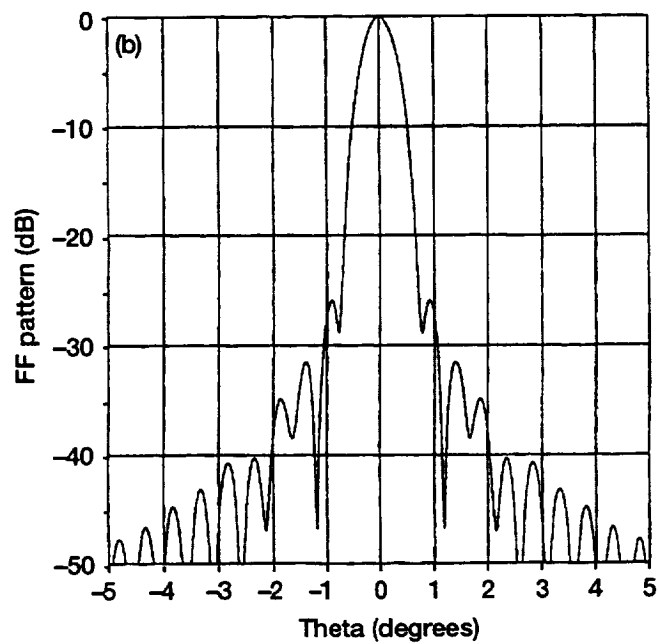
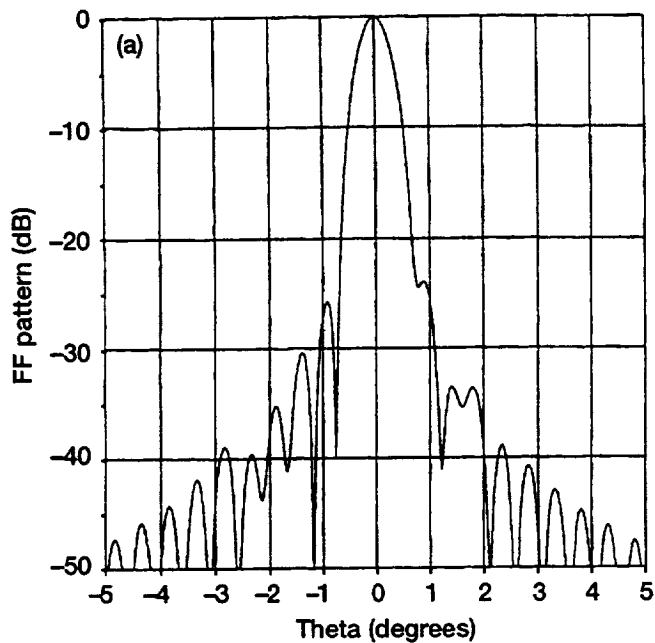


Figure 9.—Calculated far-field patterns of the 1.2 meter antenna at 29.126 GHz. Feed focussed. (a) E-Plane. (b) H-Plane.

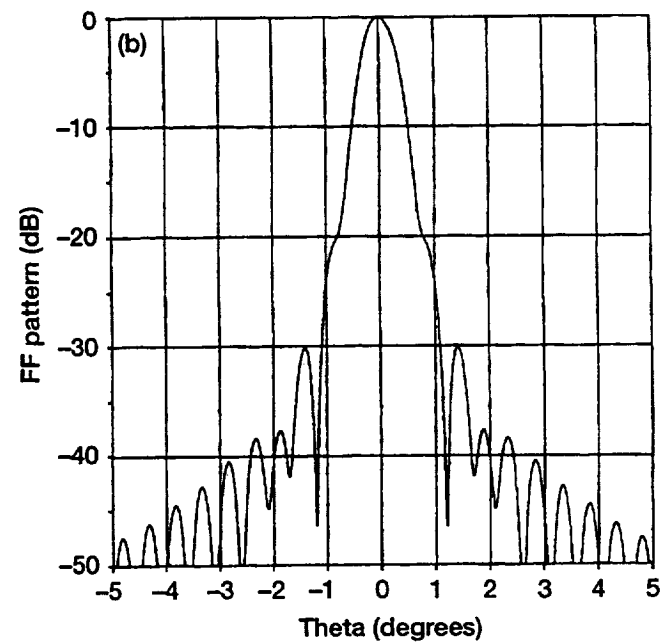
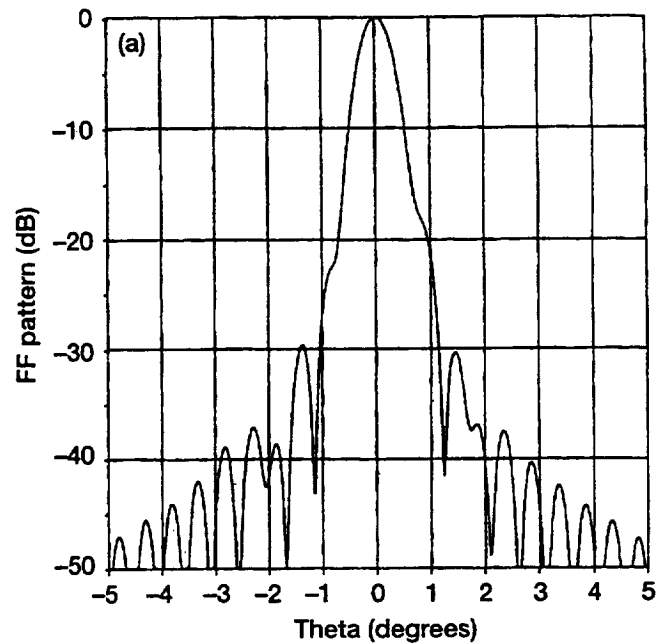


Figure 10.—Calculated far-field patterns of the 1.2 meter antenna at 29.126 GHz. Feed displaced 0.203 inch. (a) E-Plane. (b) H-Plane.

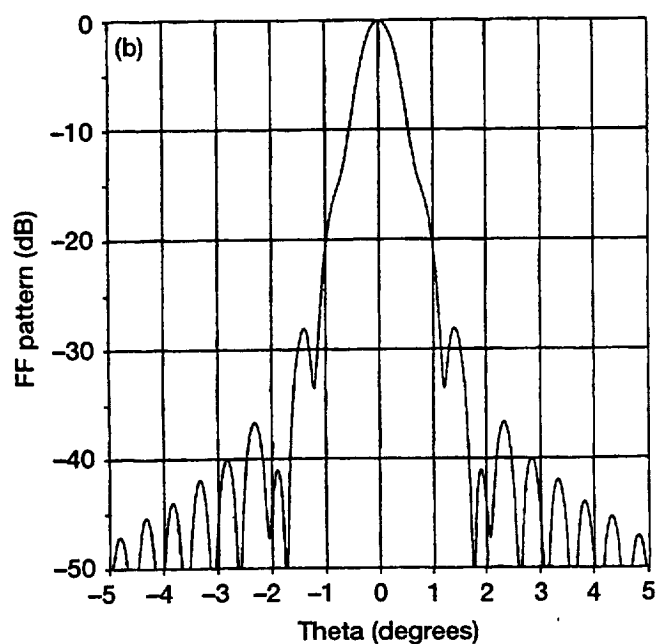
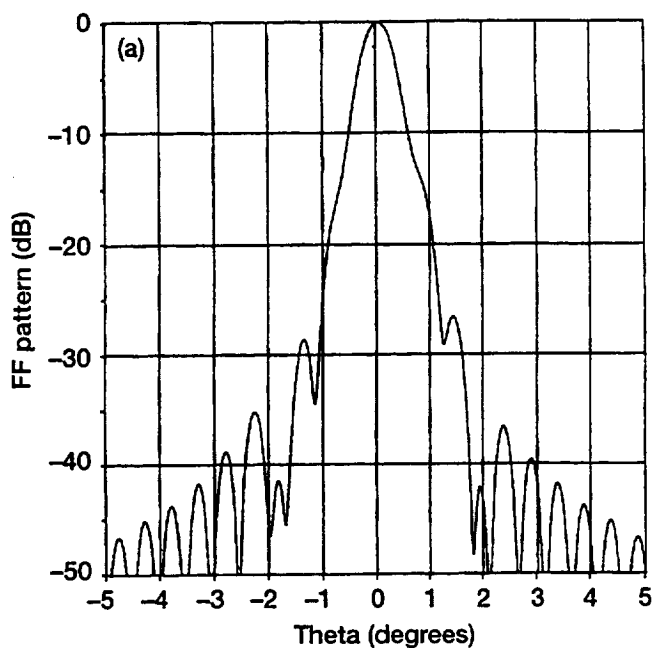


Figure 11.—Calculated far-field patterns of the 1.2 meter antenna at 29.126 GHz. Feed displaced 0.405 inch. (a) E-Plane. (b) H-Plane.

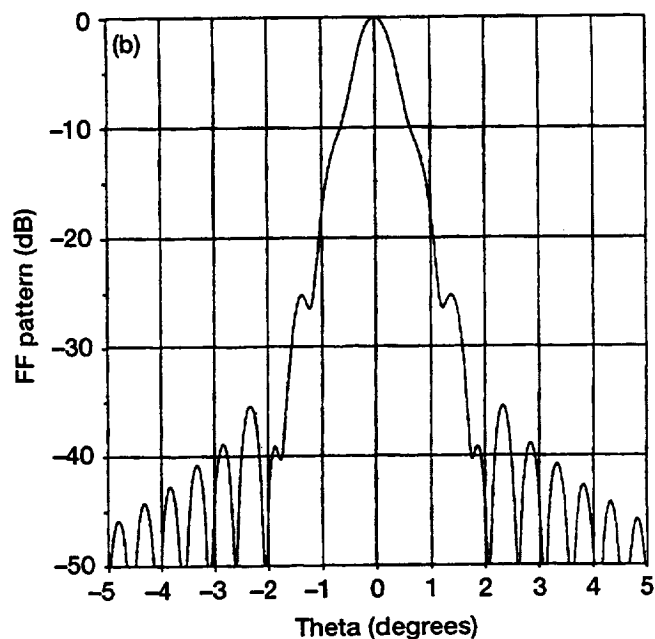
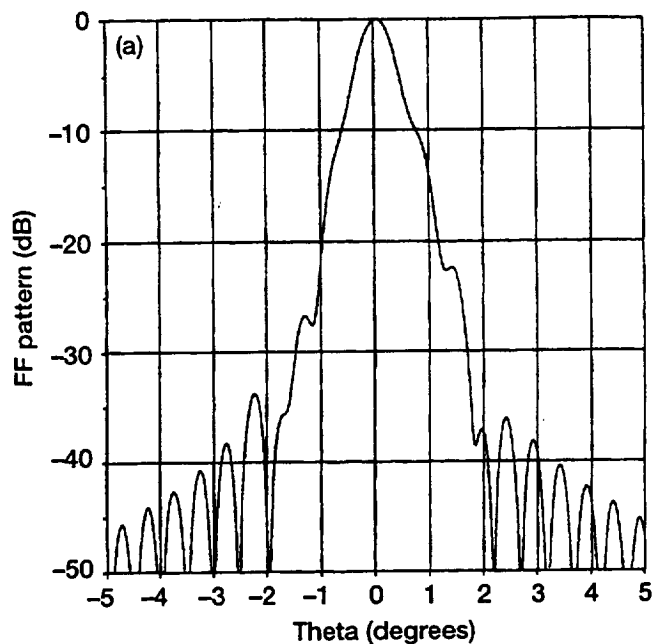


Figure 12.—Calculated far-field patterns of the 1.2 meter antenna at 29.126 GHz. Feed displaced 0.608 inch. (a) E-Plane. (b) H-Plane.

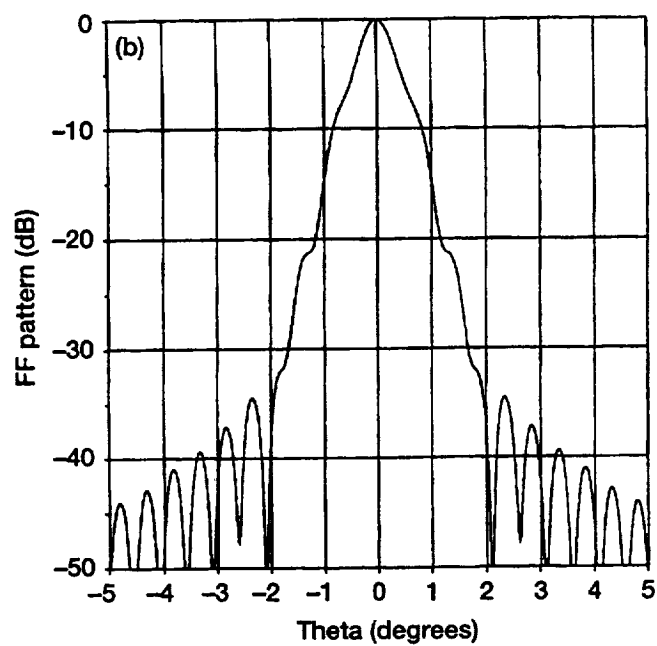
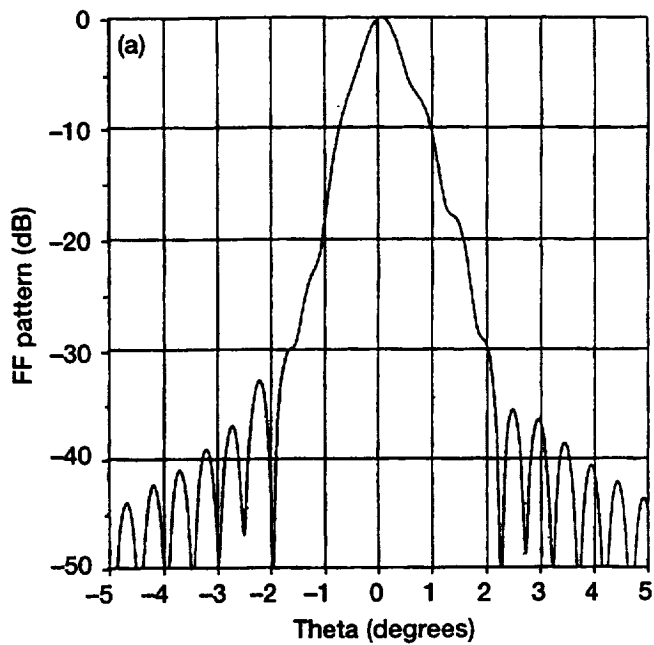


Figure 13.—Calculated far-field patterns of the 1.2 meter antenna at 29.126 GHz. Feed displaced 0.810 inch. (a) E-Plane. (b) H-Plane.

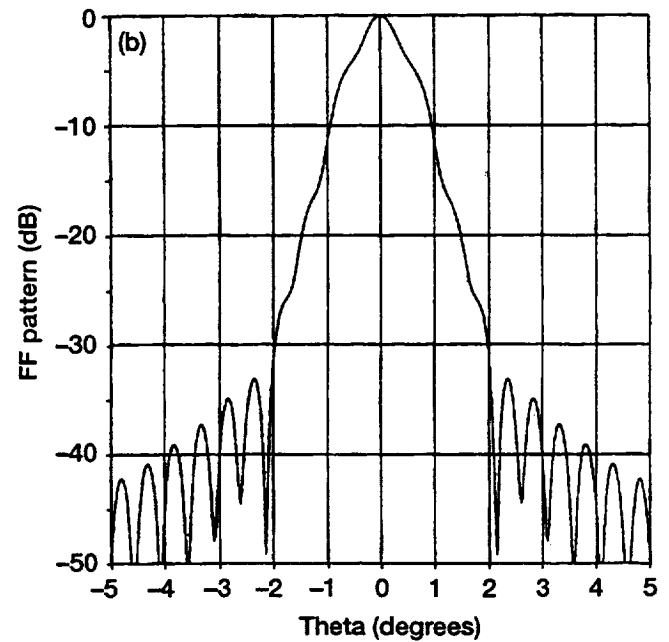
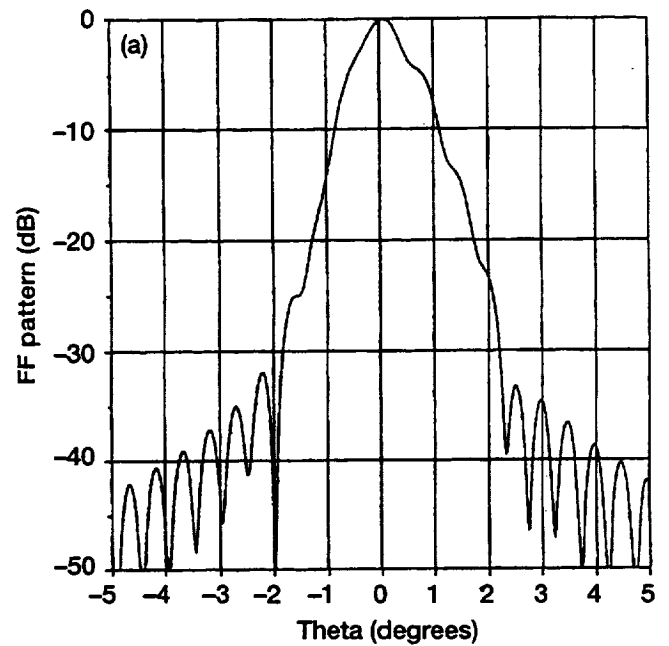


Figure 14.—Calculated far-field patterns of the 1.2 meter antenna at 29.126 GHz. Feed displaced 1.01 inch. (a) E-Plane. (b) H-Plane.

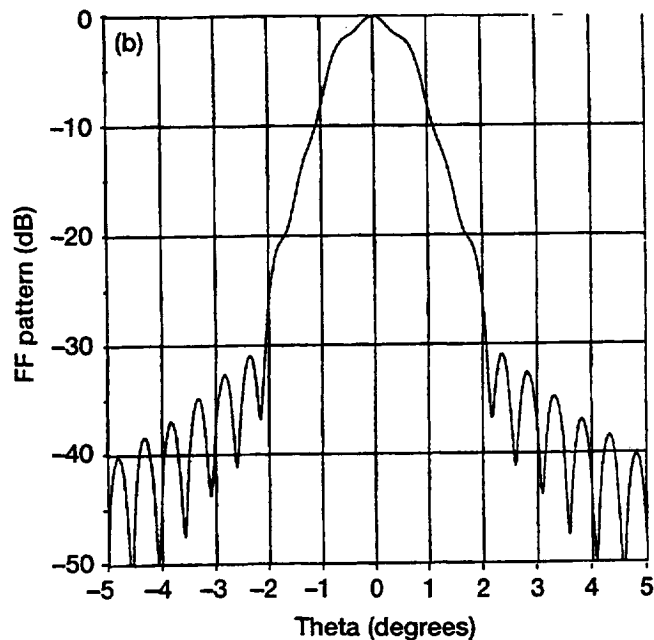
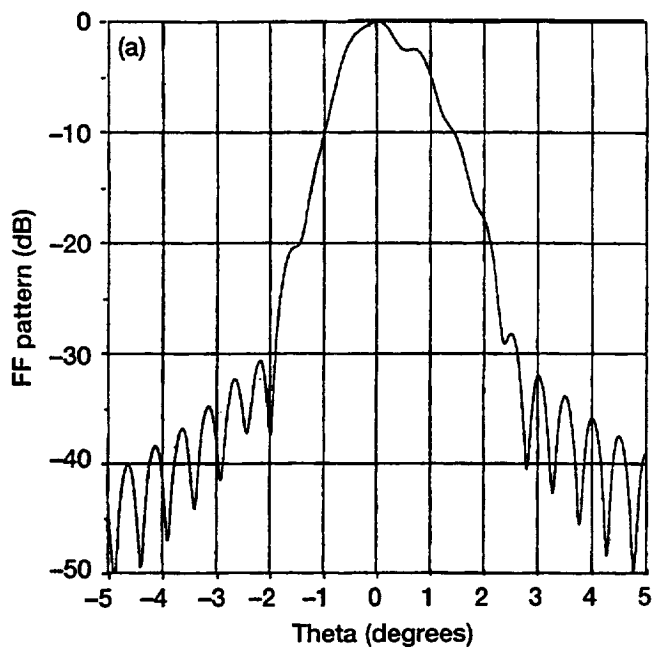


Figure 15.—Calculated far-field patterns of the 1.2 meter antenna at 29.126 GHz. Feed displaced 1.216 inch. (a) E-Plane. (b) H-Plane.

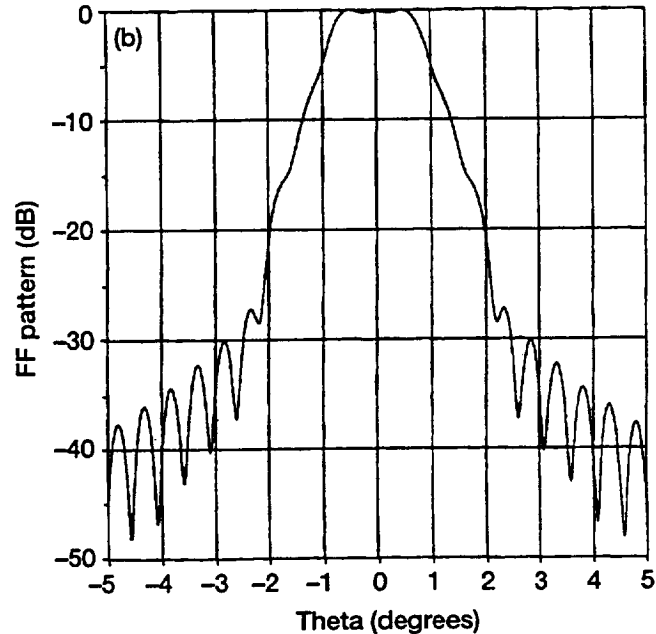
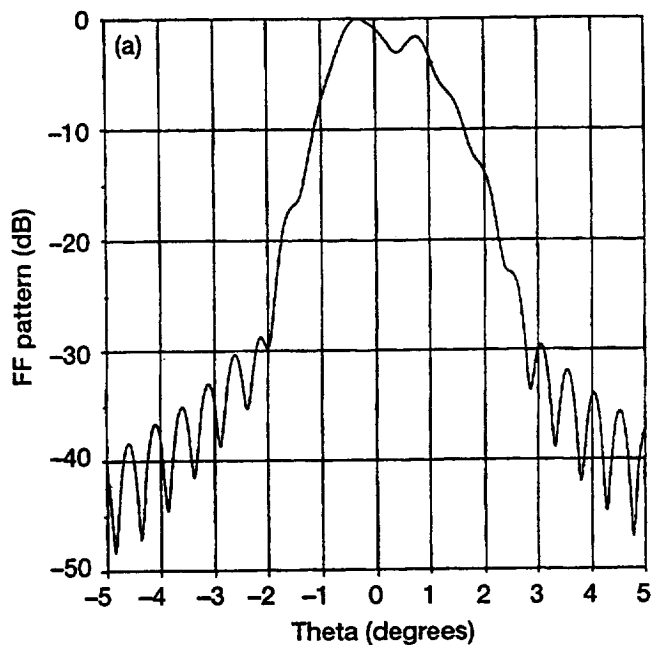


Figure 16.—Calculated far-field patterns of the 1.2 meter antenna at 29.126 GHz. Feed displaced 1.42 inch. (a) E-Plane. (b) H-Plane.

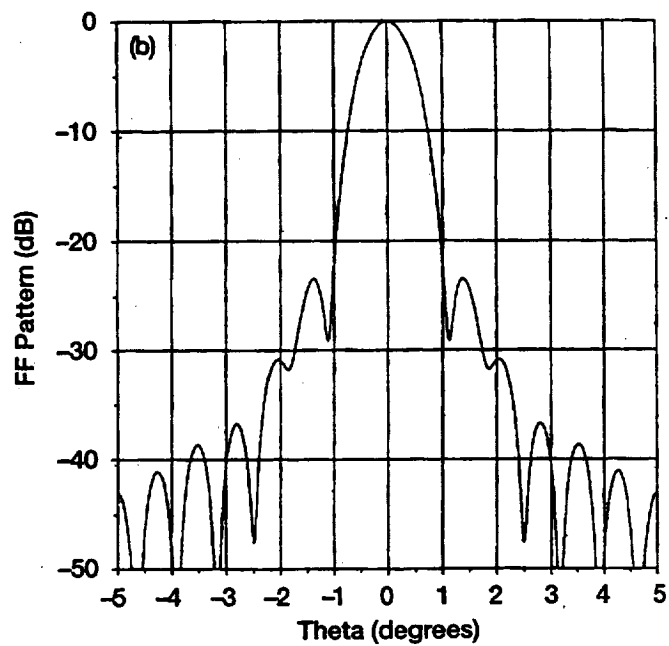
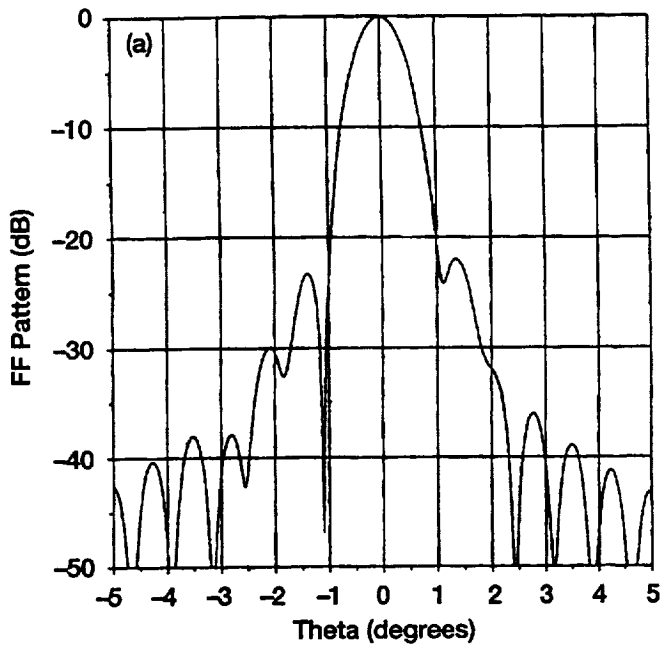


Figure 17.—Calculated far-field patterns of the 1.2 meter antenna at 19.44 GHz. Feed focussed. (a) E-Plane. (b) H-Plane.

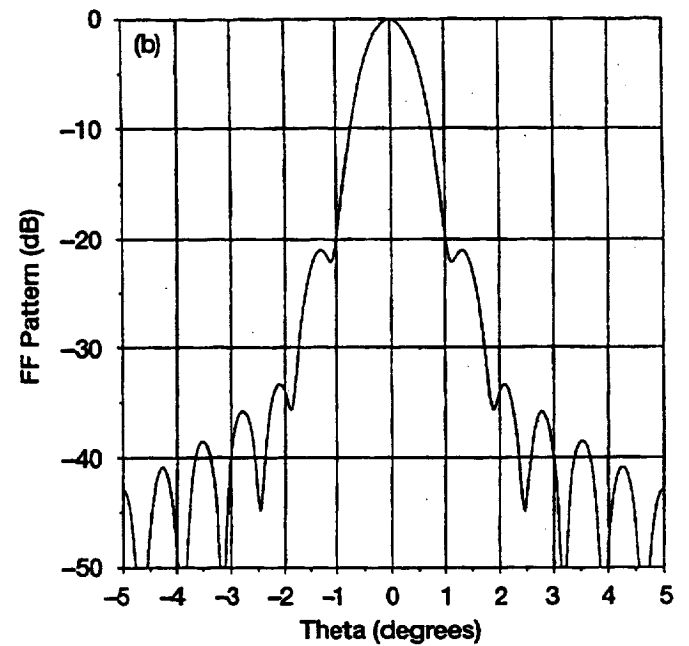
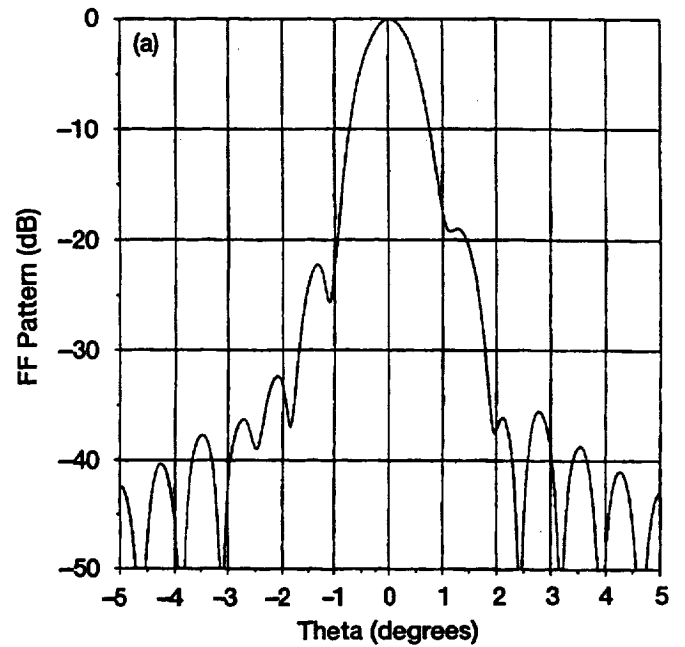


Figure 18.—Calculated far-field patterns of the 1.2 meter antenna at 19.44 GHz. Feed displaced 0.203 inch. (a) E-Plane. (b) H-Plane.

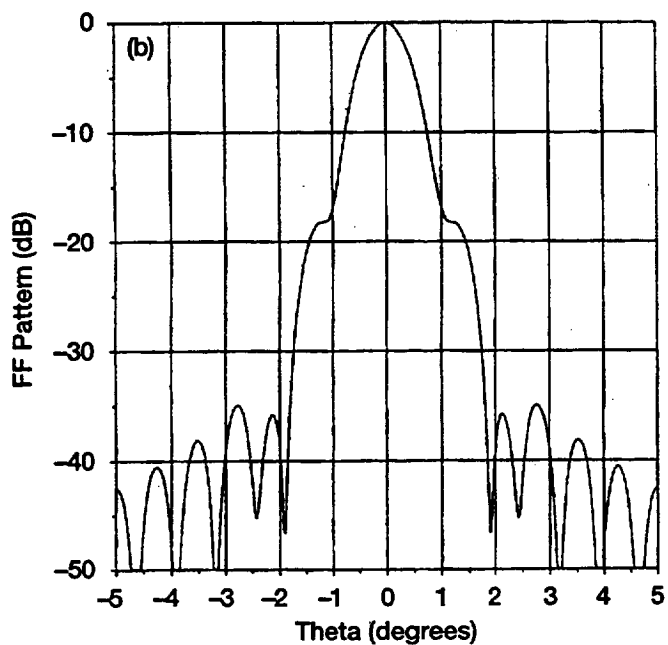
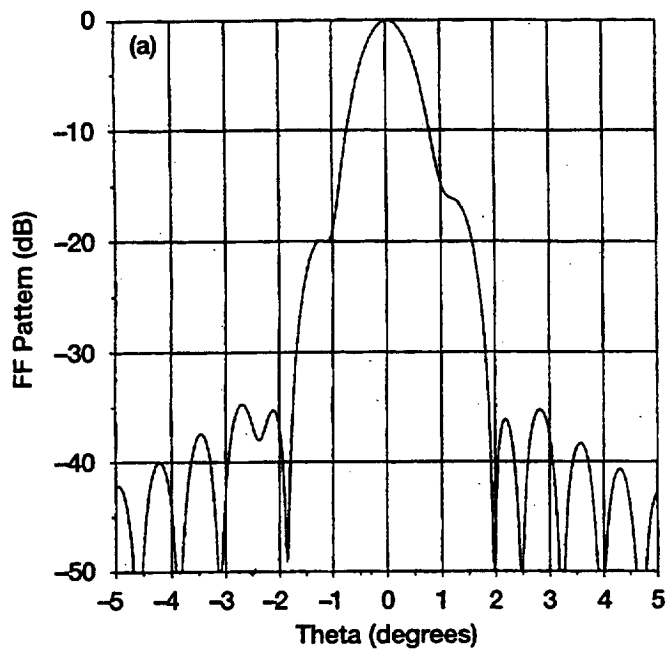


Figure 19.—Calculated far-field patterns of the 1.2 meter antenna at 19.44 GHz. Feed displaced 0.405 inch. (a) E-Plane. (b) H-Plane.

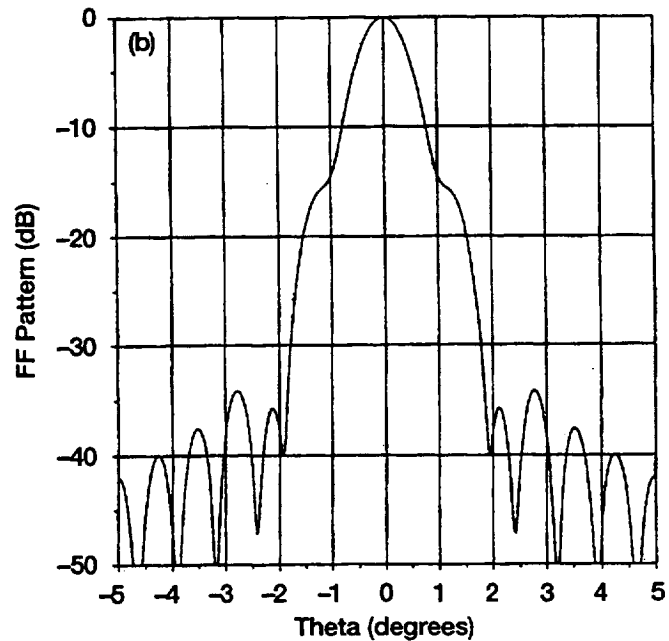
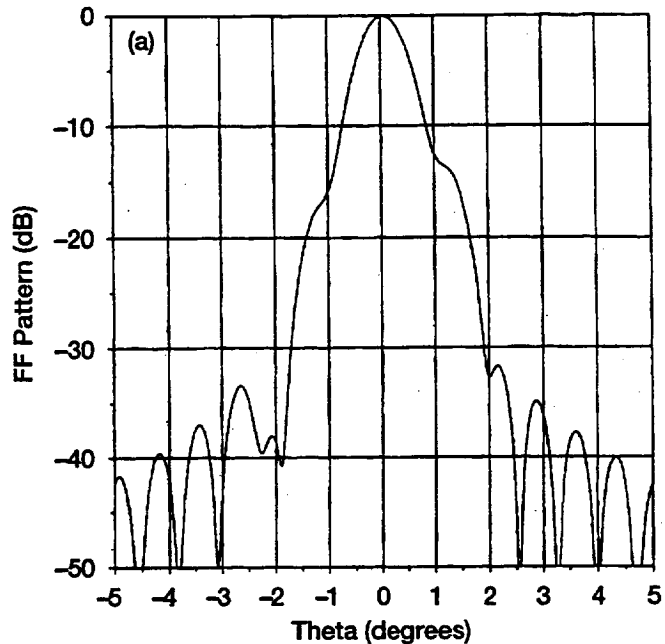


Figure 20.—Calculated far-field patterns of the 1.2 meter antenna at 19.44 GHz. Feed displaced 0.608 inch. (a) E-Plane. (b) H-Plane.

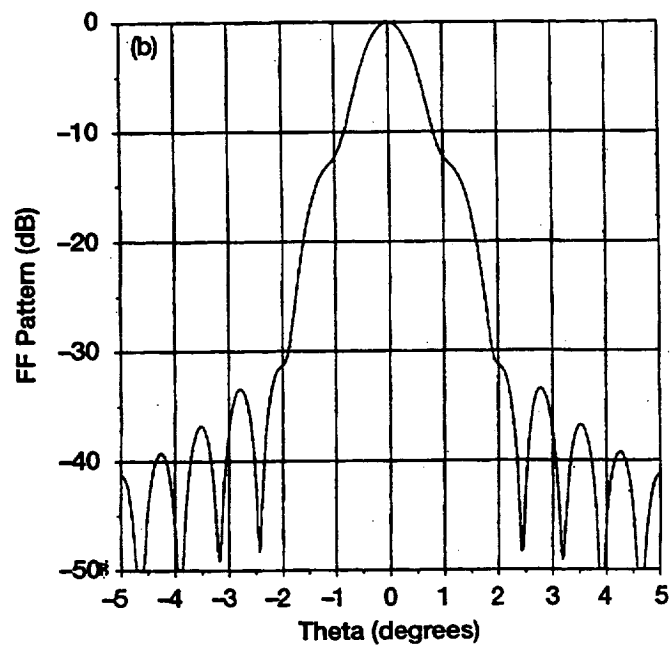
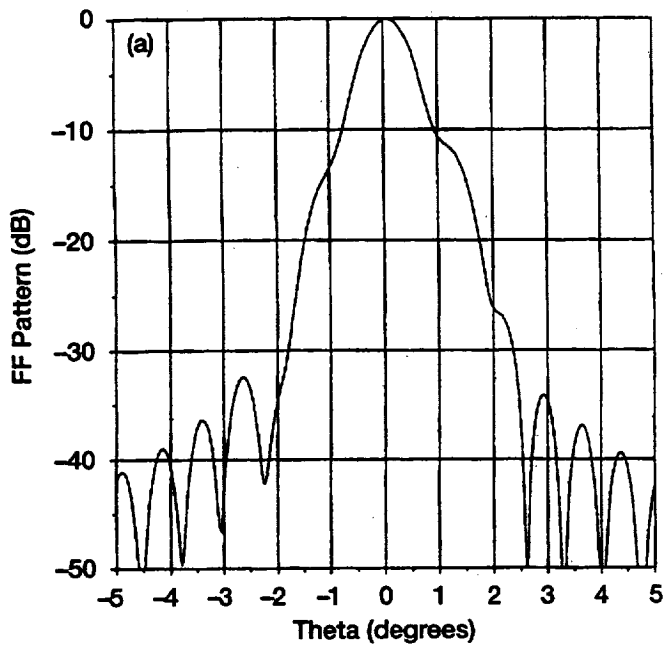


Figure 21.—Calculated far-field patterns of the 1.2 meter antenna at 19.44 GHz. Feed displaced 0.810 inch. (a) E-Plane. (b) H-Plane.

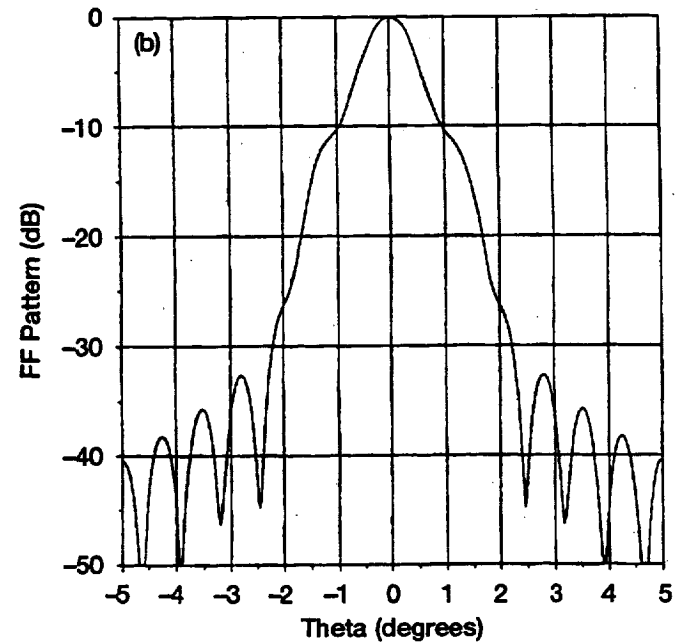
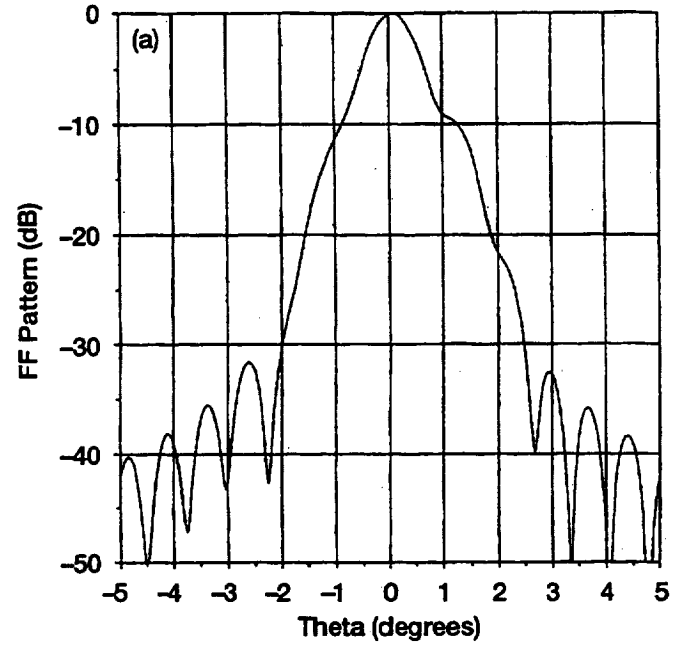


Figure 22.—Calculated far-field patterns of the 1.2 meter antenna at 19.44 GHz. Feed displaced 1.01 inch. (a) E-Plane. (b) H-Plane.

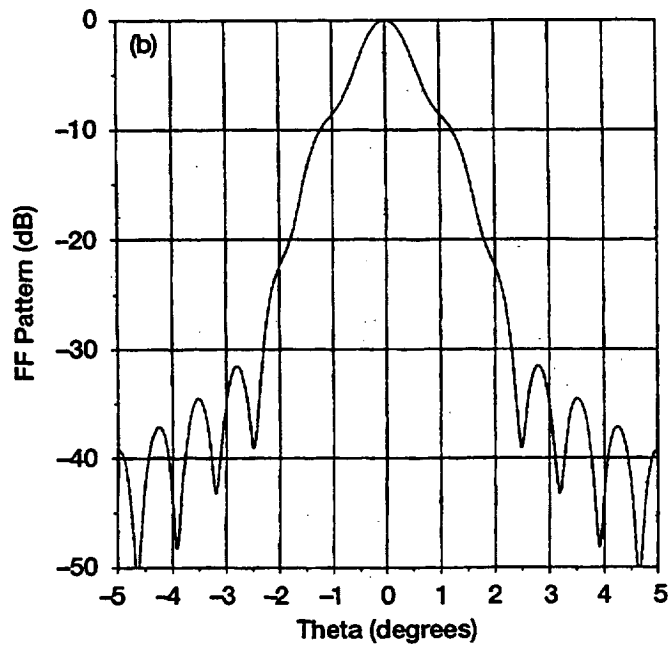
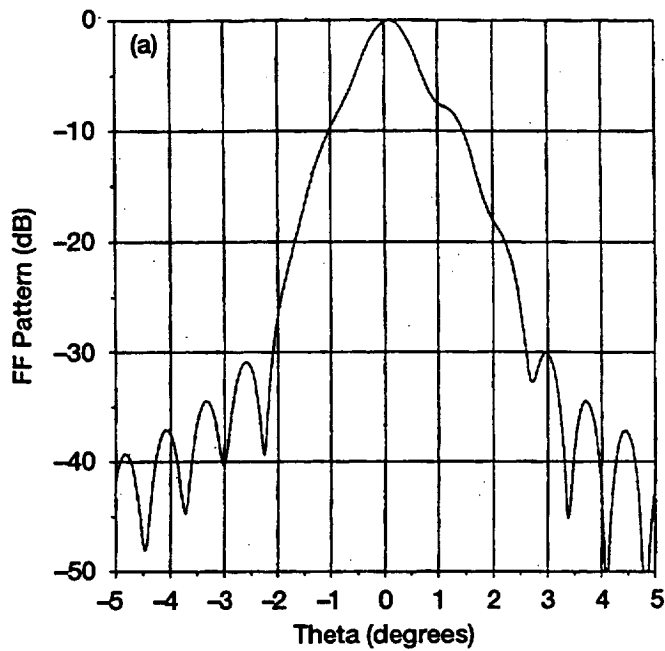


Figure 23.—Calculated far-field patterns of the 1.2 meter antenna at 19.44 GHz. Feed displaced 1.216 inch. (a) E-Plane. (b) H-Plane.

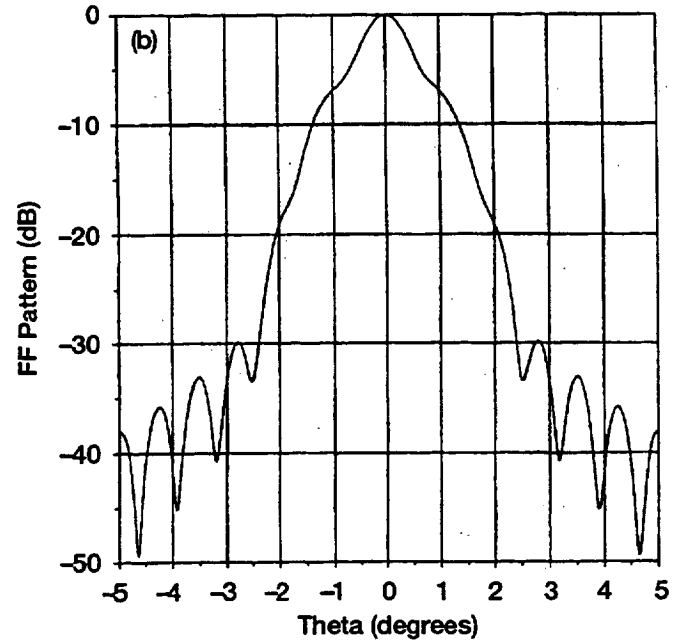
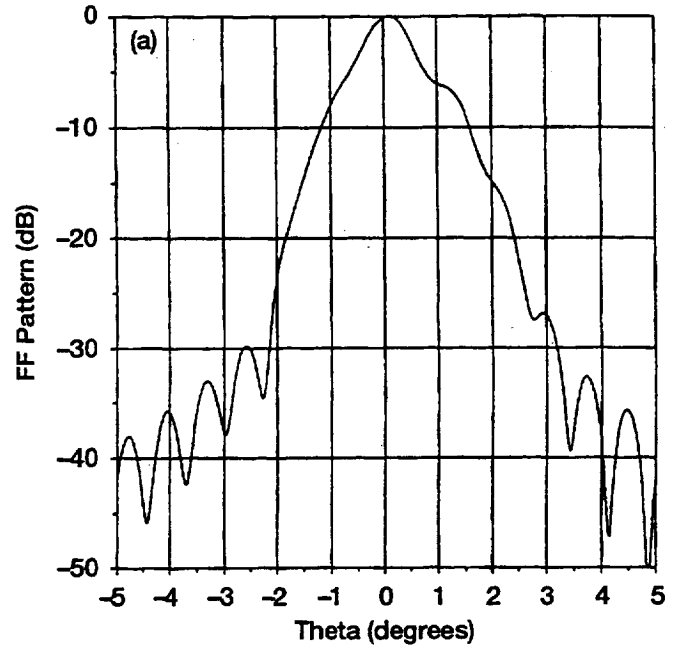


Figure 24.—Calculated far-field patterns of the 1.2 meter antenna at 19.44 GHz. Feed displaced 1.42 inch. (a) E-Plane. (b) H-Plane.

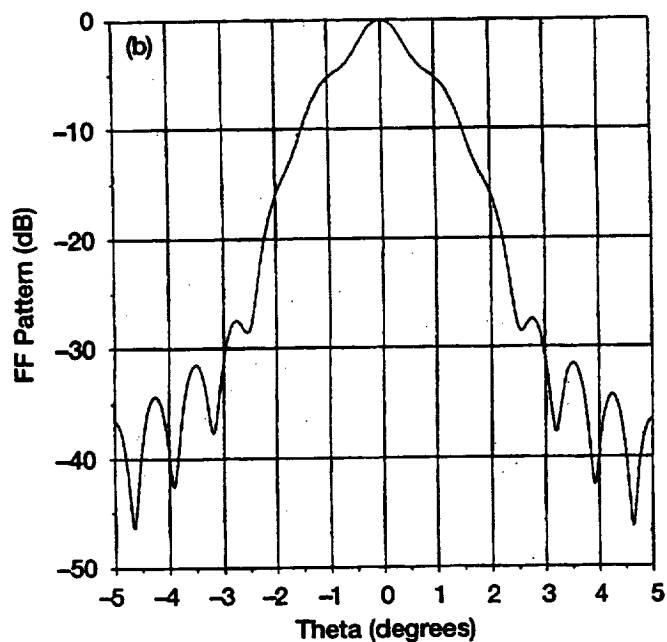
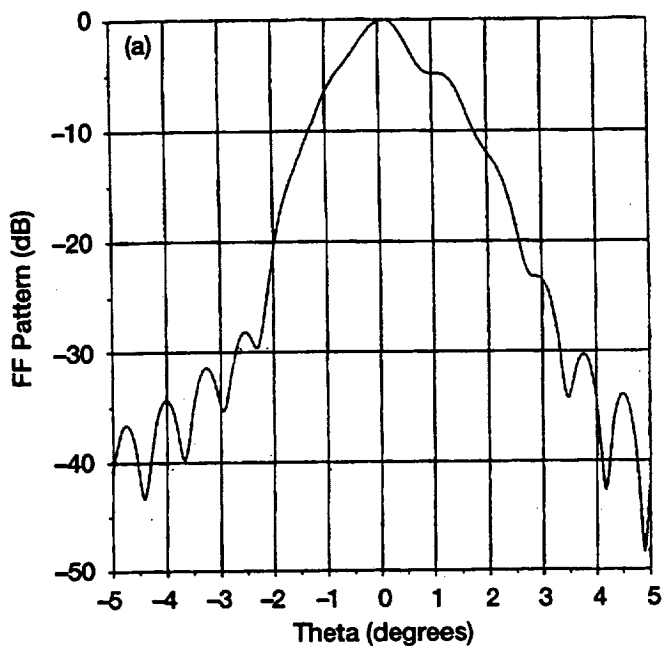


Figure 25.—Calculated far-field patterns of the 1.2 meter antenna at 19.44 GHz. Feed displaced 1.62 inch. (a) E-Plane. (b) H-Plane.

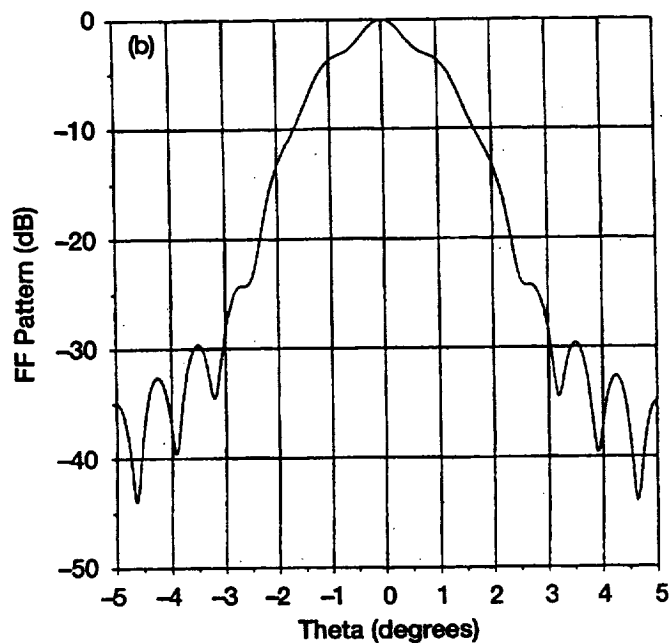
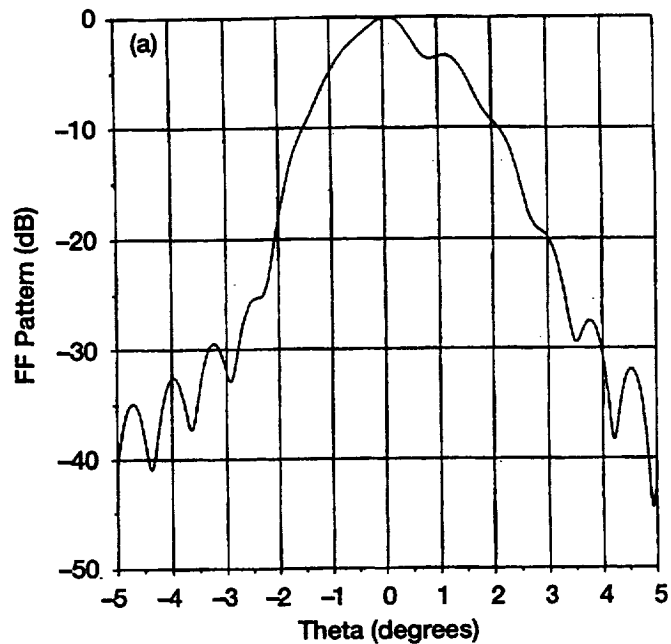


Figure 26.—Calculated far-field patterns of the 1.2 meter antenna at 19.44 GHz. Feed displaced 1.83 inch. (a) E-Plane. (b) H-Plane.

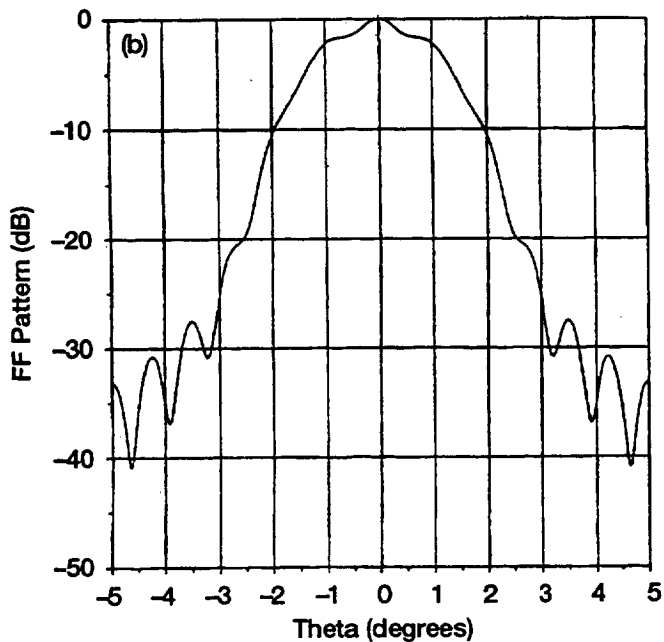
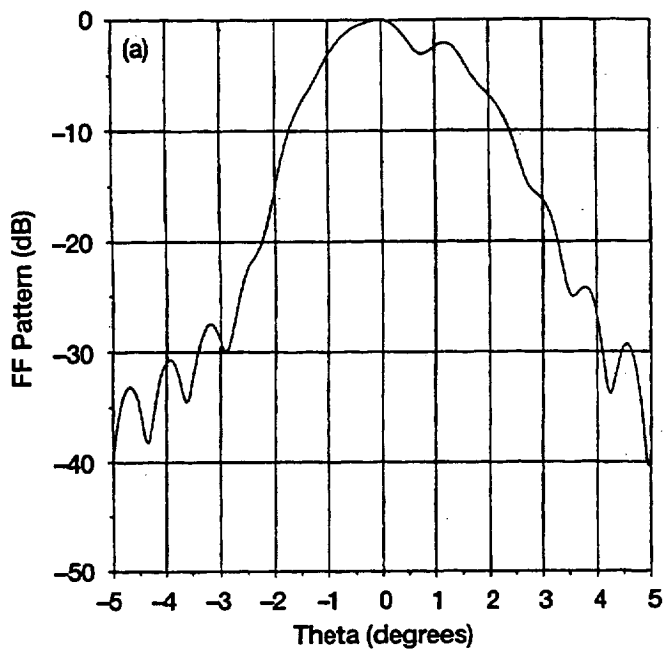


Figure 27.—Calculated far-field patterns of the 1.2 meter antenna at 19.44 GHz. Feed displaced 2.03 inch. (a) E-Plane. (b) H-Plane.

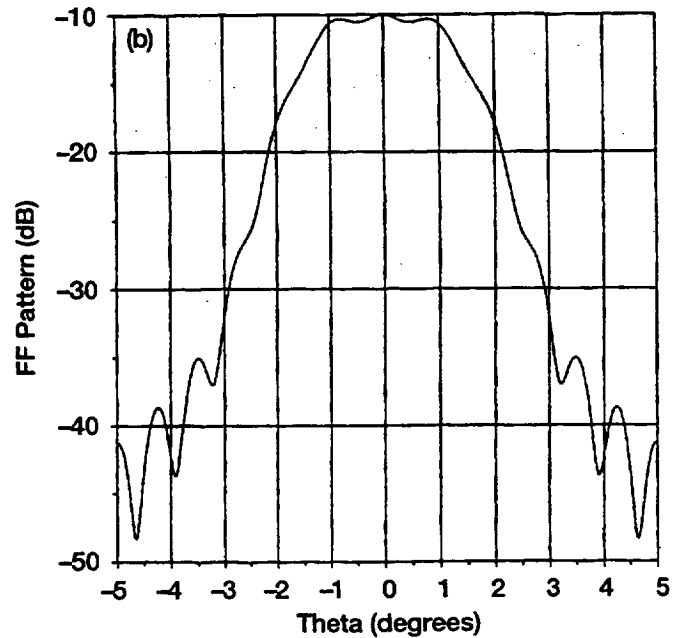
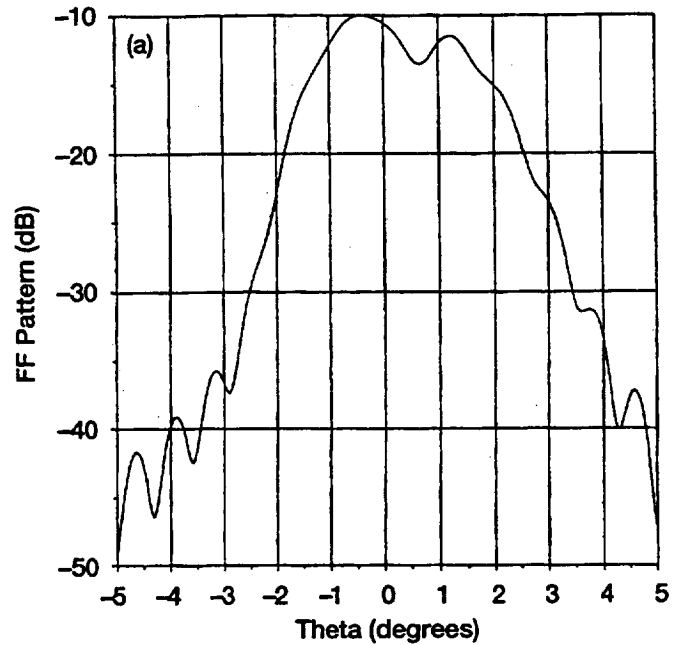


Figure 28.—Calculated far-field patterns of the 1.2 meter antenna at 19.44 GHz. Feed displaced 2.23 inch. (a) E-Plane. (b) H-Plane.

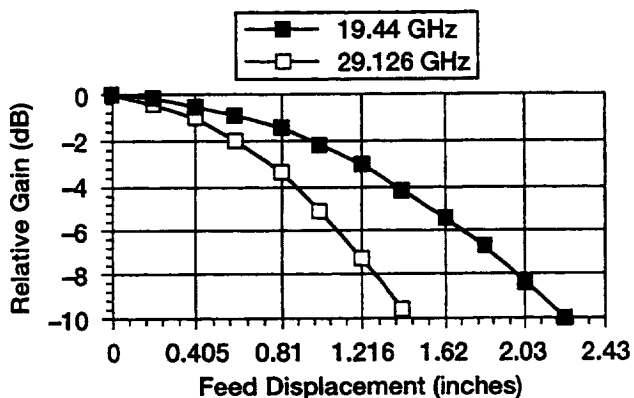


Figure 29.—Relative gain change of the 1.2 meter antenna as a function of feed displacement.

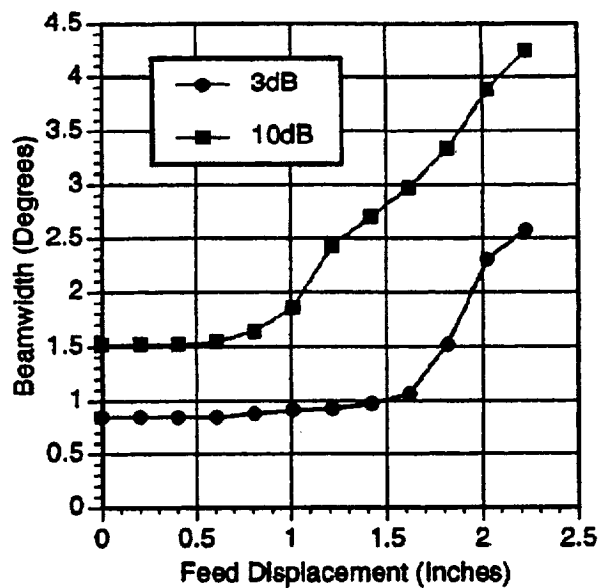


Figure 30.—Beamwidth of the 1.2 meter antenna as a function of feed displacement; 19.44 GHz.

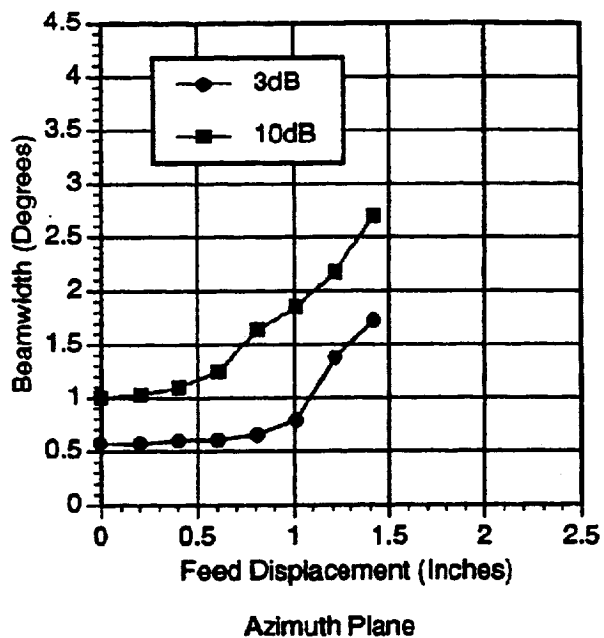


Figure 31.—Beamwidth of the 1.2 meter antenna as a function of feed displacement; 29.126 GHz.

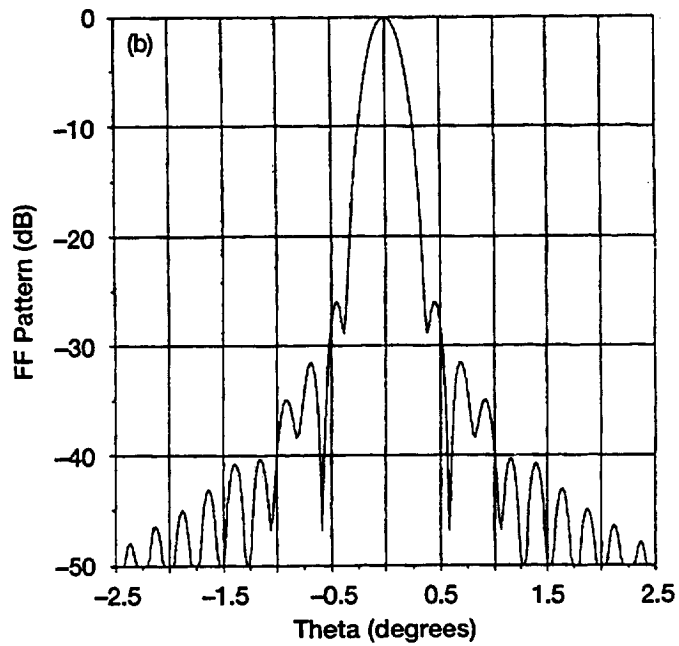
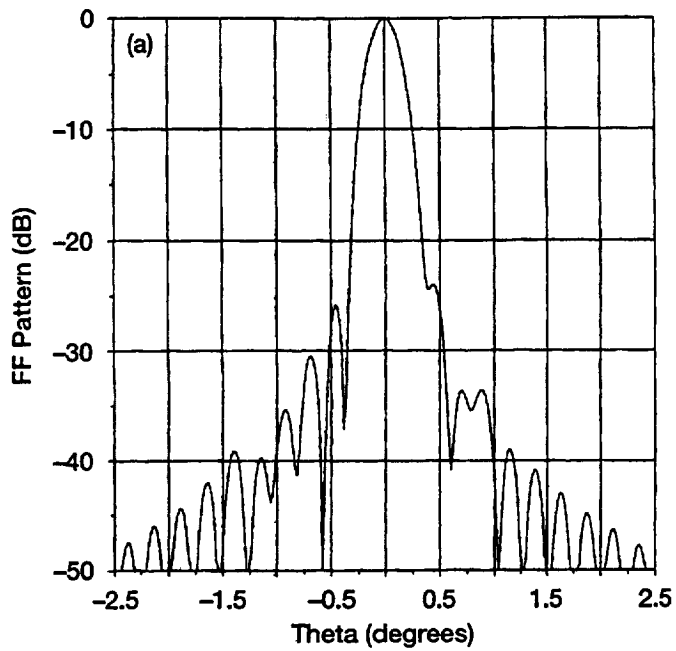


Figure 32.—Calculated far-field patterns of the 2.44 meter antenna at 29.126 GHz. Feed focussed. (a) E-Plane. (b) H-Plane.

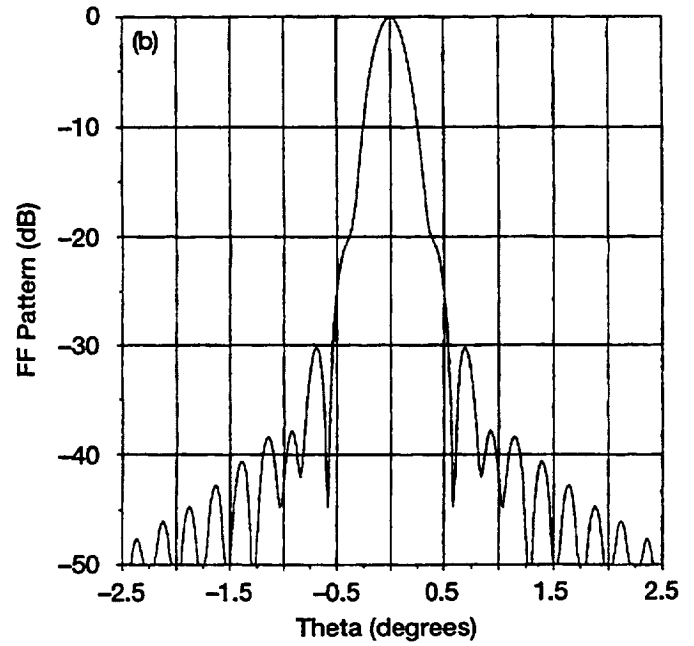
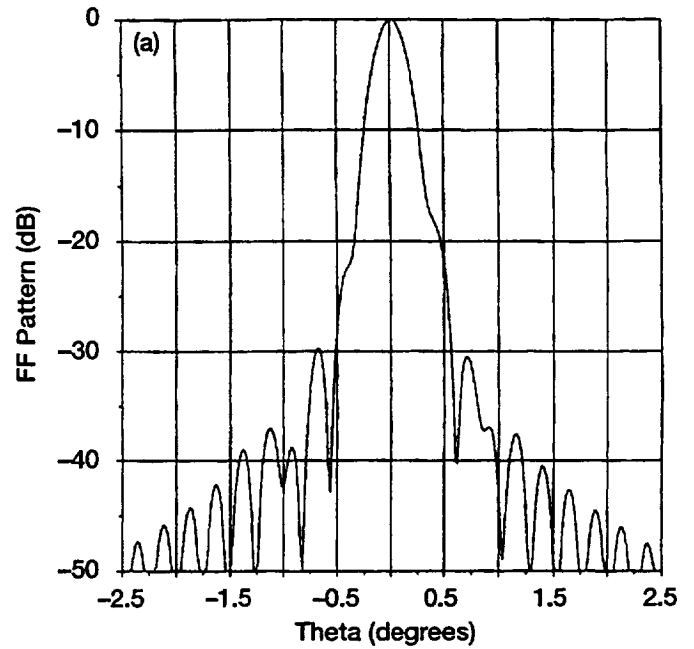


Figure 33.—Calculated far-field patterns of the 2.44 meter antenna at 29.126 GHz. Feed displaced 0.203 inch. (a) E-Plane. (b) H-Plane.

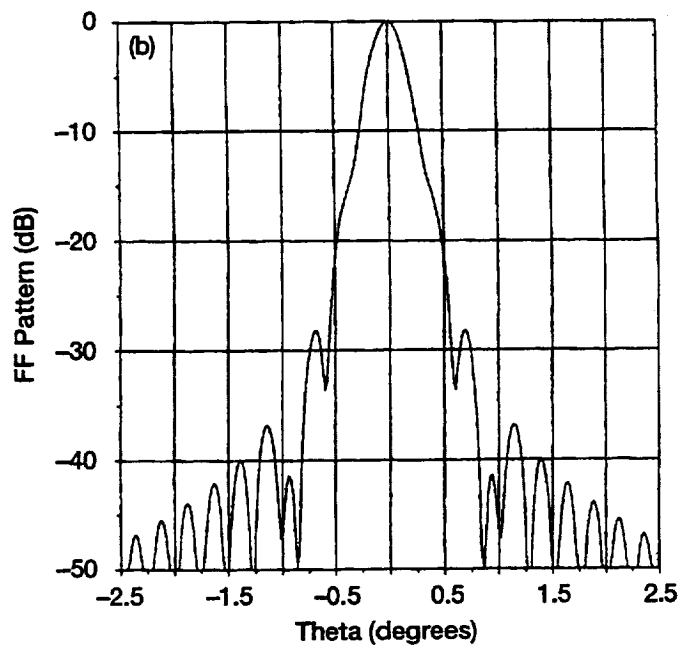
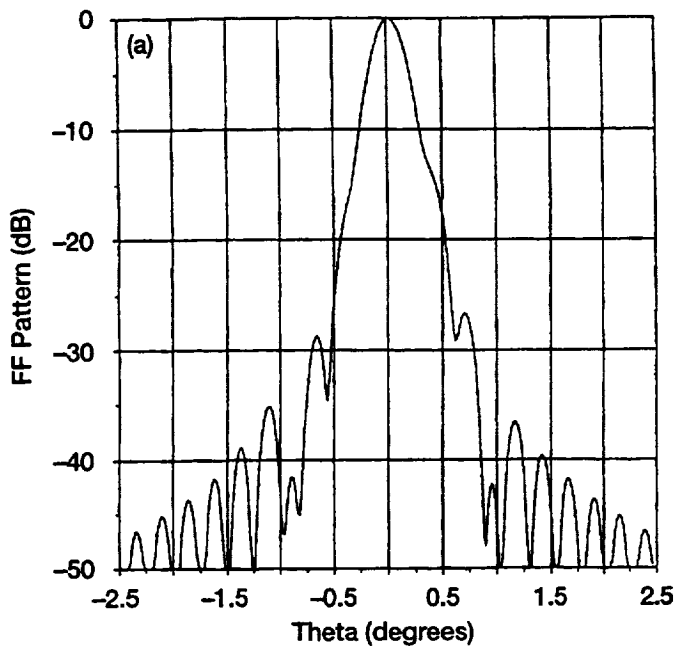


Figure 34.—Calculated far-field patterns of the 2.44 meter antenna at 29.126 GHz. Feed displaced 0.405 inch. (a) E-Plane. (b) H-Plane.

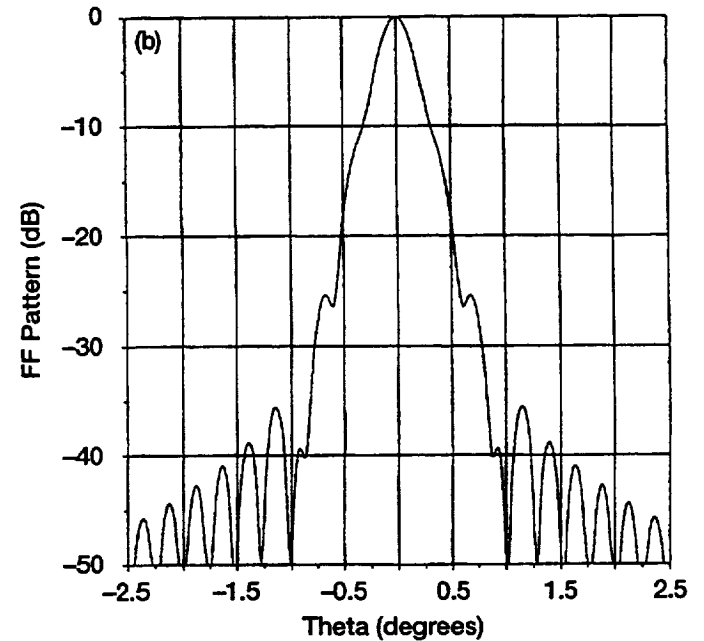
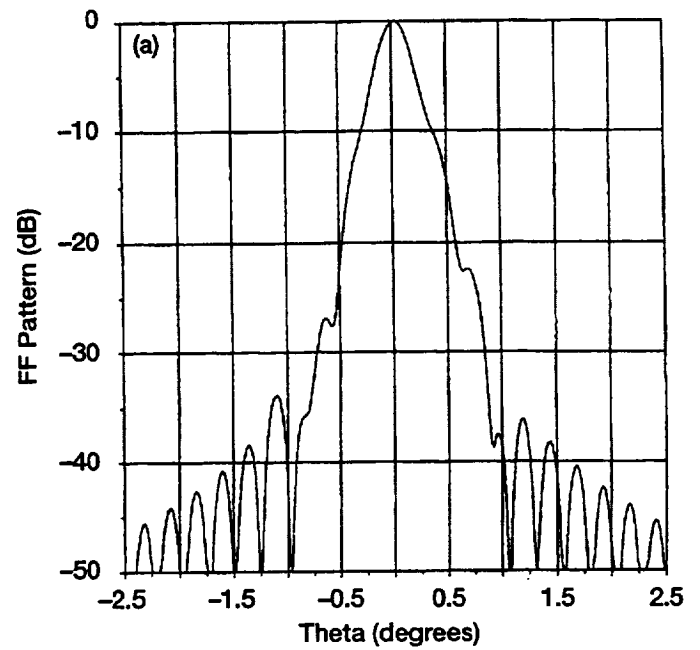


Figure 35.—Calculated far-field patterns of the 2.44 meter antenna at 29.126 GHz. Feed displaced 0.608 inch. (a) E-Plane. (b) H-Plane.

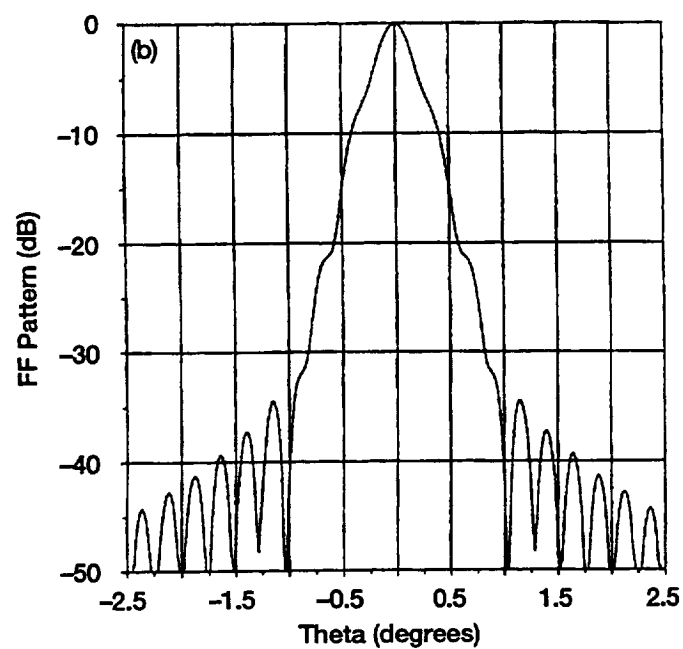
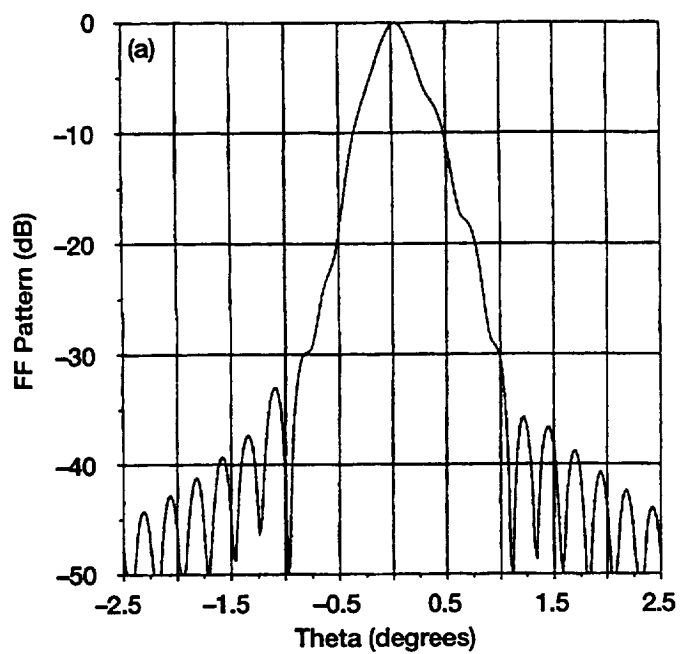


Figure 36.—Calculated far-field patterns of the 2.44 meter antenna at 29.126 GHz. Feed displaced 0.810 inch. (a) E-Plane. (b) H-Plane.

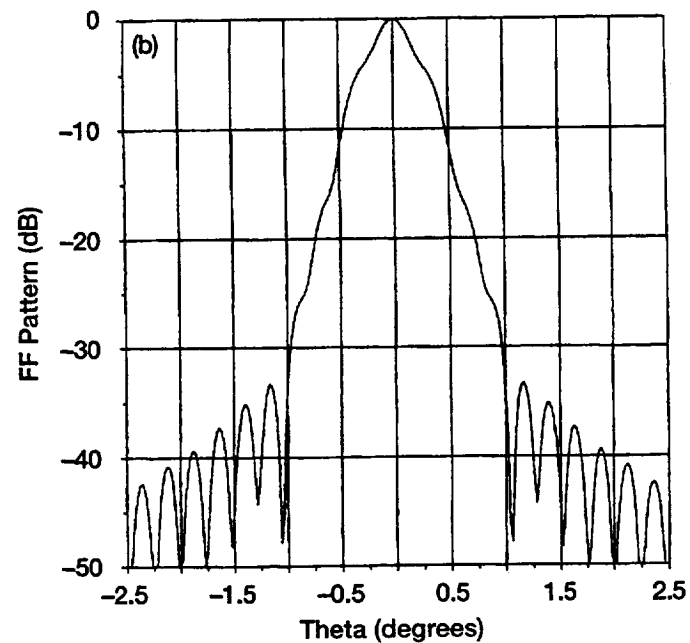
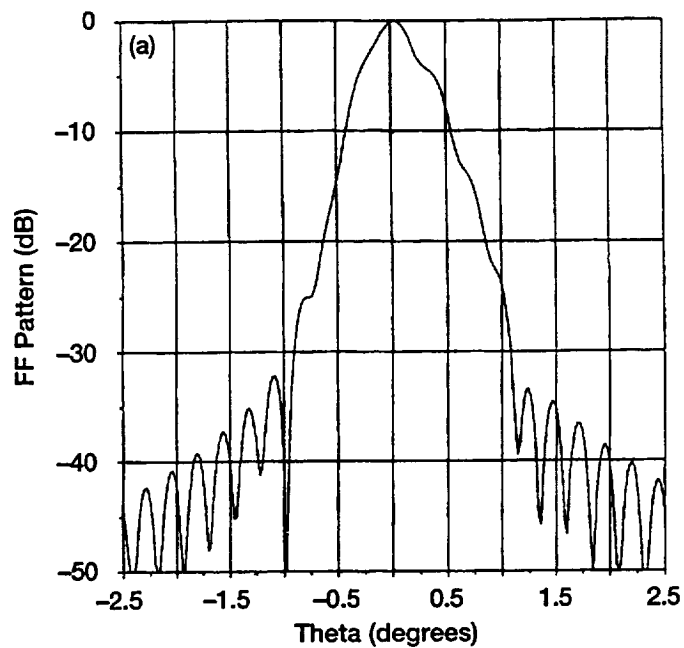


Figure 37.—Calculated far-field patterns of the 2.44 meter antenna at 29.126 GHz. Feed displaced 1.01 inch. (a) E-Plane. (b) H-Plane.

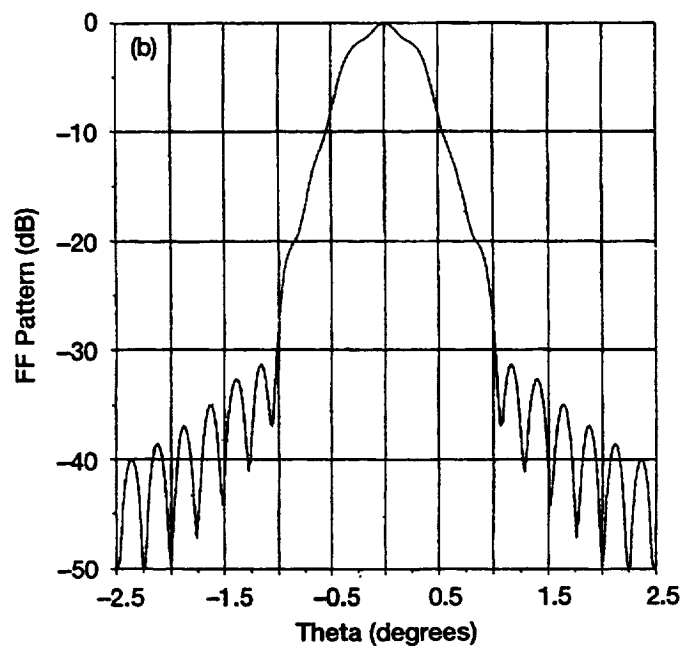
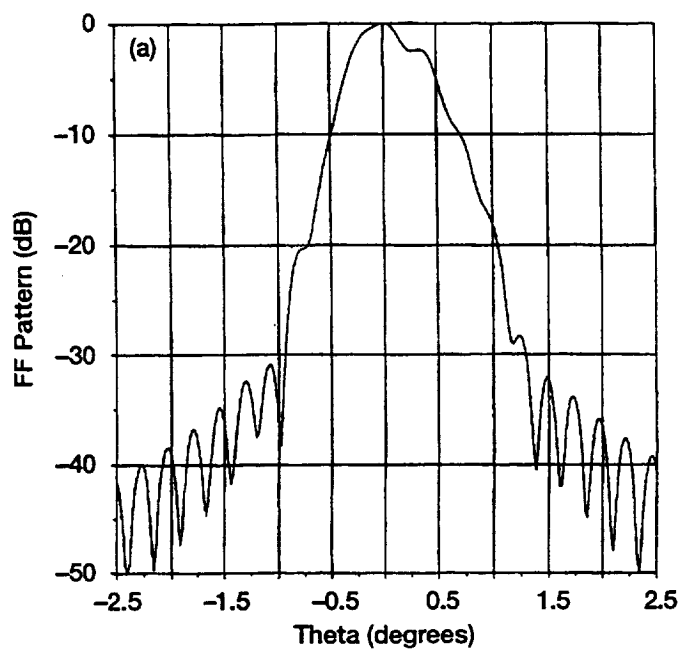


Figure 38.—Calculated far-field patterns of the 2.44 meter antenna at 29.126 GHz. Feed displaced 2.4416 inch. (a) E-Plane. (b) H-Plane.

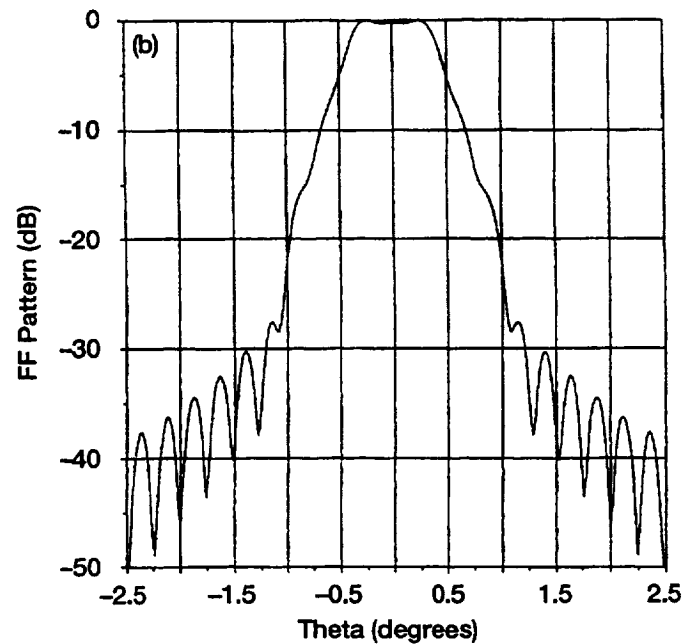
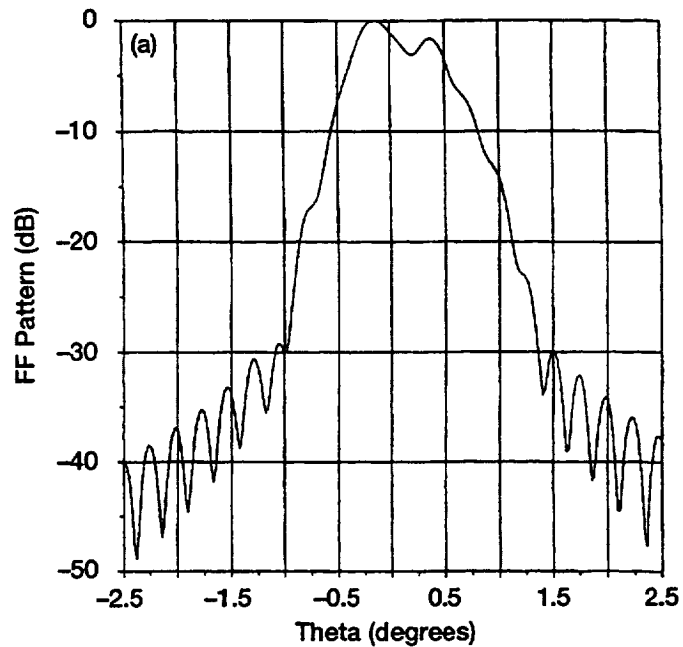


Figure 39.—Calculated far-field patterns of the 2.44 meter antenna at 29.126 GHz. Feed displaced 1.42 inch. (a) E-Plane. (b) H-Plane.

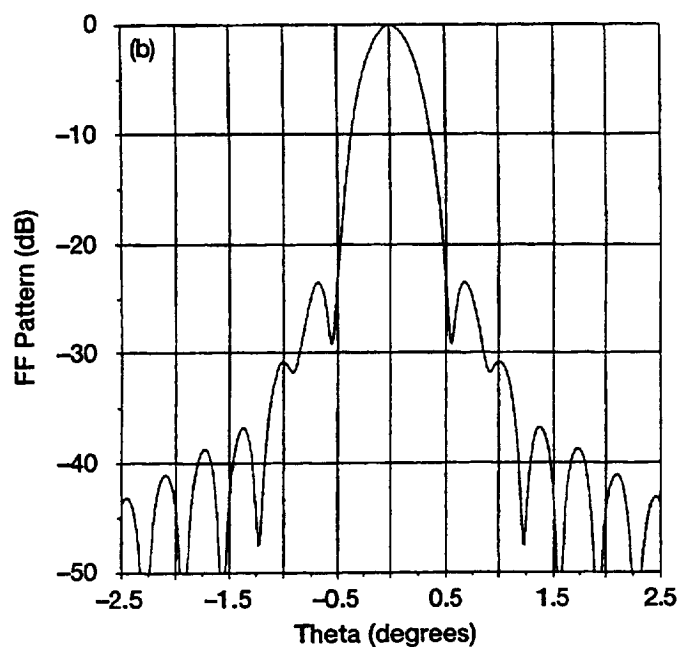
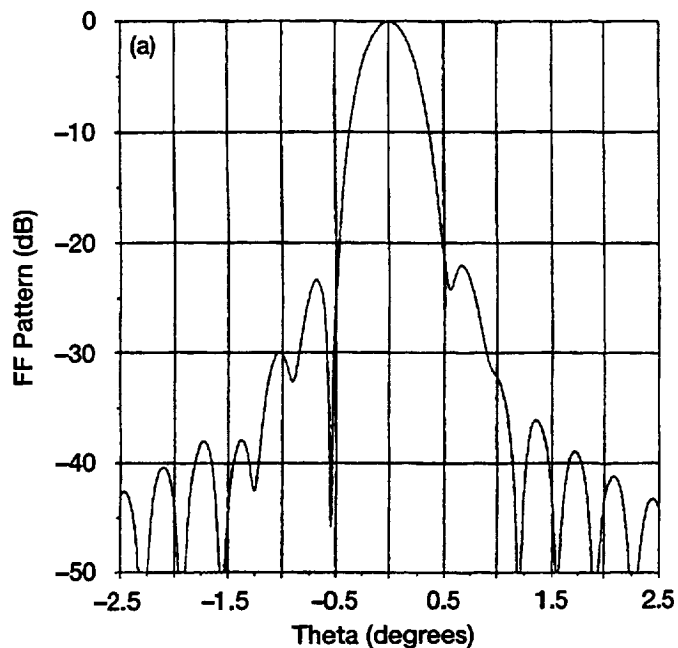


Figure 40.—Calculated far-field patterns of the 2.44 meter antenna at 19.44 GHz. Feed focussed. (a) E-Plane. (b) H-Plane.

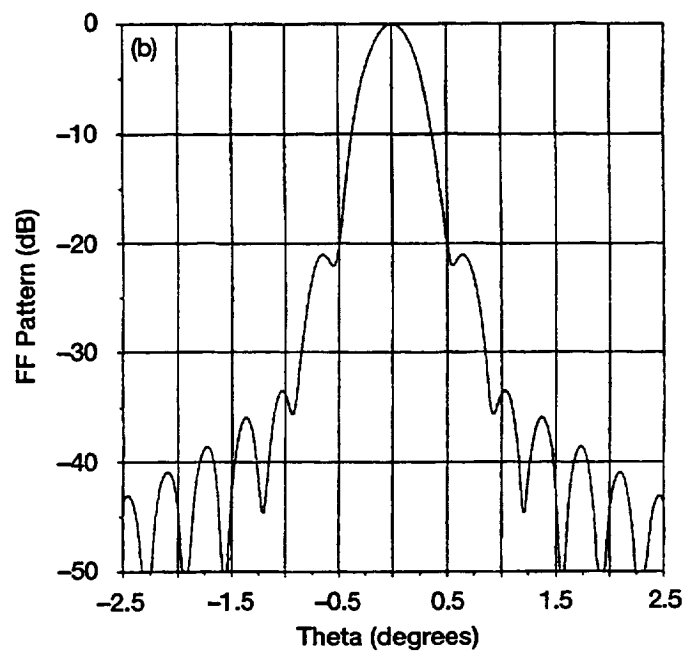
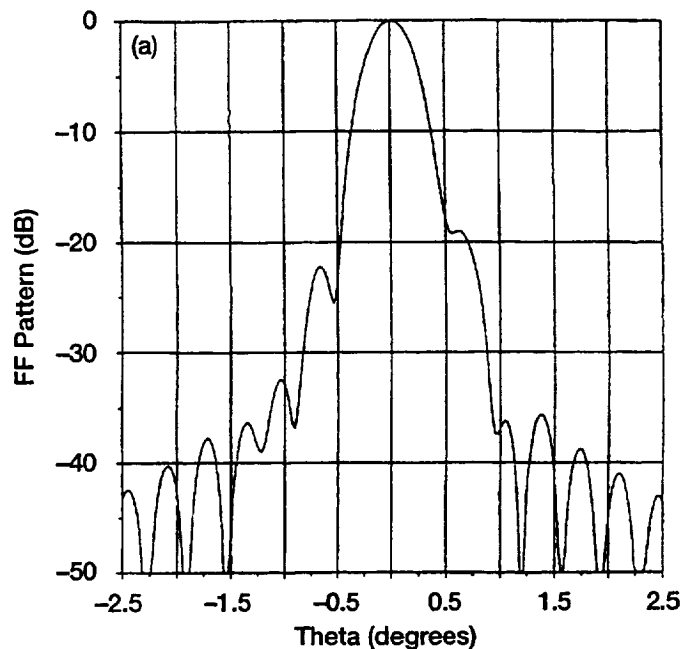


Figure 41.—Calculated far-field patterns of the 2.44 meter antenna at 19.44 GHz. Feed displaced 0.203 inch. (a) E-Plane. (b) H-Plane.

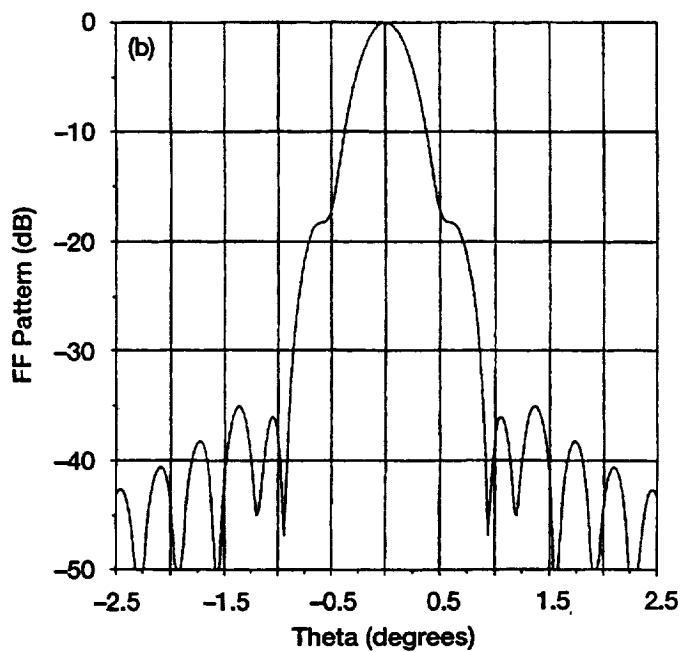
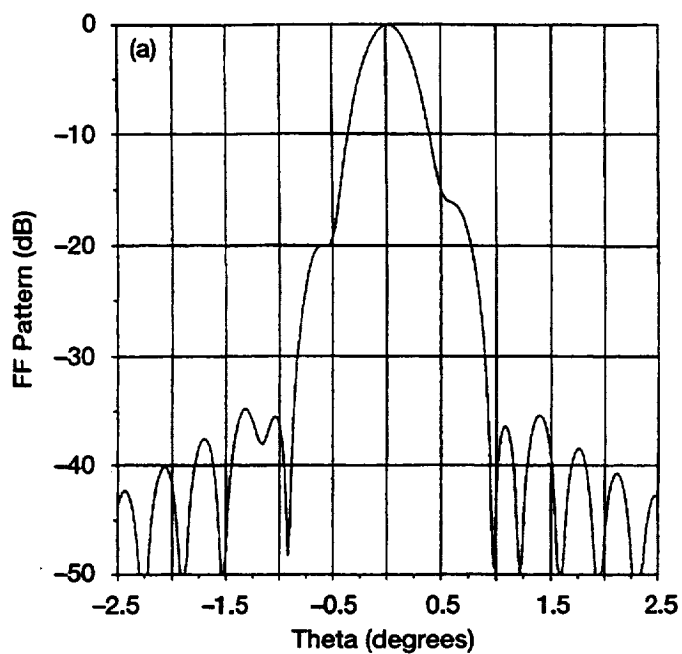


Figure 42.—Calculated far-field patterns of the 2.44 meter antenna at 19.44 GHz. Feed displaced 0.405 inch. (a) E-Plane. (b) H-Plane.

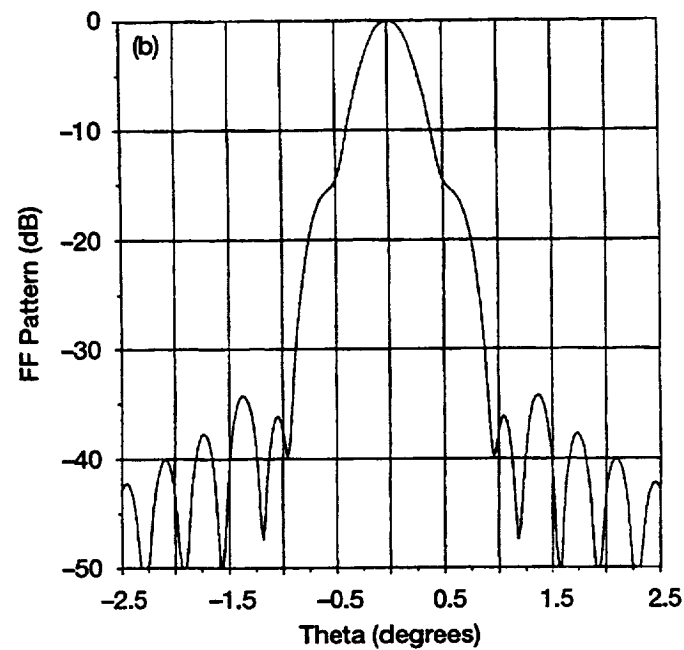
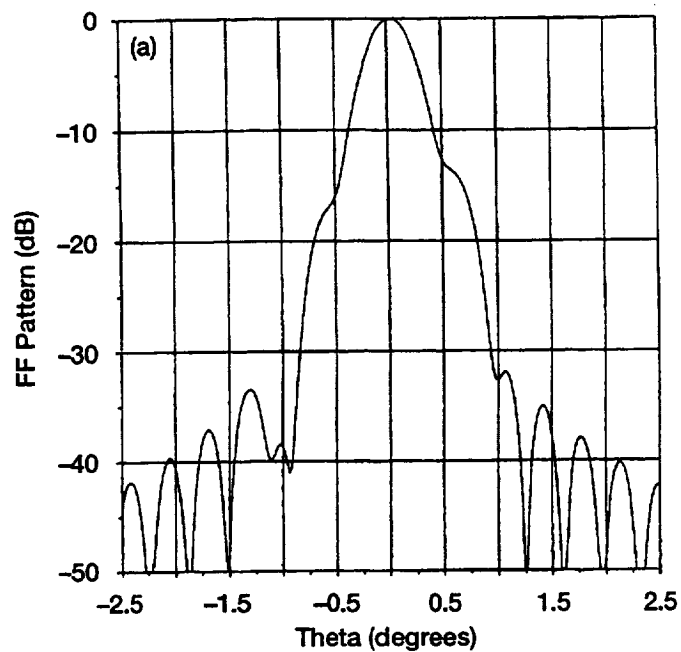


Figure 43.—Calculated far-field patterns of the 2.44 meter antenna at 19.44 GHz. Feed displaced 0.608 inch. (a) E-Plane. (b) H-Plane.

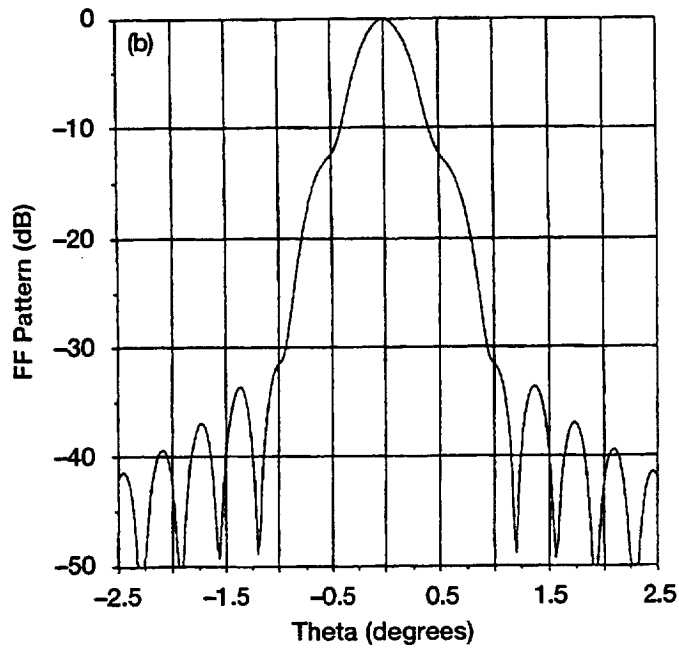
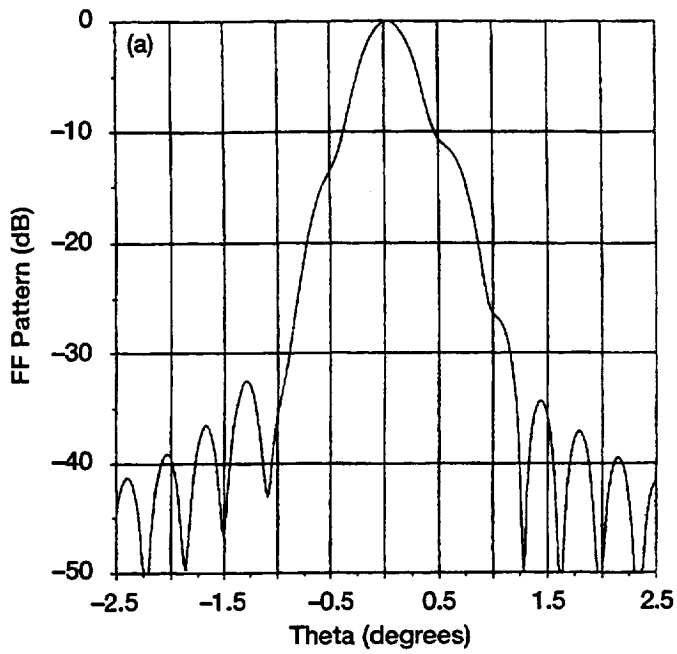


Figure 44.—Calculated far-field patterns of the 2.44 meter antenna at 19.44 GHz. Feed displaced 0.810 inch. (a) E-Plane. (b) H-Plane.

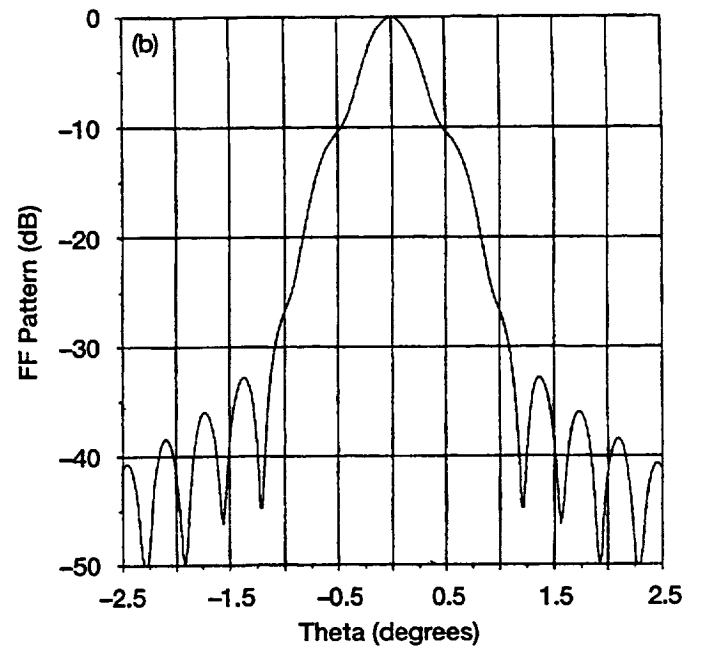
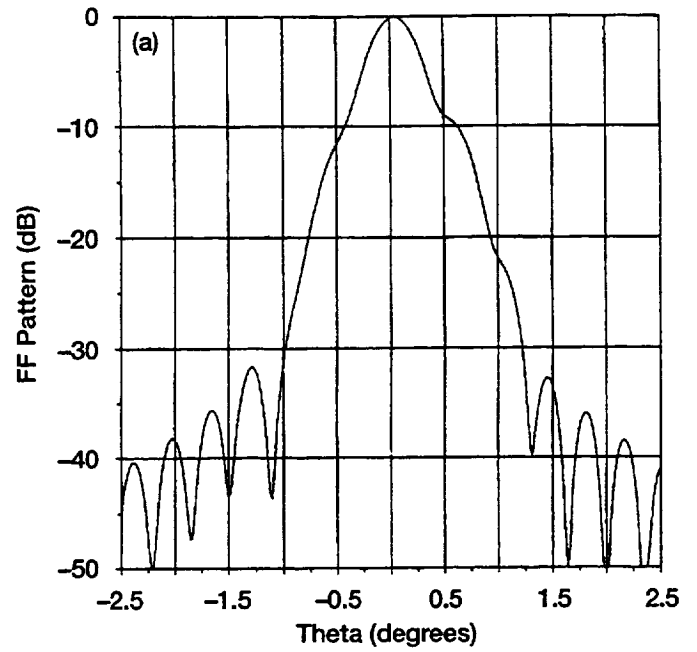


Figure 45.—Calculated far-field patterns of the 2.44 meter antenna at 19.44 GHz. Feed displaced 1.01 inch. (a) E-Plane. (b) H-Plane.

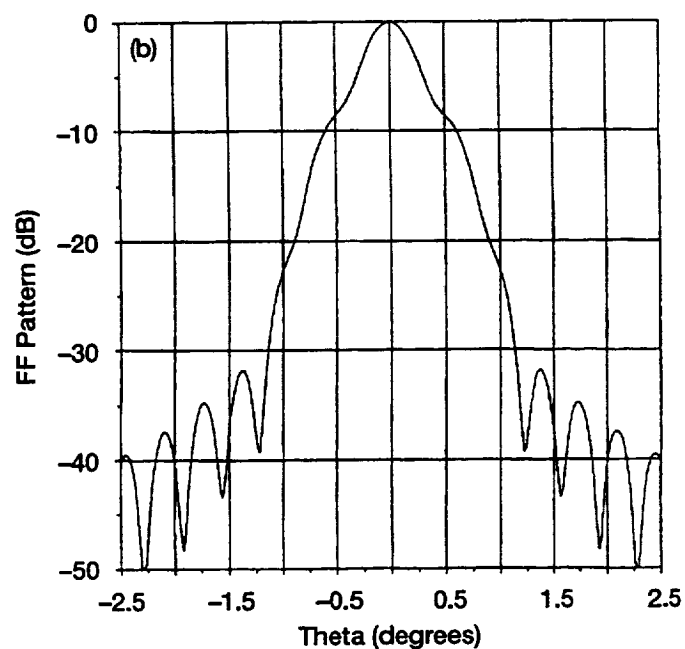
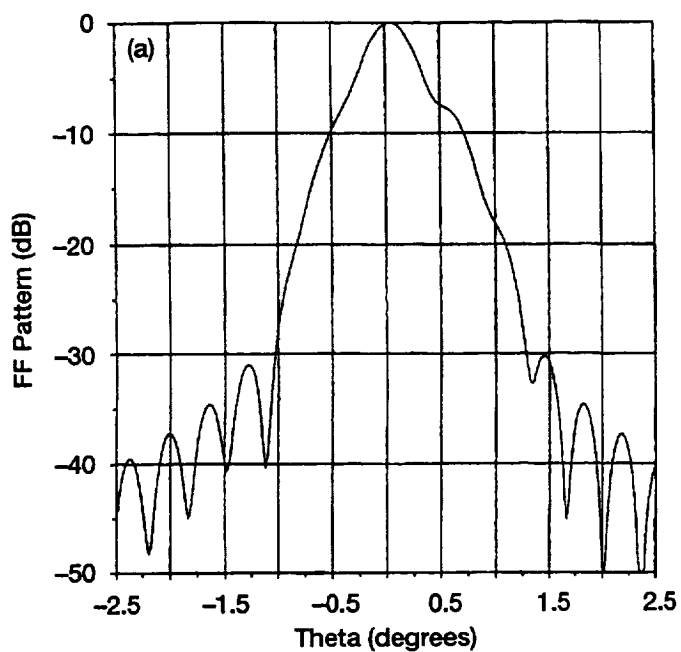


Figure 46.—Calculated far-field patterns of the 2.44 meter antenna at 19.44 GHz. Feed displaced 2.4416 inch. (a) E-Plane. (b) H-Plane.

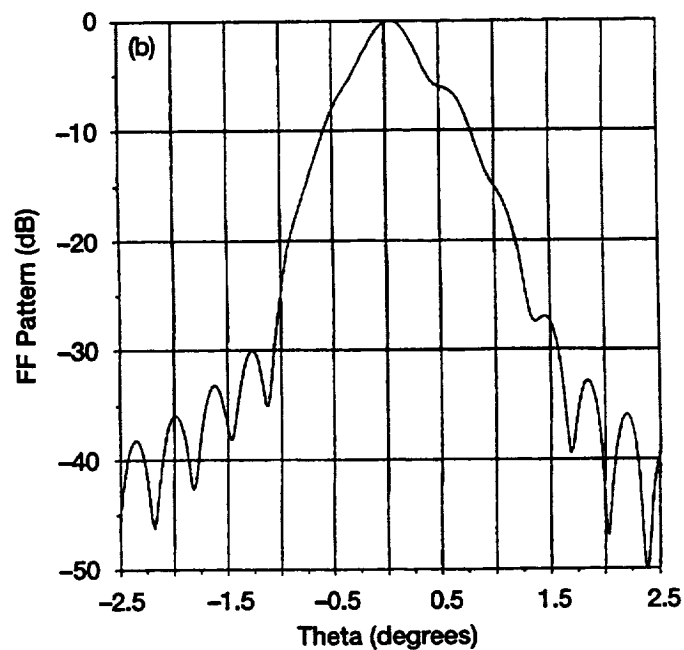
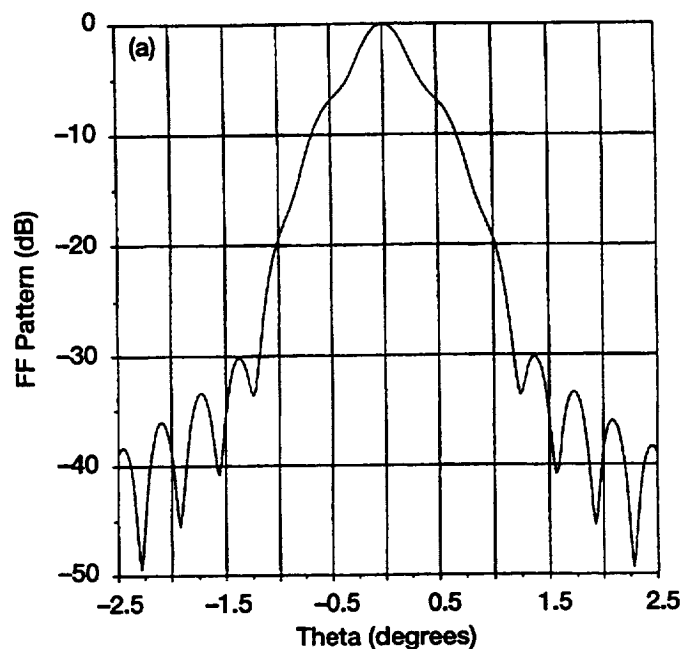


Figure 47.—Calculated far-field patterns of the 2.44 meter antenna at 19.44 GHz. Feed displaced 1.42 inch. (a) E-Plane. (b) H-Plane.

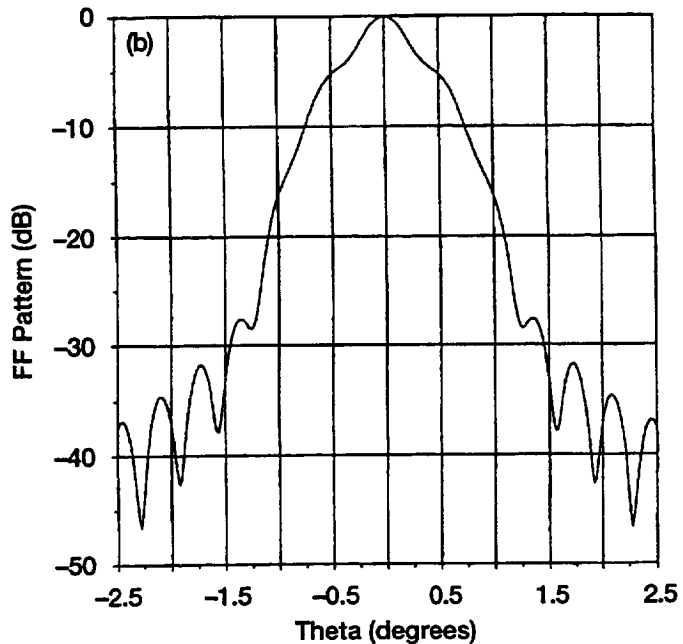
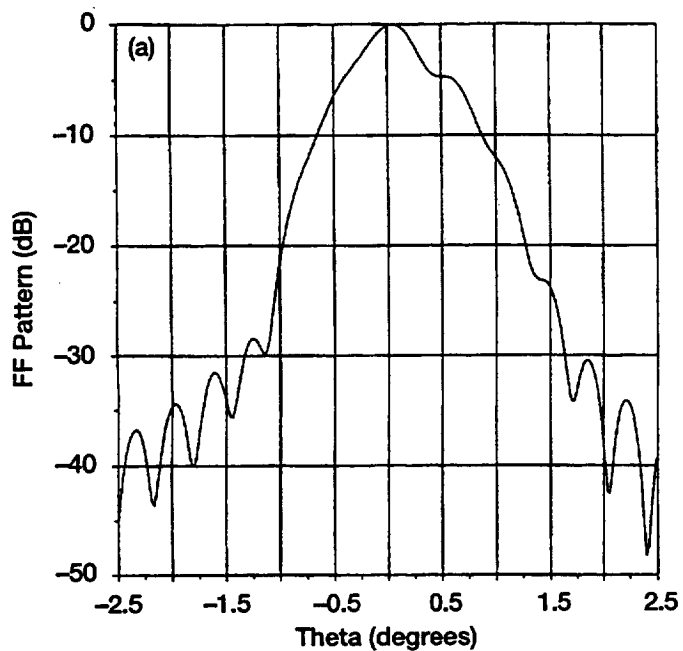


Figure 48.—Calculated far-field patterns of the 2.44 meter antenna at 19.44 GHz. Feed displaced 1.62 inch. (a) E-Plane. (b) H-Plane.

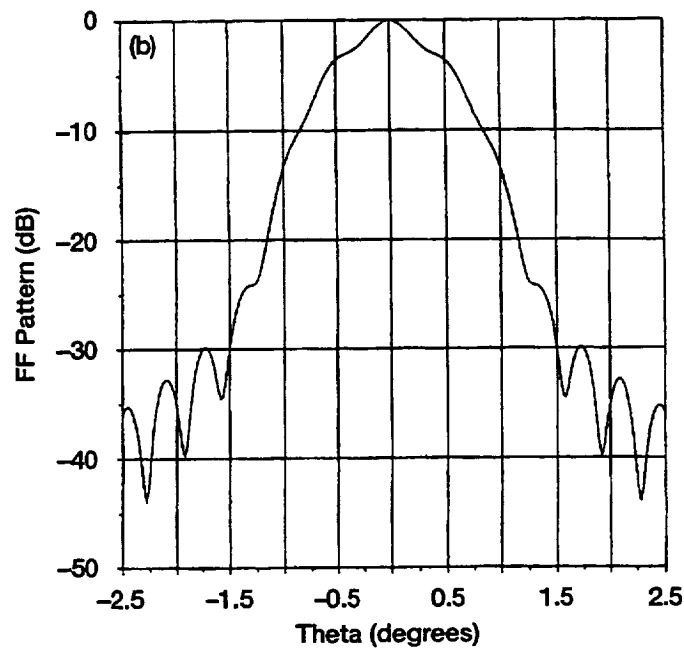
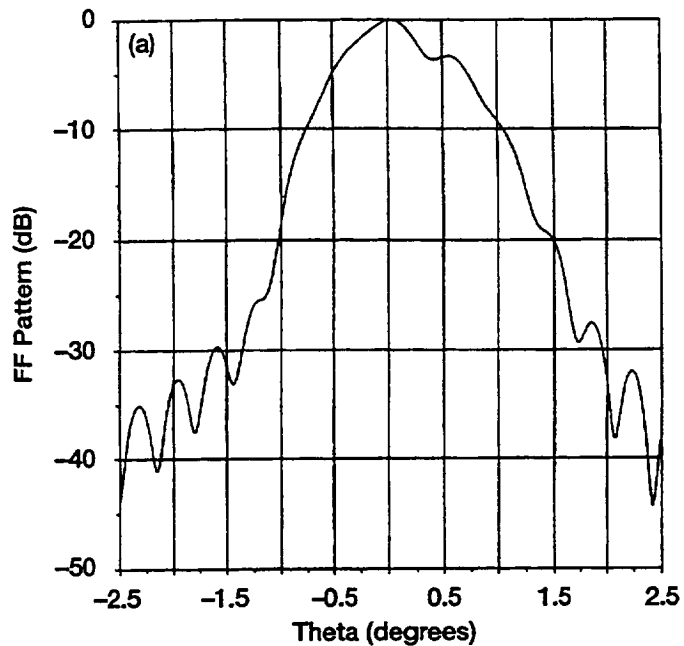


Figure 49.—Calculated far-field patterns of the 2.44 meter antenna at 19.44 GHz. Feed displaced 1.83 inch. (a) E-Plane. (b) H-Plane.

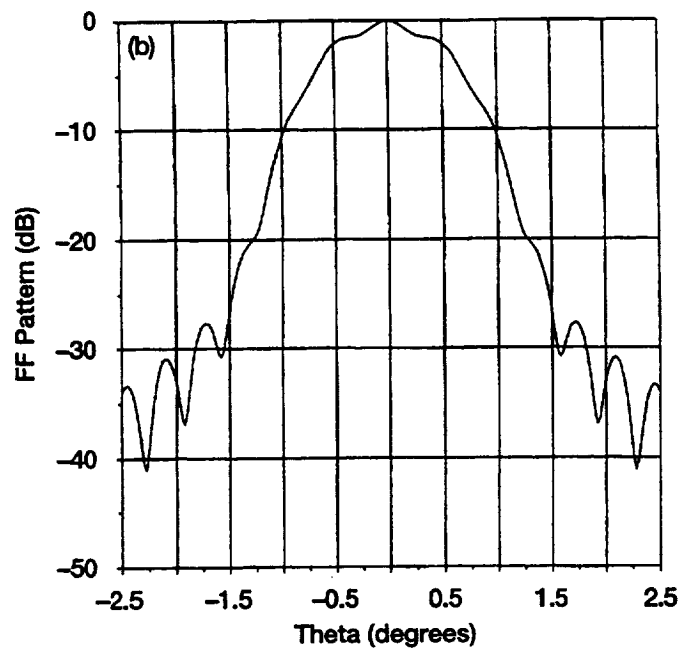
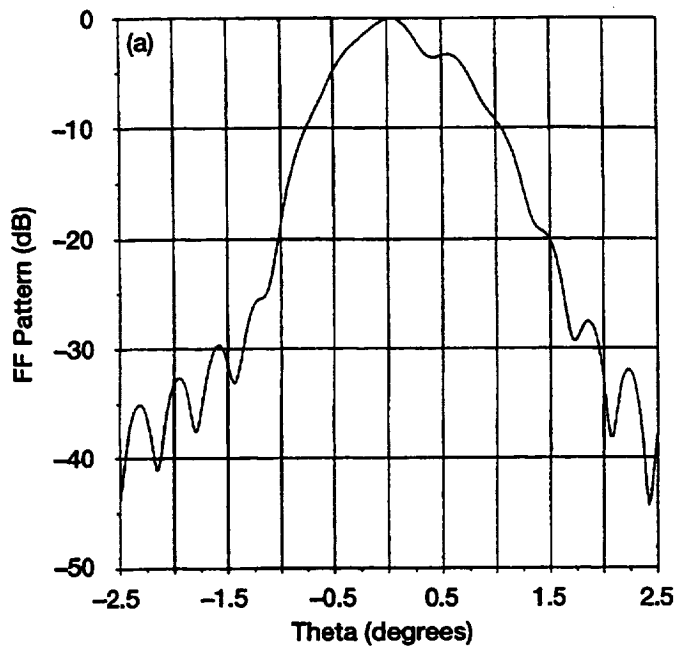


Figure 50.—Calculated far-field patterns of the 2.44 meter antenna at 19.44 GHz. Feed displaced 2.03 inch. (a) E-Plane. (b) H-Plane.

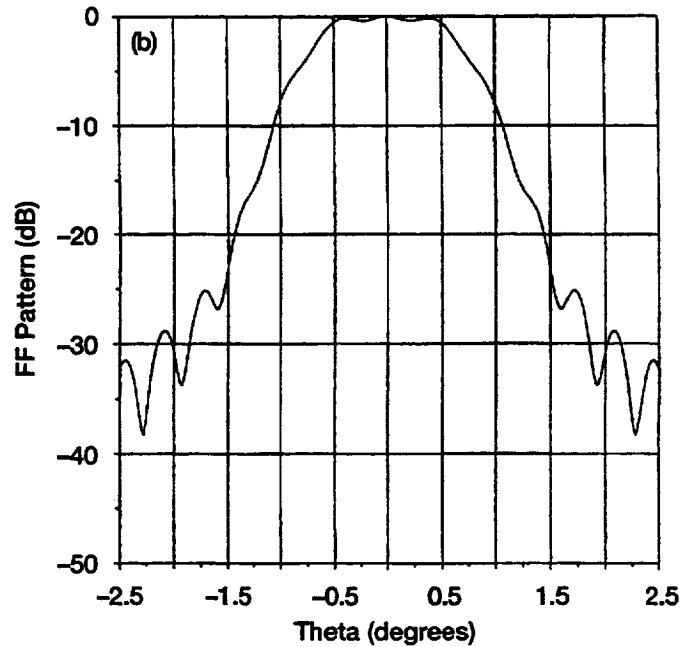
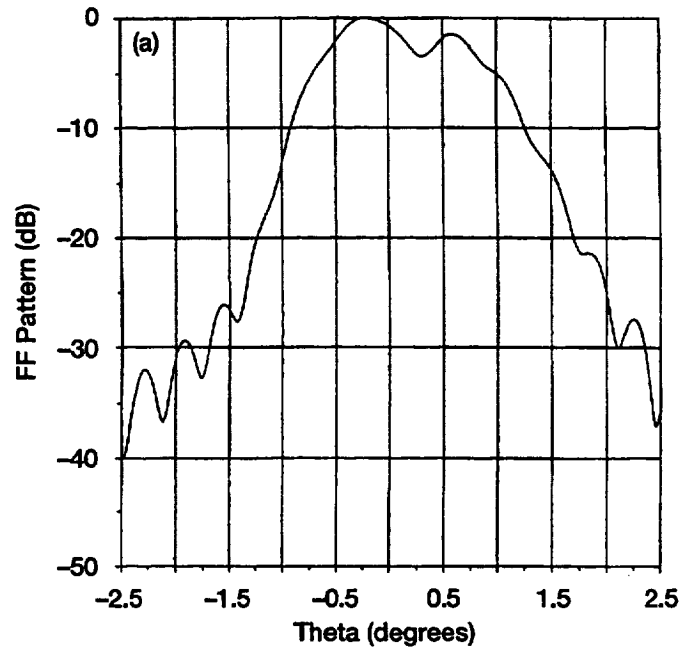


Figure 51.—Calculated far-field patterns of the 2.44 meter antenna at 19.44 GHz. Feed displaced 2.23 inch. (a) E-Plane. (b) H-Plane.

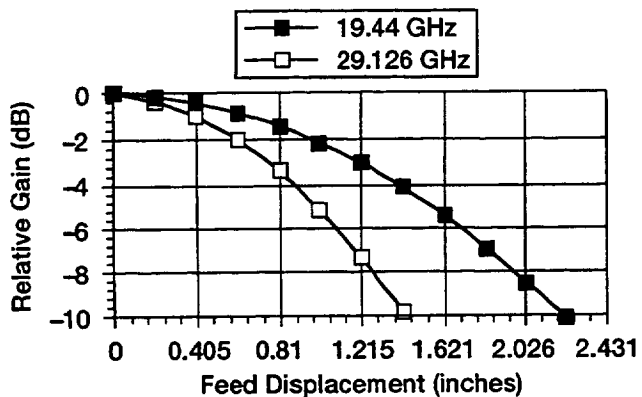


Figure 52.—Relative gain change of the 2.44 meter antenna as a function of feed displacement.

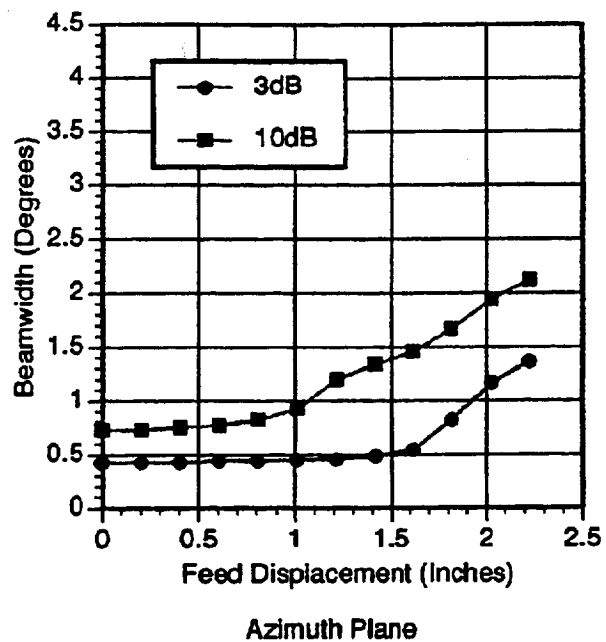


Figure 53.—Beamwidth of the 2.44 meter antenna as a function of feed displacement; 19.44 GHz.

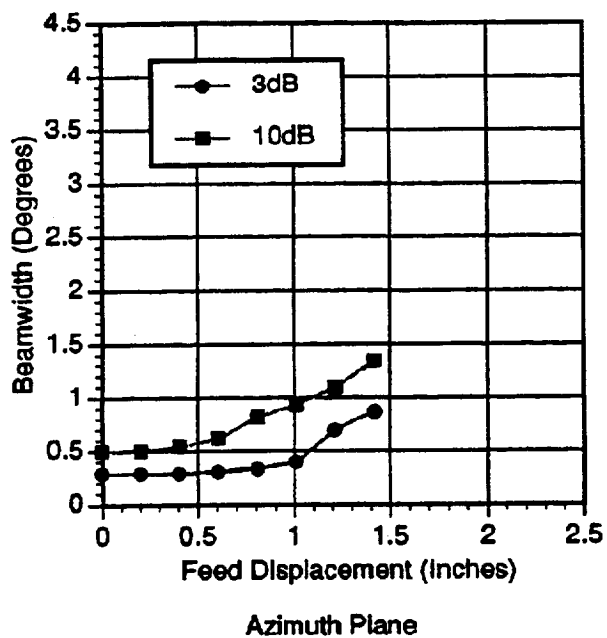


Figure 54.—Beamwidth of the 2.44 meter antenna as a function of feed displacement; 29.126 GHz.

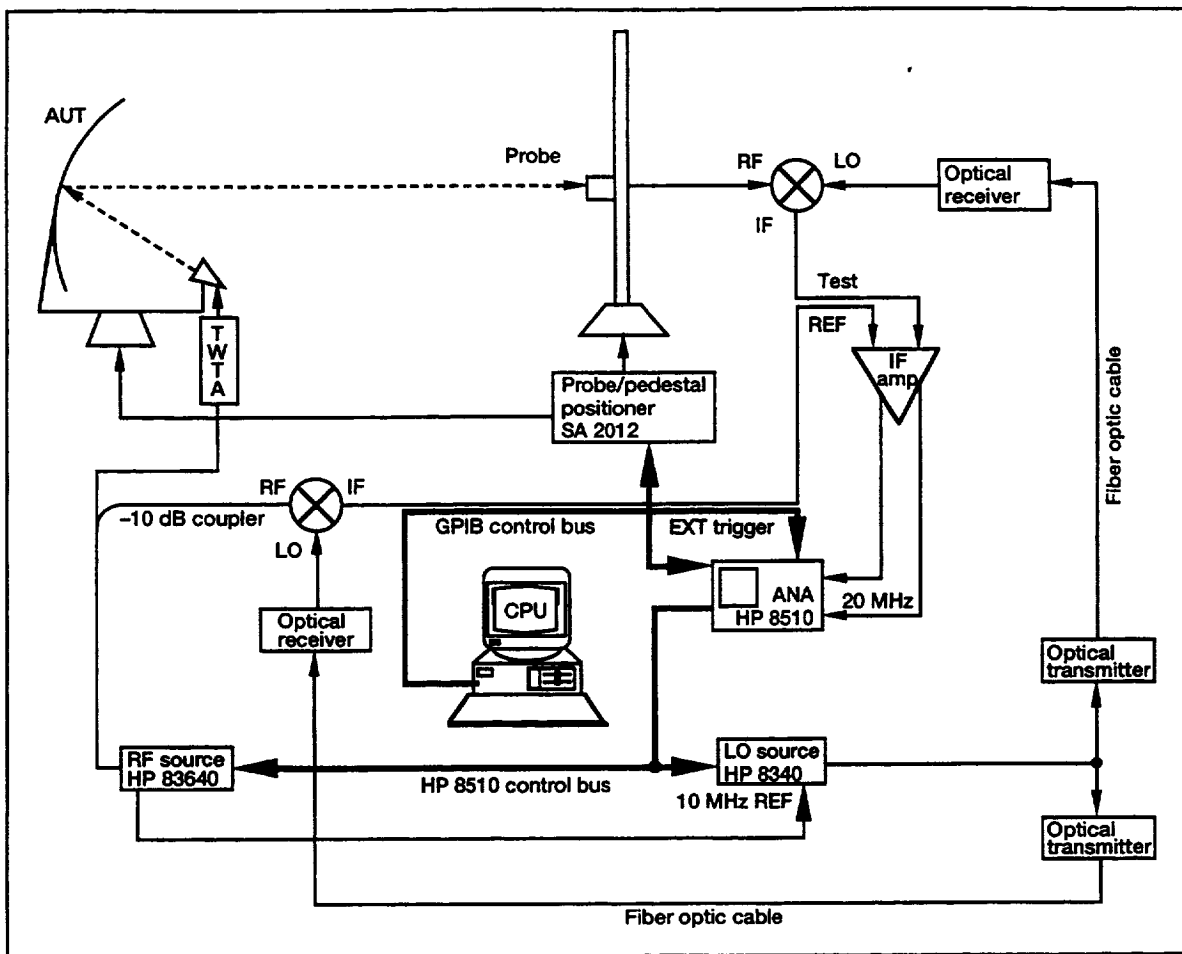


Figure 55.—Near field antenna test facility configuration.

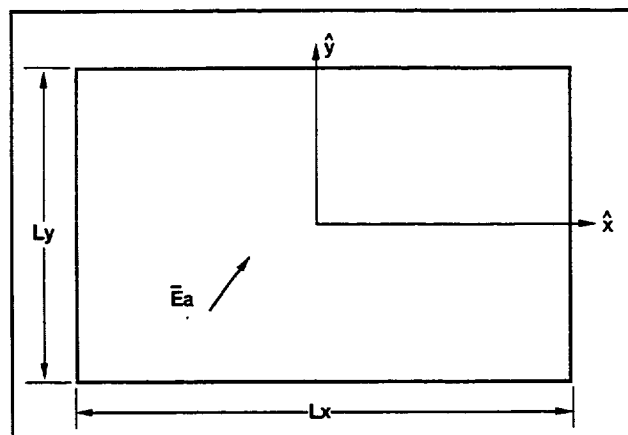


Figure 56.—Scan plane surface (Sa).

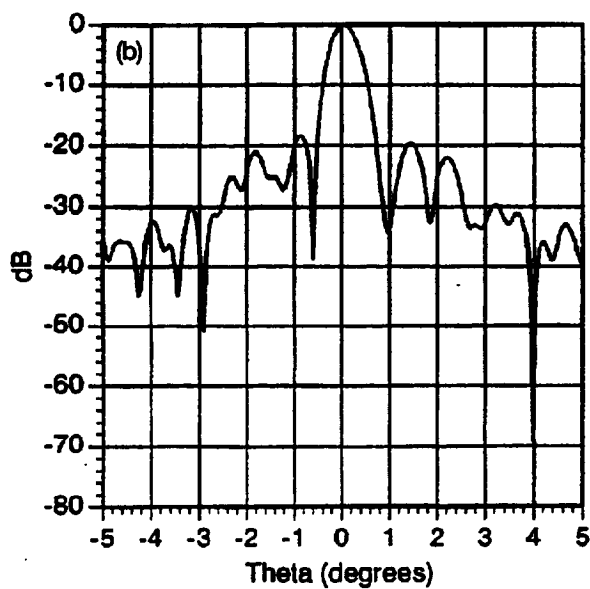
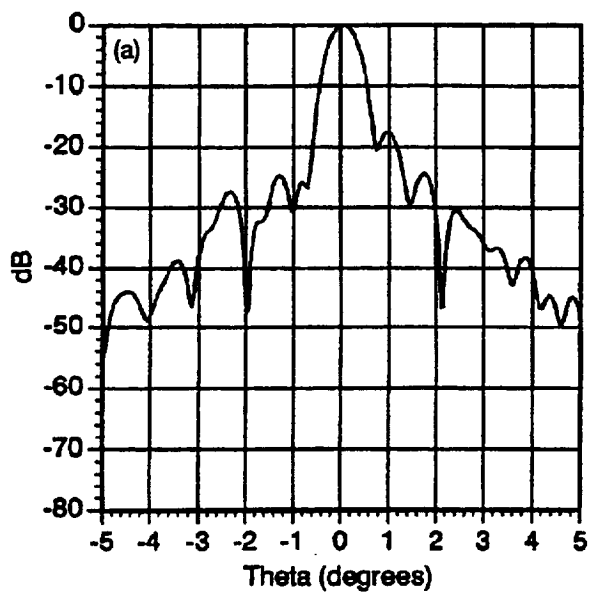


Figure 57.—Measured far-field patterns of the 1.2 meter antenna at 29.126 GHz. Feed displaced focussed. (a) E-Plane. (b) H-Plane.

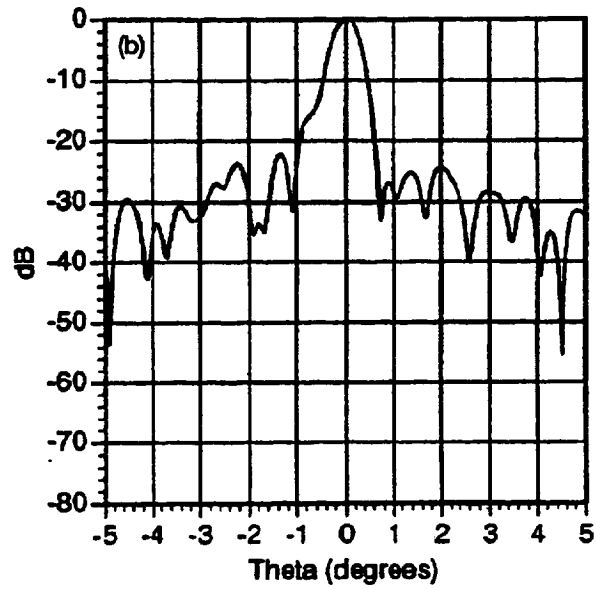
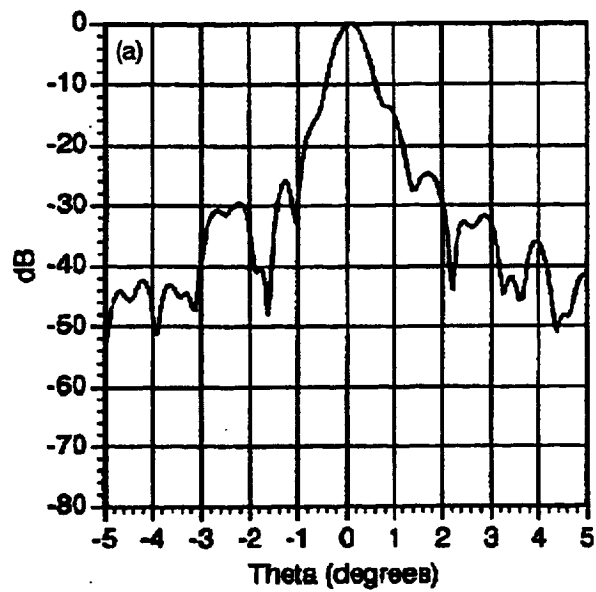


Figure 58.—Measured far-field patterns of the 1.2 meter antenna at 29.126 GHz. Feed displaced 0.41 inches. (a) E-Plane. (b) H-Plane.

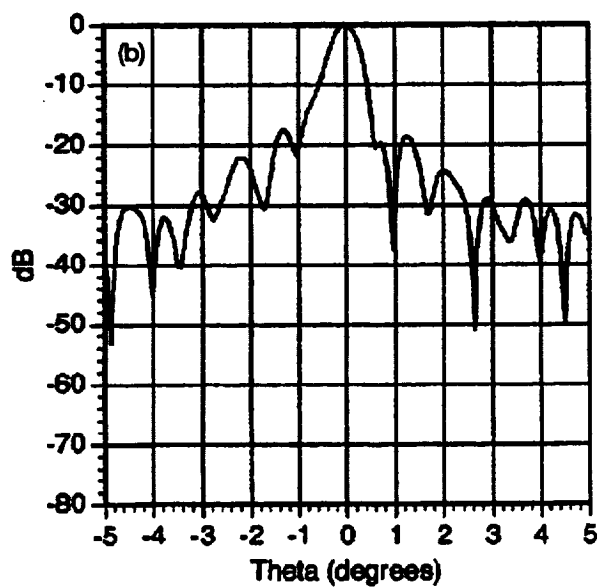
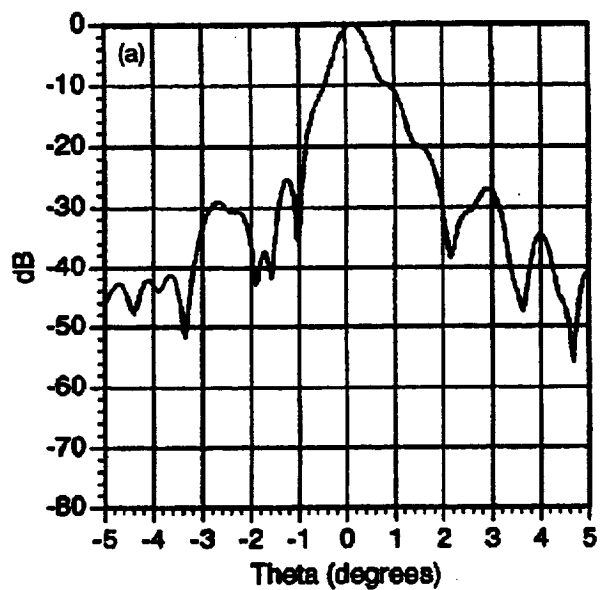


Figure 59.—Measured far-field patterns of the 1.2 meter antenna at 29.126 GHz. Feed displaced 0.60 inches. (a) E-Plane. (b) H-Plane.

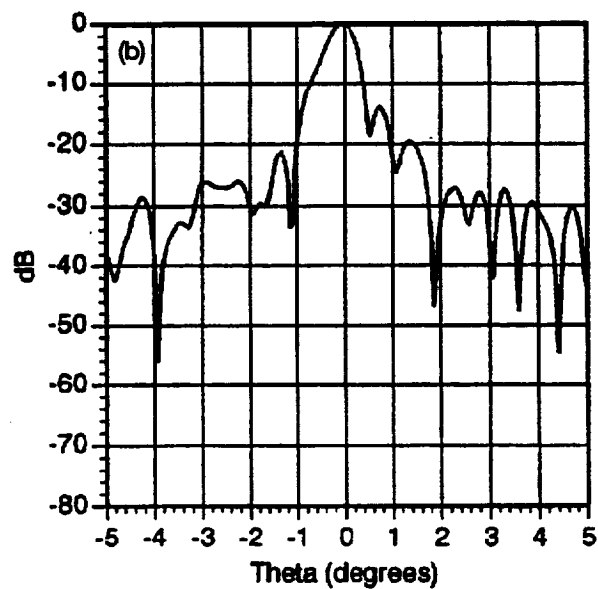
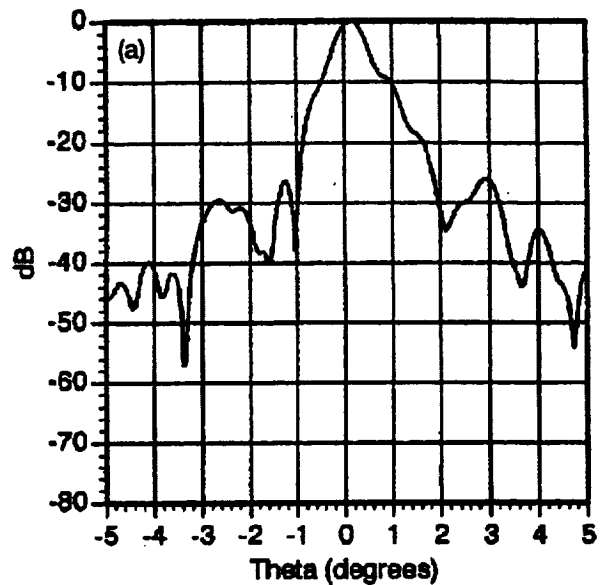


Figure 60.—Measured far-field patterns of the 1.2 meter antenna at 29.126 GHz. Feed displaced 0.74 inches. (a) E-Plane. (b) H-Plane.

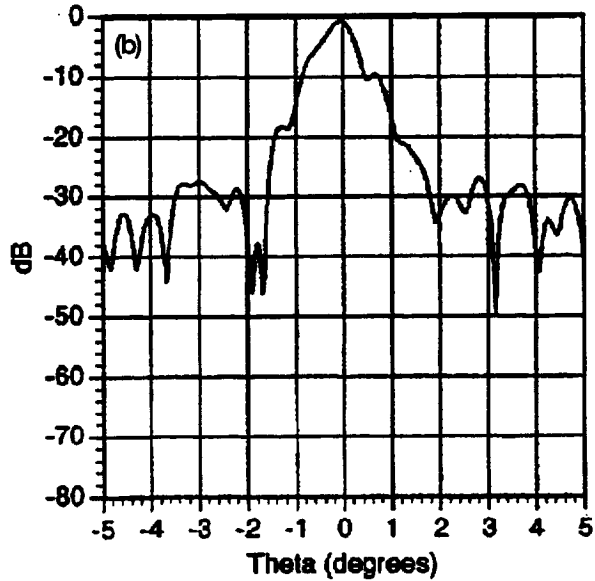
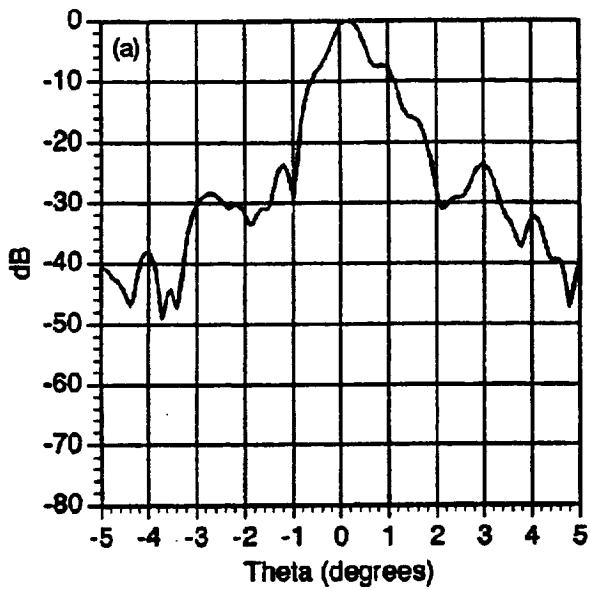


Figure 61.—Measured far-field patterns of the 1.2 meter antenna at 29.126 GHz. Feed displaced 0.87 inches. (a) E-Plane. (b) H-Plane.

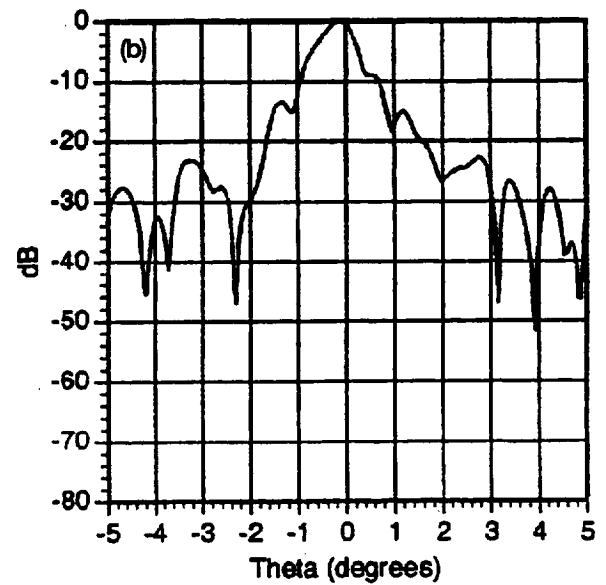
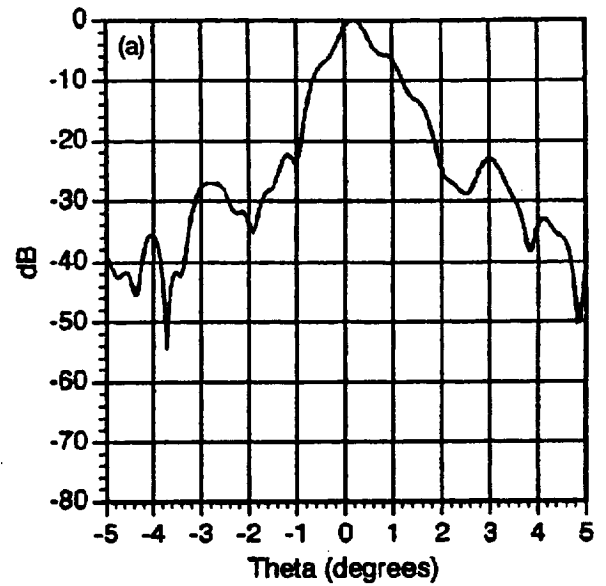


Figure 62.—Measured far-field patterns of the 1.2 meter antenna at 29.126 GHz. Feed displaced 0.99 inches. (a) E-Plane. (b) H-Plane.

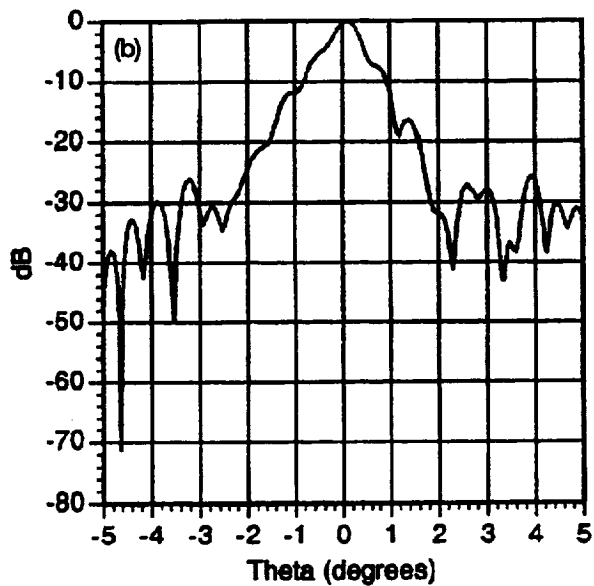
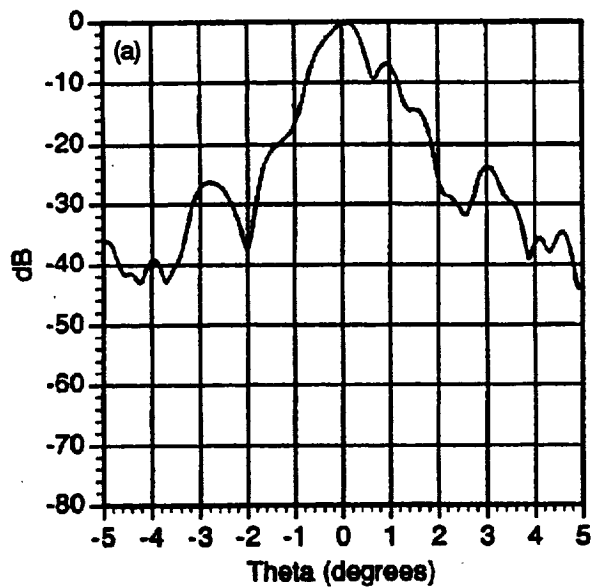


Figure 63.—Measured far-field patterns of the 1.2 meter antenna at 29.126 GHz. Feed displaced 1.09 inches. (a) E-Plane. (b) H-Plane.

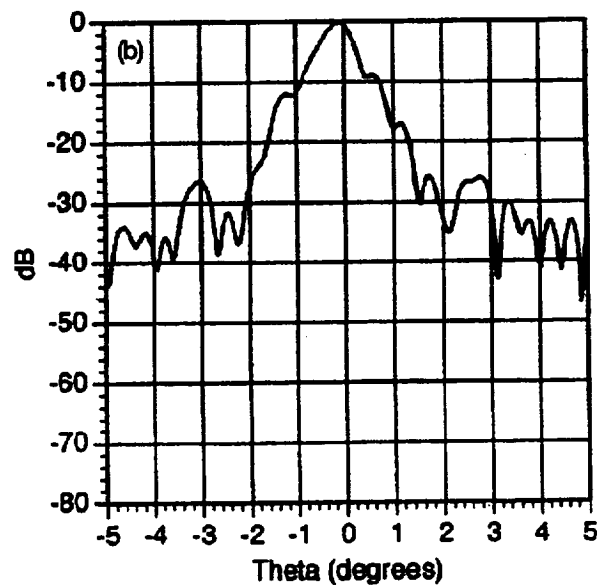
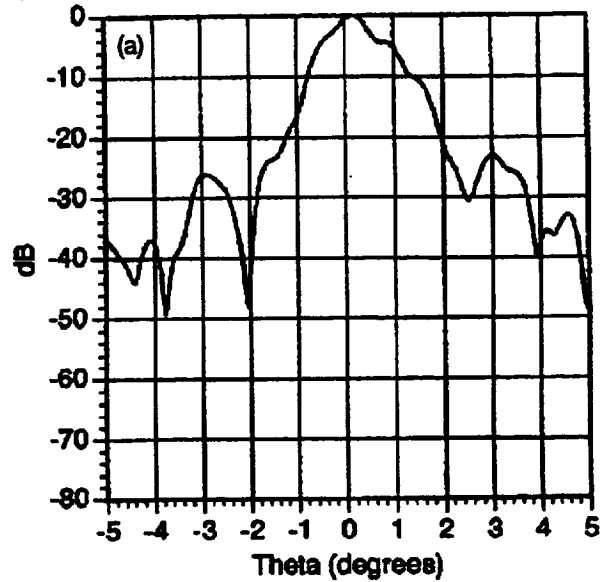


Figure 64.—Measured far-field patterns of the 1.2 meter antenna at 29.126 GHz. Feed displaced 1.18 inches. (a) E-Plane. (b) H-Plane.

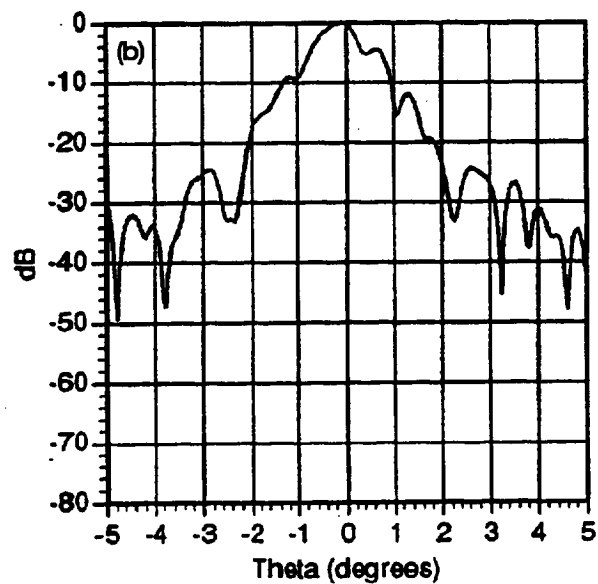
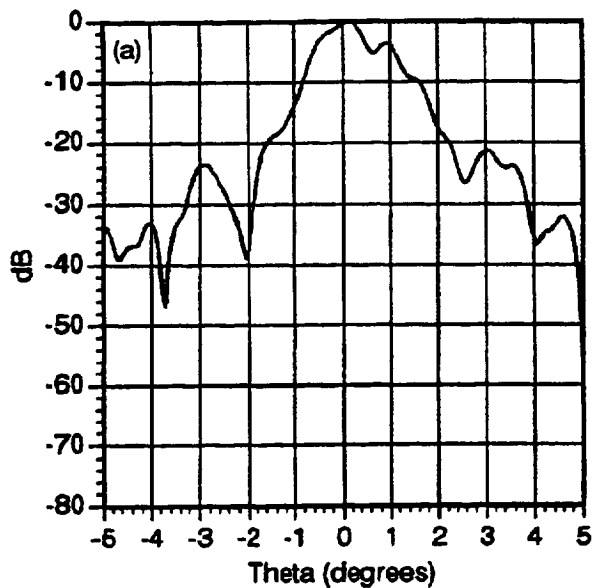


Figure 65.—Measured far-field patterns of the 1.2 meter antenna at 29.126 GHz. Feed displaced 1.28 inches. (a) E-Plane. (b) H-Plane.

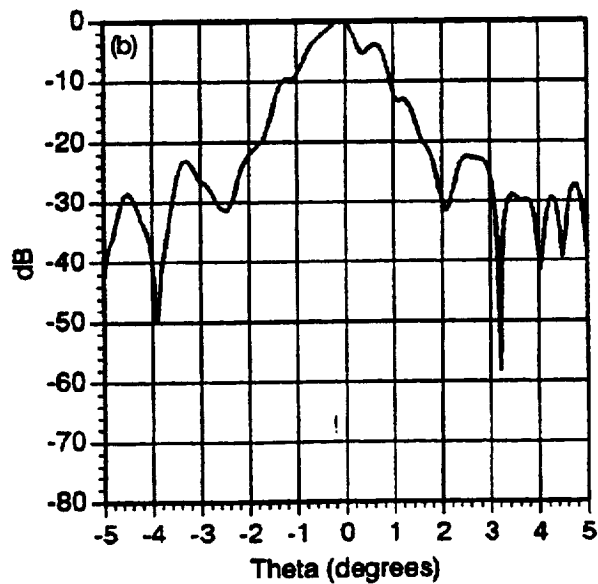
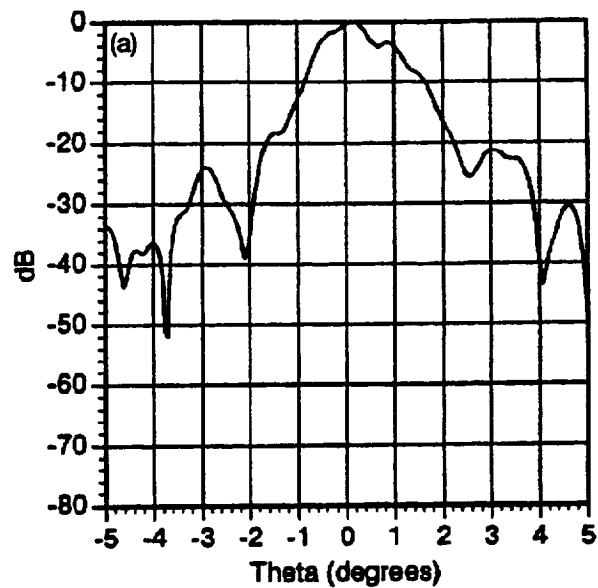


Figure 66.—Measured far-field patterns of the 1.2 meter antenna at 29.126 GHz. Feed displacement 1.37 inches. (a) E-plane. (b) H-plane.

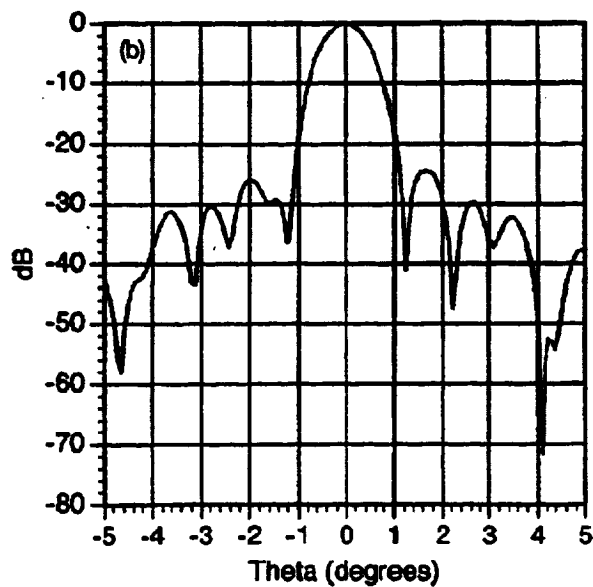
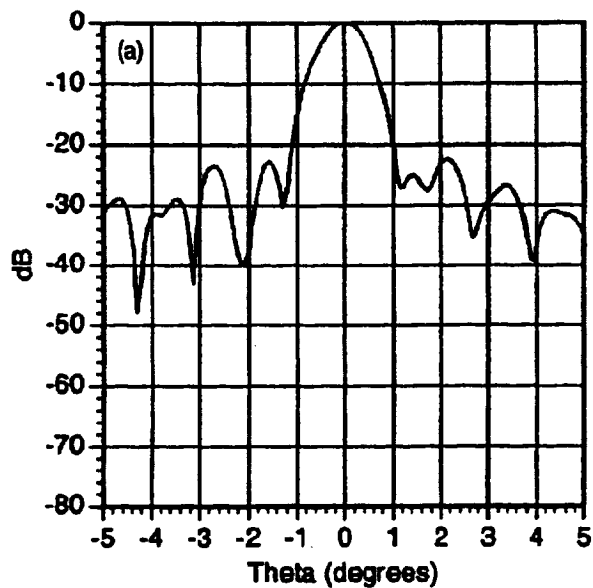


Figure 67.—Measured far-field patterns of the 1.2 meter antenna at 19.44 GHz. Feed displaced focussed. (a) E-Plane. (b) H-Plane.

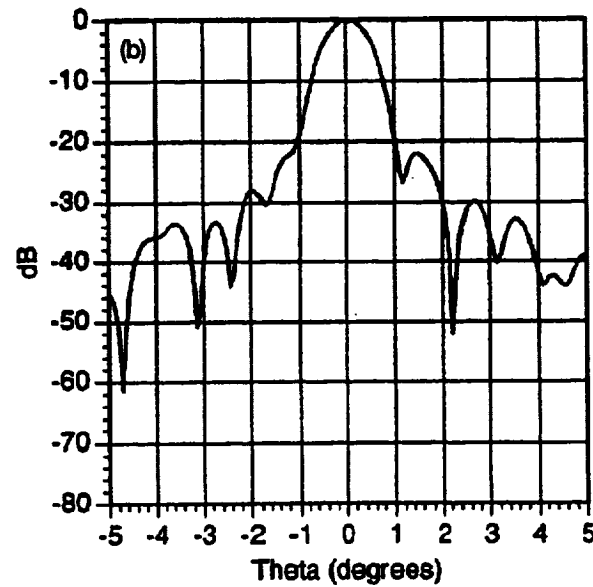
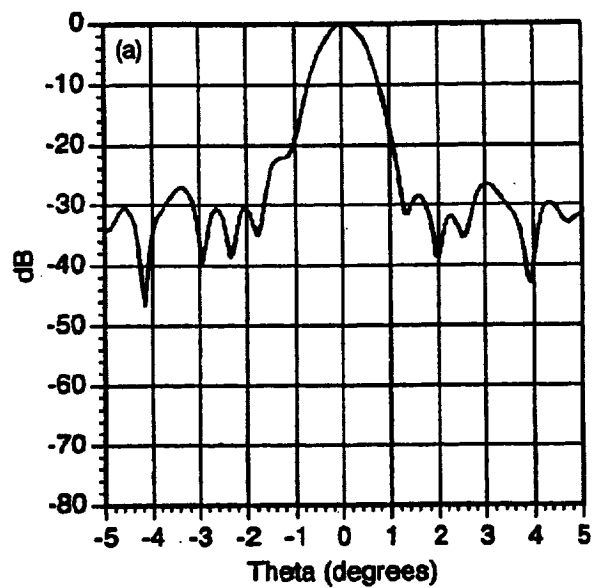


Figure 68.—Measured far-field patterns of the 1.2 meter antenna at 19.44 GHz. Feed displaced 0.41 inches. (a) E-Plane. (b) H-Plane.

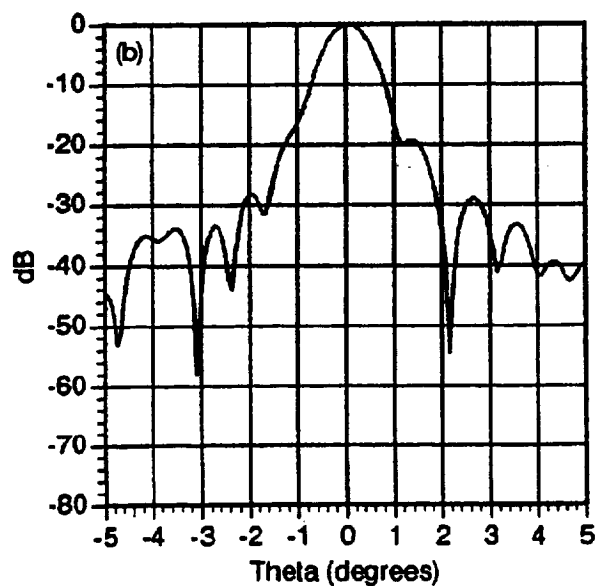
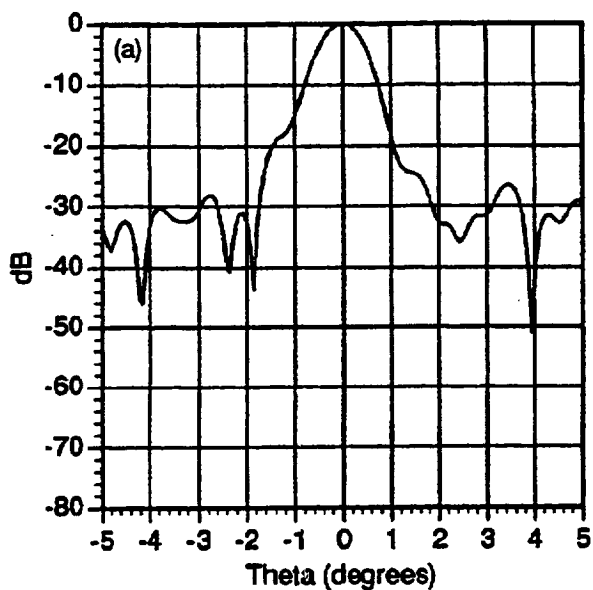


Figure 69.—Measured far-field patterns of the 1.2 meter antenna at 19.44 GHz. Feed displaced 0.60 inches. (a) E-Plane. (b) H-Plane.

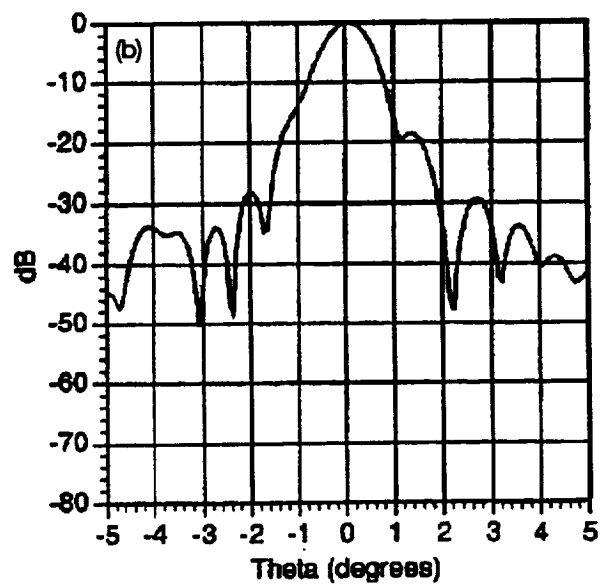
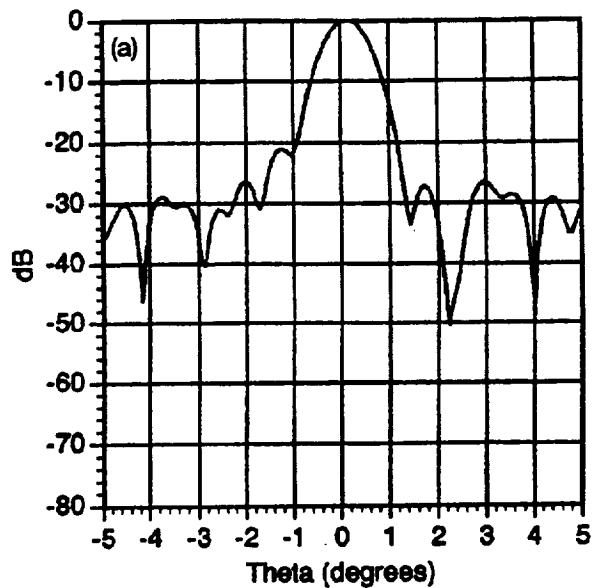


Figure 70.—Measured far-field patterns of the 1.2 meter antenna at 19.44 GHz. Feed displaced 0.74 inches. (a) E-Plane. (b) H-Plane.

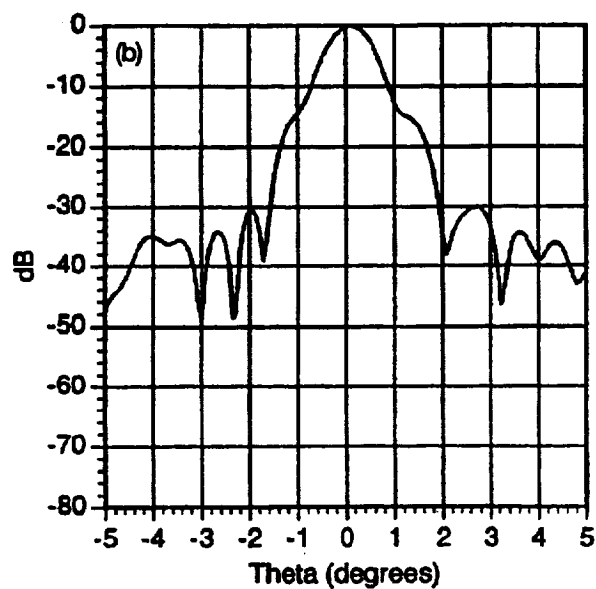
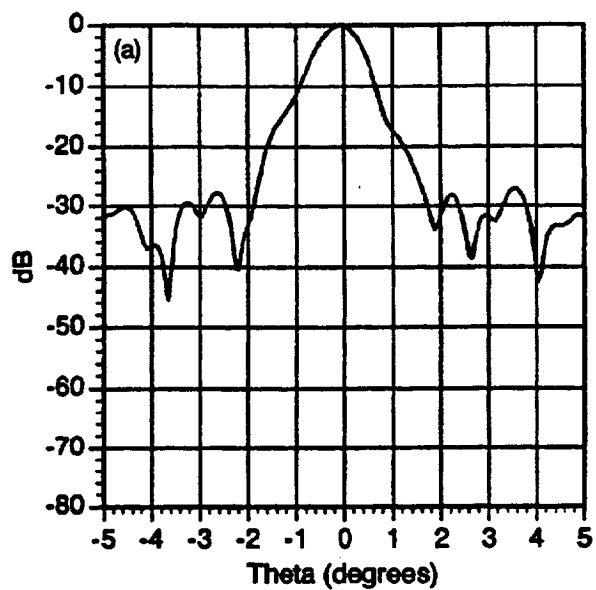


Figure 71.—Measured far-field patterns of the 1.2 meter antenna at 19.44 GHz. Feed displaced 0.87 inches. (a) E-Plane. (b) H-Plane.

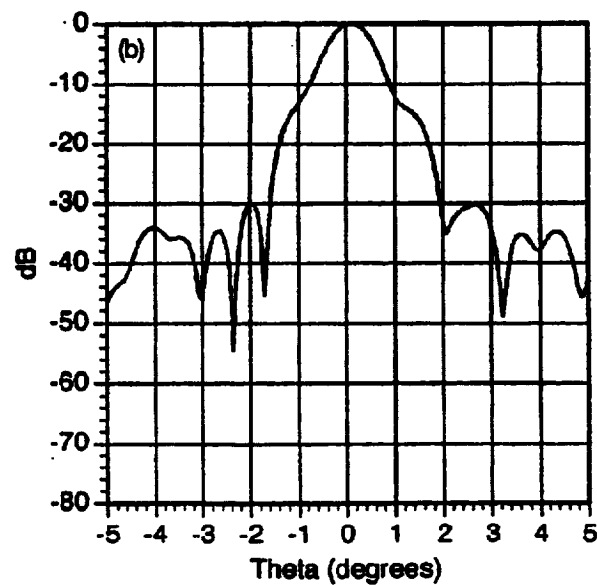
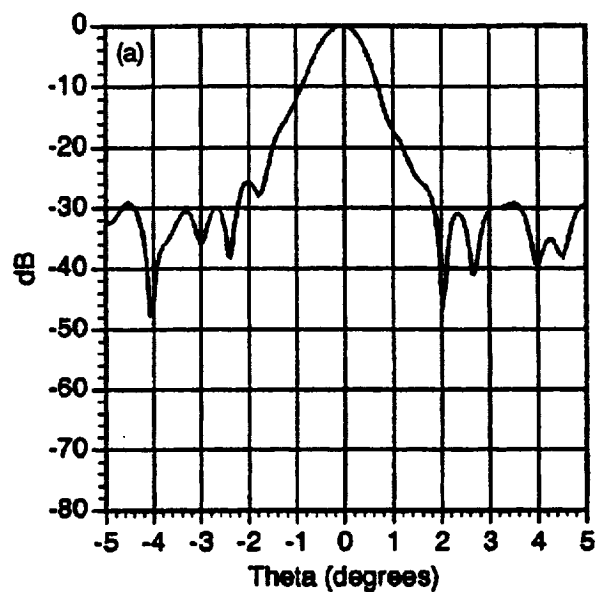


Figure 72.—Measured far-field patterns of the 1.2 meter antenna at 19.44 GHz. Feed displaced 0.99 inches. (a) E-Plane. (b) H-Plane.

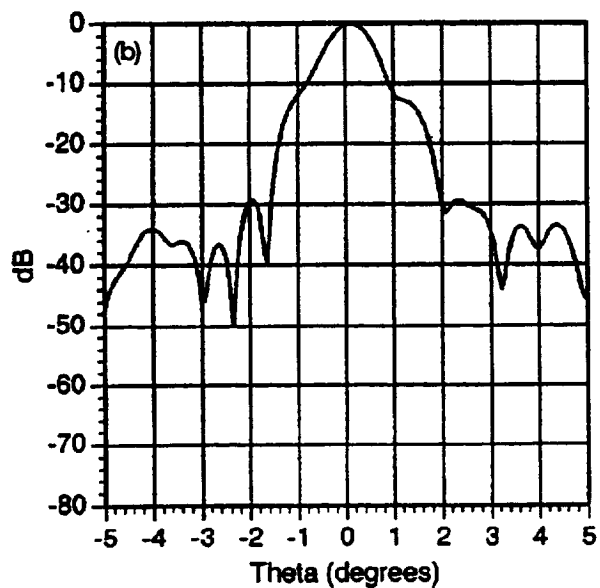
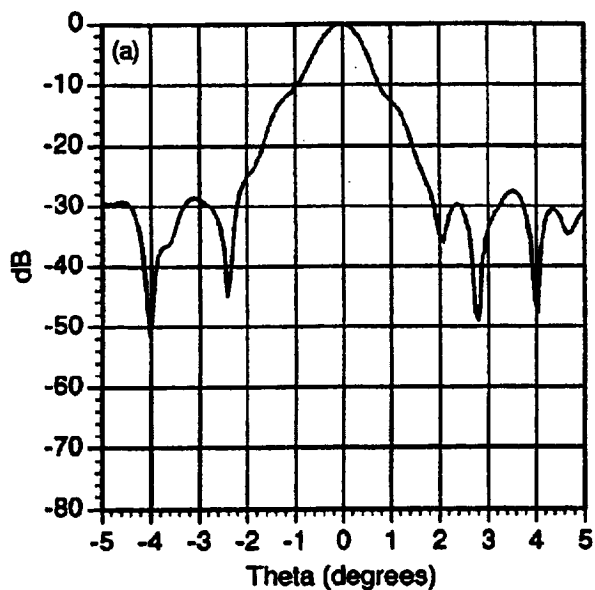


Figure 73.—Measured far-field patterns of the 1.2 meter antenna at 19.44 GHz. Feed displaced 1.09 inches. (a) E-Plane. (b) H-Plane.

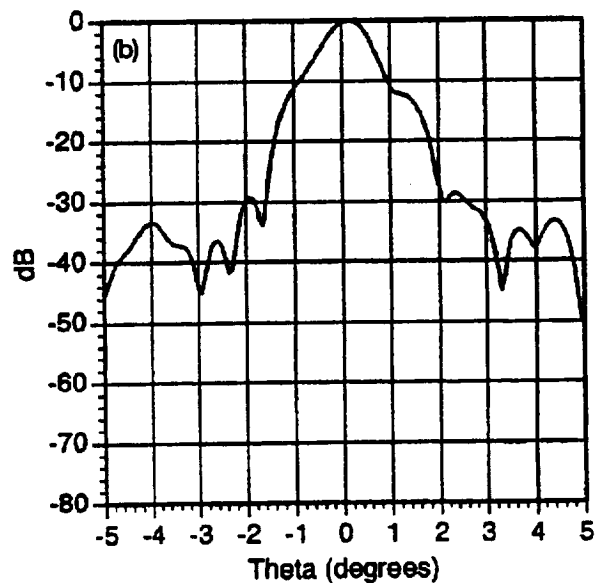
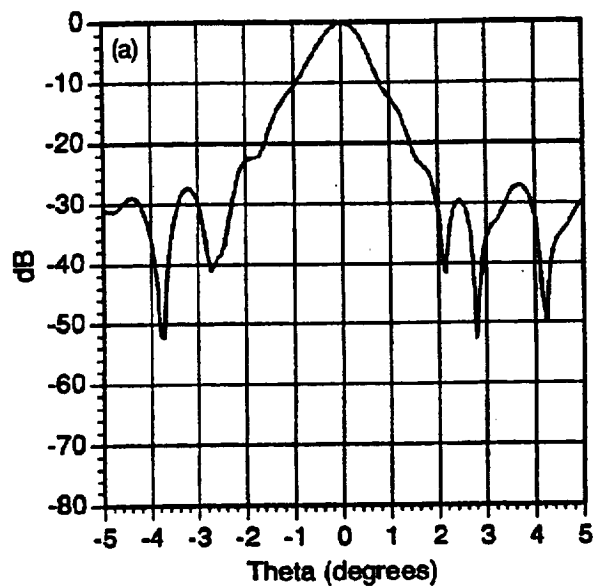


Figure 74.—Measured far-field patterns of the 1.2 meter antenna at 19.44 GHz. Feed displaced 1.18 inches. (a) E-Plane. (b) H-Plane.

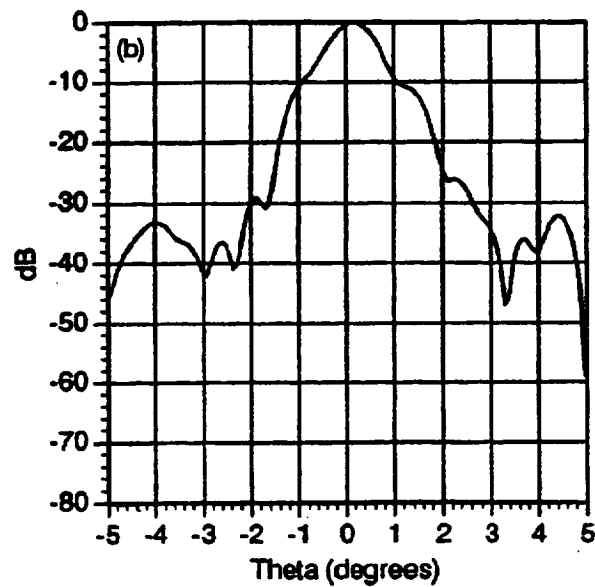
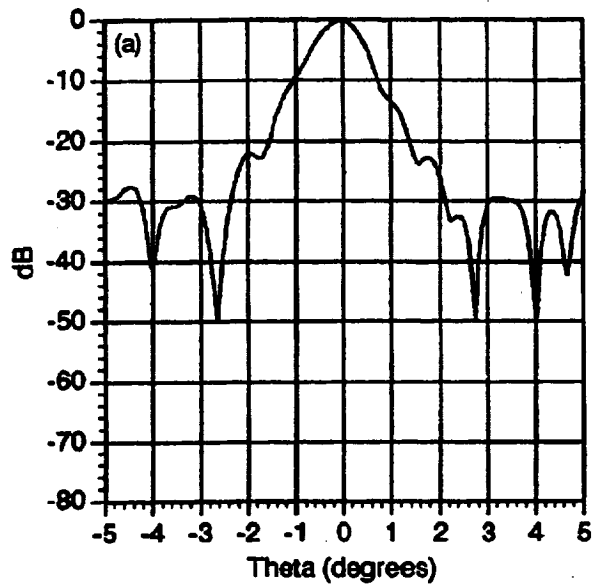


Figure 75.—Measured far-field patterns of the 1.2 meter antenna at 19.44 GHz. Feed displaced 1.28 inches. (a) E-Plane. (b) H-Plane.

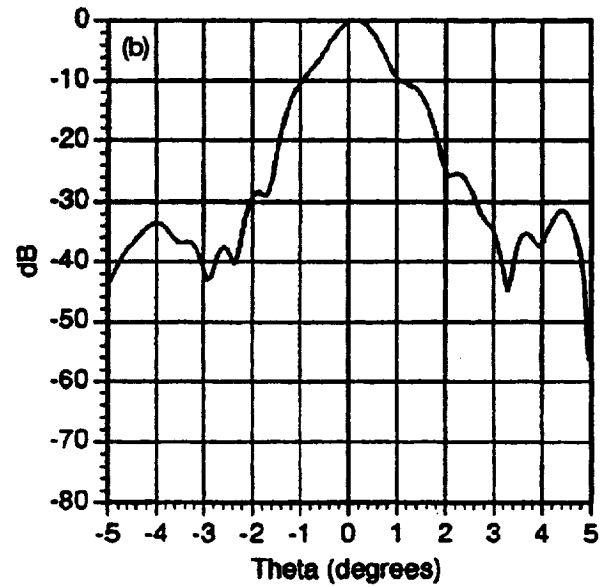
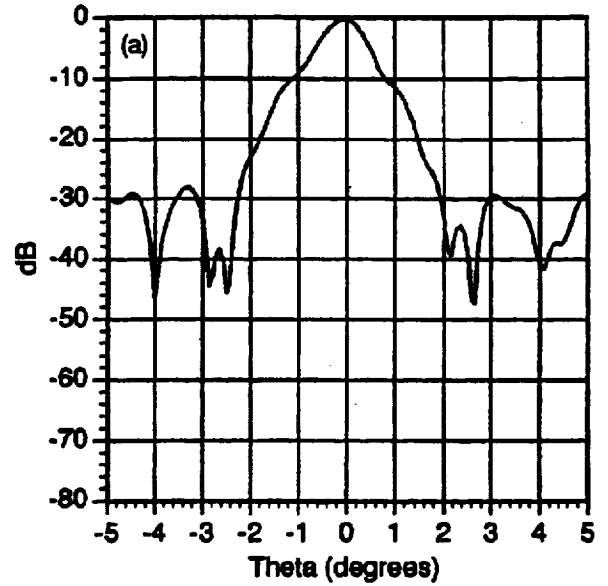


Figure 76.—Measured far-field patterns of the 1.2 meter antenna at 19.44 GHz. Feed displaced 1.37 inches. (a) E-Plane. (b) H-Plane.

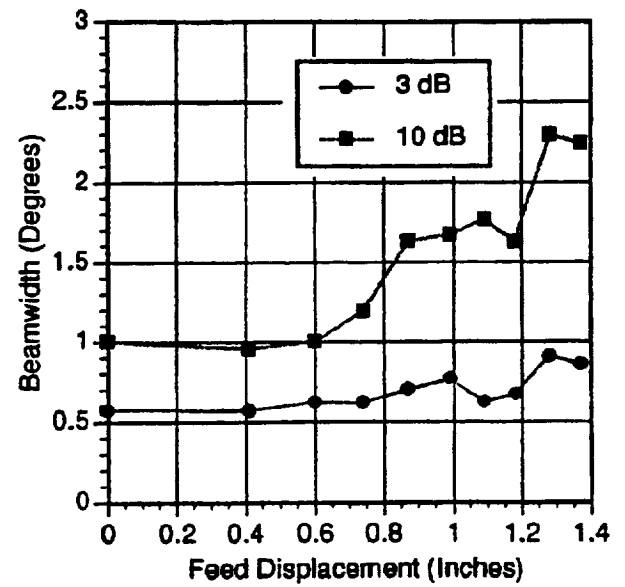
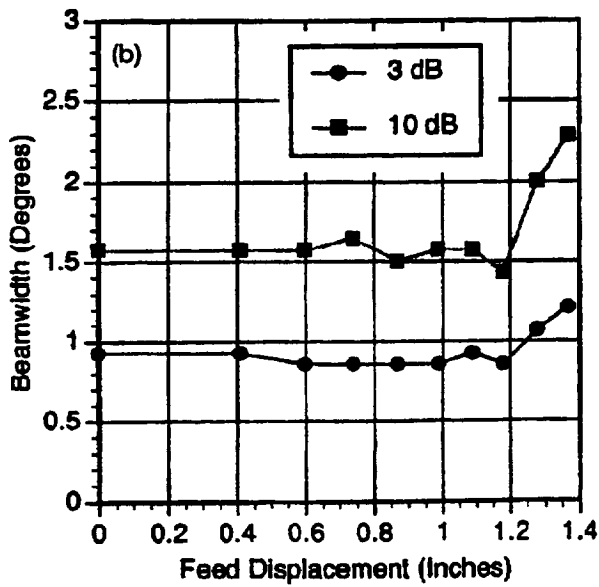
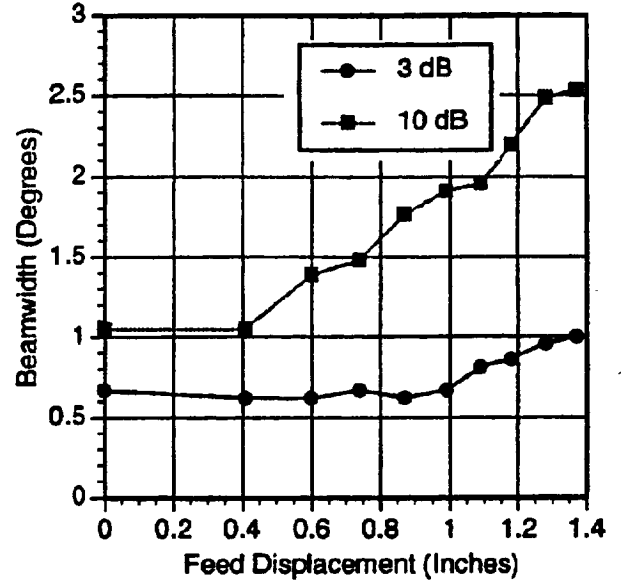
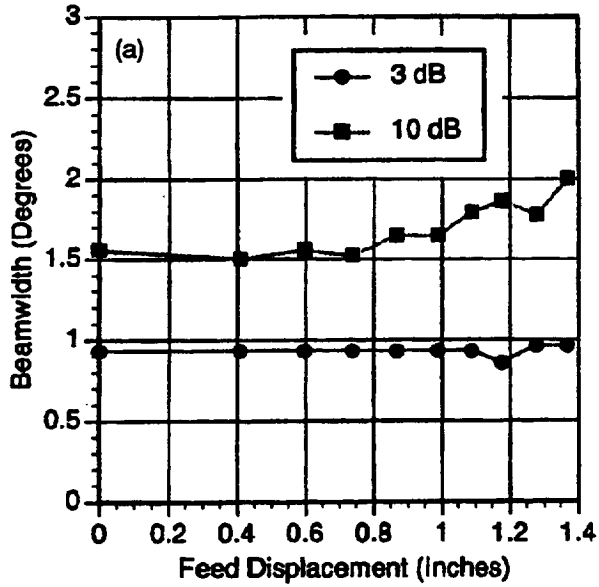


Figure 77.—Beamwidth of the 1.2 meter antenna as a function of feed displacement at 19.44 GHz. (a) E-plane. (b) H-plane.

Figure 78.—Beamwidth of the 1.2 meter antenna as a function of feed displacement at 29.126 GHz. (a) E-plane. (b) H-plane.

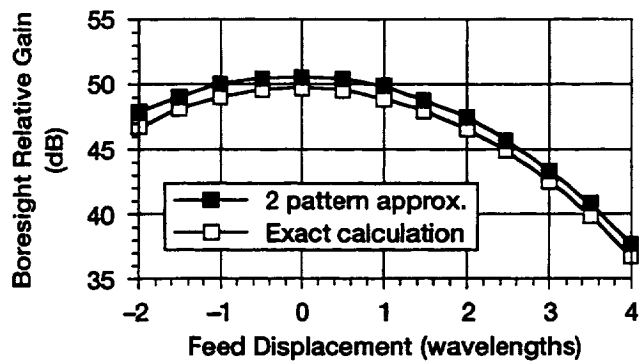


Figure 79.—Comparison of absolute gain calculations provided by the OSU Reflector Code and by the two pattern approximation.

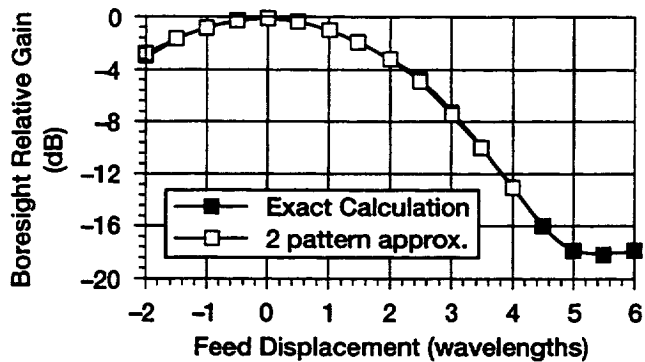


Figure 80.—Comparison of relative gain calculations provided by the OSU Reflector Code and by the two pattern approximation (curves are coincident).

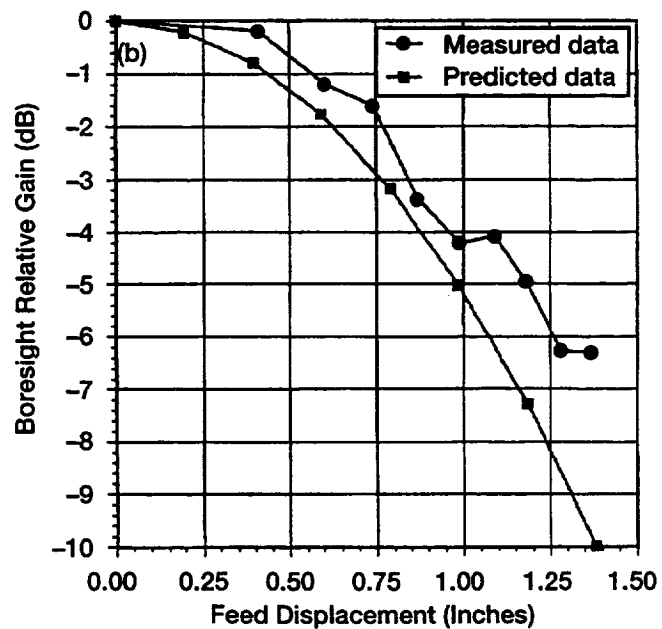
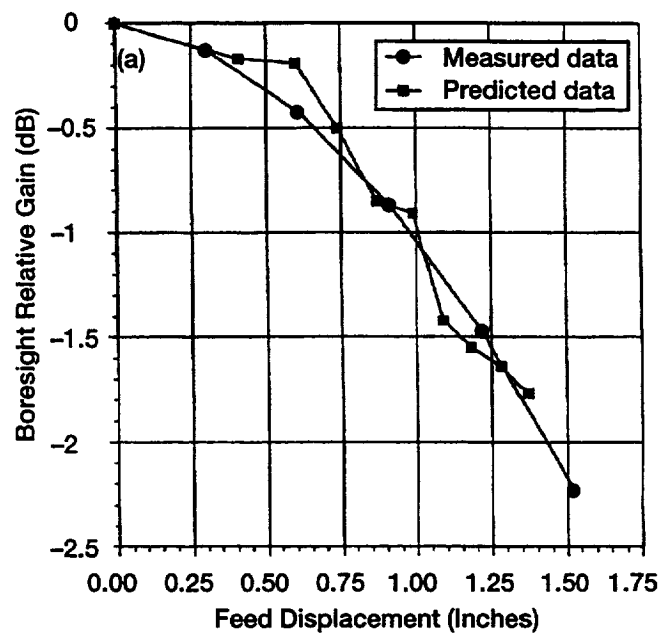


Figure 81.—Comparison of relative gain predicted from the OSU Reflector Code with the gain obtained from the near-field measurements. (a) 19.44 GHz. (b) 29.126 GHz.

REPORT DOCUMENTATION PAGE			Form Approved OMB No. 0704-0188	
Public reporting burden for this collection of information is estimated to average 1 hour per response, including the time for reviewing instructions, searching existing data sources, gathering and maintaining the data needed, and completing and reviewing the collection of information. Send comments regarding this burden estimate or any other aspect of this collection of information, including suggestions for reducing this burden, to Washington Headquarters Services, Directorate for Information Operations and Reports, 1215 Jefferson Davis Highway, Suite 1204, Arlington, VA 22202-4302, and to the Office of Management and Budget, Paperwork Reduction Project (0704-0188), Washington, DC 20503.				
1. AGENCY USE ONLY (Leave blank)		2. REPORT DATE January 1994	3. REPORT TYPE AND DATES COVERED Technical Memorandum	
4. TITLE AND SUBTITLE Defocussing Characteristics of the ACTS, T1-VSAT Earth Terminal Antennas			5. FUNDING NUMBERS WU-506-72-1C	
6. AUTHOR(S) Kevin M. Lambert and Walter M. Strickler				
7. PERFORMING ORGANIZATION NAME(S) AND ADDRESS(ES) National Aeronautics and Space Administration Lewis Research Center Cleveland, Ohio 44135-3191			8. PERFORMING ORGANIZATION REPORT NUMBER E-8257	
9. SPONSORING/MONITORING AGENCY NAME(S) AND ADDRESS(ES) National Aeronautics and Space Administration Washington, D.C. 20546-0001			10. SPONSORING/MONITORING AGENCY REPORT NUMBER NASA TM-106420	
11. SUPPLEMENTARY NOTES Kevin M. Lambert, Analox Corporation, 3001 Aerospace Parkway, Brook Park, Ohio 44142 (work funded by NASA Contract NAS3-25776) and Walter M. Strickler, NASA Lewis Research Center. Responsible person, Walter M. Strickler, (216) 433-8860.				
12a. DISTRIBUTION/AVAILABILITY STATEMENT Unclassified - Unlimited Subject Category 32			12b. DISTRIBUTION CODE	
13. ABSTRACT (Maximum 200 words) This report describes a study, the purpose of which was to determine the characteristics of two reflector antennas, as the reflector feed is moved away from the focus. The antennas are a 1.2 meter and a 2.44 meter reflector that will be used in the T1-VSAT earth terminals for the Advanced Communications Technology Satellite (ACTS). These terminals have been constructed in such a way that is inconvenient to use attenuators to control the gain of the signal that is directed toward the satellite. Feed defocussing was proposed as a simple, convenient way to achieve the required gain control. The study was performed in two parts. In order to determine the feasibility of the technique, a theoretical analysis was performed to obtain the gain, beamwidth and far-field pattern of the antennas, as a function of feed displacement. An experimental investigation followed in which patterns of the 1.2 meter antenna were obtained through measurement in the NASA Lewis Research Center, Near-Field Antenna Test Facility. Results of the theoretical and experimental investigation are presented for both uplink (30 GHz) and downlink (20 GHz) frequencies.				
14. SUBJECT TERMS Reflector antennas; Antenna metrology			15. NUMBER OF PAGES 54	
			16. PRICE CODE A04	
17. SECURITY CLASSIFICATION OF REPORT Unclassified	18. SECURITY CLASSIFICATION OF THIS PAGE Unclassified	19. SECURITY CLASSIFICATION OF ABSTRACT Unclassified	20. LIMITATION OF ABSTRACT	